Silicon Based Lithium-Ion Battery Anodes: a Chronicle Perspective Review

Xiuxia Zuo[1], Jin Zhu[1], Peter Müller-Buschbaum[2], and Ya-Jun Cheng[1, 3*]

1. Polymers and Composites Division, Ningbo Institute of Materials Technology & Engineering, 1219 Zhongguan West Rd, Zhenhai District, Ningbo, 315201, Zhejiang Province, P. R. China

2. Physik-Department, Lehrstuhl für Funtionelle Materielien, Technische Universität MÜnchen, James-Franck-Strasse 1, 85748 Garching, Germany

3. Department of Materials, University of Oxford, Parks Rd, OX1 3PH, Oxford, United Kingdom

Abstract

Si has been regarded as one of the most promising next generation lithium-ion battery (LIB) anodes due to its exceptional capacity and proper working voltage. However, the dramatic volume change during lithiation/delithiation processes has caused severe detrimental consequences, leading to very poor cyclic stability. It has been one of the critical problems hampering the practical applications of the silicon based LIB anode. Extensive research has been carried out to resolve the problem since early 1990s. For the first time, the studies on the Si anode in the time frame more than two decades are summarized and discussed in this review with a novel chronicle perspective. Through this article, the evolution of the concept, fundamental scientific and technology development of the silicon LIB anode are clearly presented. It

provides unique eyesight into this rapid developing field and will shed light on the future trend of the Si LIB anode research.

Keywords: Silicon; Lithium-Ion Battery; Anode; Volume Change; Cyclic Stability; Energy Storage

Contents

1. Introduction

Lithium-ion batteries (LIBs) are one of the most widely used secondary battery systems. Compared to other rechargeable batteries, such as nickel-cadmium and nickel metal hydride batteries, LIBs are featured with higher energy density, higher operating voltages, limited self-discharging and lower maintenance requirements[1-4]. However, the current commercial graphite anode cannot meet the increasing demand on energy density, operation reliability and system integration arising from portable electronic devices, electric vehicles, and energy storage applications. Graphite anodes exhibit only a moderate intrinsic specific capacity (372 mAh g^{-1}) and serious safety concerns due to lithium plating and further formation of lithium dendrites[5]. As a consequence, studies on new generation anode materials with the characteristics of high capacities, a proper charging/discharging potential, as well as safe and low cost manufacturing and usage have attracted great attention from both, academia and industry[6].

Among all potential lithium-ion battery (LIB) anodes, silicon (Si) is one of the most promising candidates to replace graphite due to following reasons: (1) Si possesses the highest gravimetric capacity (4200 mAh g^{-1}, lithiated to $Li_{4.4}Si$)[7] and volumetric capacity (9786 mAh cm^{-3}, calculated based on the initial volume of Si) other than lithium metal; (2) Si exhibits an appropriate discharge voltage at *ca*. 0.4 V in average, which finds a good balance between retaining reasonable open circuit voltage and avoiding adverse lithium plating process[5, 8]; (3) Si is abundant (second richest in earth crust), potentially low cost, environment friendly, and non-toxic[9].

However, drastic volume expansion (around 360 % for $Li_{4.4}Si$)[10] and huge stress generation are accompanied with the lithiation/delithiation process of Si, which causes series of severe destructive consequences (**Figure 1**)[5, 9, 11, 12]. (1) Electrode structure integrity is deteriorated due to gradually enhanced pulverization during repeated discharge/charge processes; (2) disconnection between electrode and current collector happens induced by the interfacial stress; (3) continuous consumption of lithium ions occurs during the continuous formation-breaking-reformation process of solid electrolyte interface (SEI) layer[13-15]. All these processes accelerate electrode collapse and capacity fading in a synergistic way. Besides, the critical problem of volume expansion, the poor intrinsic electron conductivity of Si also contributes to the sluggish electrochemical kinetics[16].

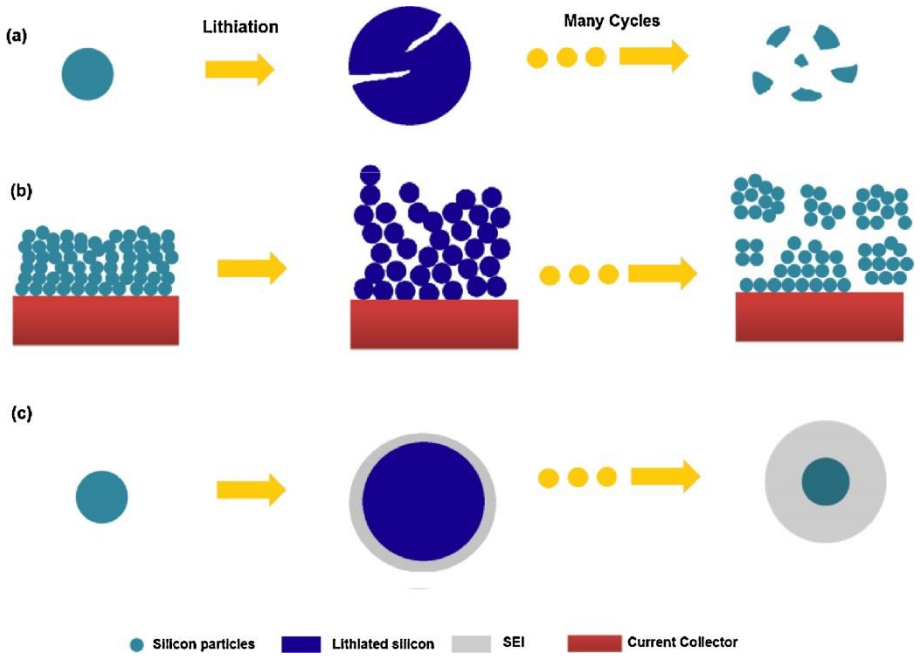

Figure 1. Three different failure mechanism of Si electrode, a) electrode pulverization, b) collapse of the entire electrode, and c) continuous breaking and re-growth of the

SEI layer. Reprinted with permission from Ref 6. Copyright 2012 Elsevier. B.V.

To tackle the aforementioned critical issues, tremendous efforts have been made since 1990s [17-23]. The strategies developed include utilizing nanoscale silicon, compositing with stress-relief buffer matrix, and constructing physical compartment to accommodate volume expansion.

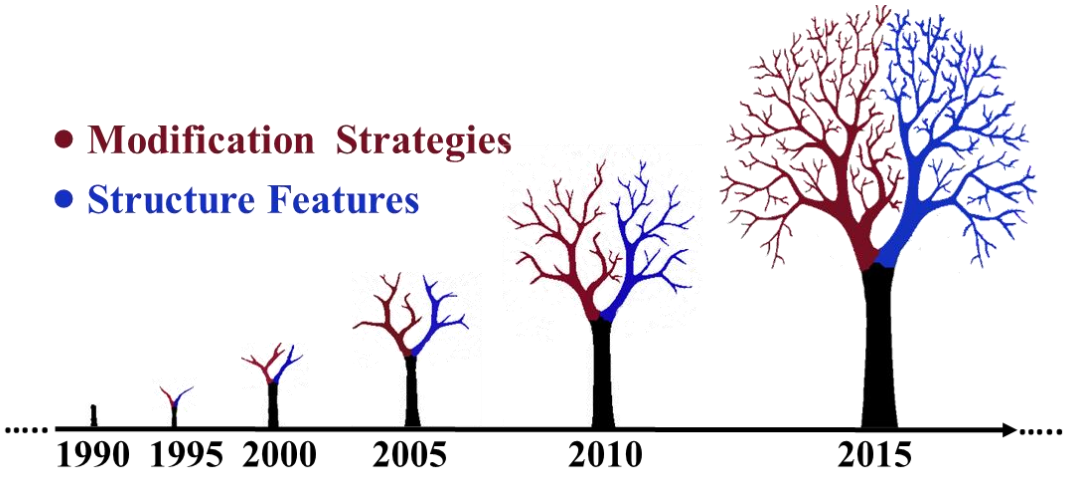

Figure 2. Three criteria applied in this review to classify the Si-based anode research.

In this manuscript, the progress of the basic research activities on Si-based LIB anodes will be reviewed. The research work will be classified based on three criteria (**Figure 2**). The first criterion is the structure feature of Si, such as zero-dimension Si nanoparticles, one-dimensional Si (Si nanowire, Si nanotube), two-dimensional Si (thick and thin Si film), and three-dimensional Si (three-dimensional continuous bulk Si). The second one is about modification strategies of Si. It includes composition (further classified with different carbon species, metals, metal oxides, and other materials), and hierarchical structure construction (core-shell, embedding, yolk-shell, etc.). The third criterion is the chronical scale ranging from the early 1990s to 2015. Particularly, unlike typical

reviews on Si anodes that have been published so far [8, 16, 24], this new chronicle perspective will be applied as a mayor line to address the advance of the Si-based LIB anode research in the last twenty years. The two other criteria are used to substructure the review article. We hope that with our review approach unique insights will be obtained to inspire future research on Si anodes.

2. Emergence of Si as LIB Anodes

Experimental work on anodes using chemical elements which form alloys with lithium was started in the early 1970s. In 1971, Dey found that lithium could electrochemically alloy with a number of metals at room temperature, including Sn, Pb, Al, Au, Pt, Zn, Cd, Ag and Mg[25]. In 1976, Sharma and Seefurth reported the formation of Li–Si alloys at high temperature cells operating in the range between 400 °C and 500 °C [26, 27]. The phases in the Li-Si system were confirmed as $Li_{12}Si_7$, $Li_{14}Si_6$, $Li_{13}i_4$, and $Li_{22}Si_5$. Particularly, the formation of $Li_{22}Si_5$ generates a total theoretical capacity of 4200 mAh g^{-1}, which is the highest among the above various Li alloy compounds [5, 7, 9, 26, 28]. But the reversibility of normal Si powder at room temperature was found to be very poor due to the huge volume expansion[7, 10]. Developing effective strategies to resolve the problem of volume expansion has been identified as a central issue of the research on Si-based LIB anodes.

3. Preliminary Stage of the Si-Based Anodes Research between 1990 and 2000

Dahn *et al*. appears to be the first few groups to synthesize Si-containing anode by pyrolyzing various Si containing polymers under inert atmosphere conditions.

Typical polymers explored include polysiloxanes, epoxy-silane composites, and pitch-polysilane blends [29-34]. The main pyrolysis product is amorphous non-stoichiometric $Si_xO_yC_z$ glass composited with free carbon matrix. The exact composition of the SiOC can be tuned by modifying the molecular structure of the polymers, and tuning the pyrolysis protocols as well [31, 32, 35-39]. The reversible capacity can reach the range between 360 mAh g^{-1} and 900 mAh g^{-1}. The exact mechanism for the lithiation of SiOC is not well understood. The non-stoichiometric nature is reported to endow the SiOC compounds electrochemical activity and exhibit lithiation capability. However, there are also some references claiming that SiOC is mainly electrochemical inactive and it is the free carbon matrix that exhibits the lithiation capability [31, 35, 36]. The capacity can be increased by fine tuning the composition of the Si element within the SiOC. Nevertheless, the room for performance improvement is relatively limited because the main active component is unlikely the Si element itself.

In the late 1990s, using nano-sized Si composited with carbonaceous materials has been regarded as one promising method to improve the electrochemical performance of the Si anode preparation. Wilson dispersed nano-sized Si synthesized by CVD into carbons matrix (11 % by molar ratio over carbon) to lift the overall capacity of the composite[34]. It was found that the capacity reached 600 mAh g^{-1}, which was nearly 50 % higher than the capacity of the commercial graphite. Besides CVD, Wang used ball milling to prepare Si/graphite composites. The mixture of micrometer-sized Si and graphite (both 325 mesh) was ball-milled with different

molar ratios ($C_{1-x}Si_x$, x = 0, 0.1, 0.2, 0.25)[40]. The reversible capacity of the ball-milled products was increased from 437 mAh g^{-1} (pure graphite) to 1039 mAh g^{-1} ($C_{0.8}Si_{0.2}$) at the current density of 45 mA g^{-1}. The increased capacity originated from the lithium insertion/extraction of Si. One year later, Huang prepared Si/C composite by manual grinding the mixture of nano-sized Si (78 nm) and carbon black under ambient condition[41]. The composite exhibited a capacity of 1700 mAh g^{-1} after ten cycles. Particularly, the authors pointed out that the use of nano-sized Si particles played an important role in the improvement of the cyclic stability due to their good plasticity and deformability. Besides the use of carbon matrix, Kumta synthesized Si/TiN composite by high-energy mechanical milling (HEMM)[42]. The HEMM process generated very fine Si particles, which are homogeneously dispersed in the TiN matrix. The composite containing 33.3 mol% of Si exhibited a stable capacity of 300 mAh g^{-1} after 20 cycles at a current density of 0.25 mA cm^{-2}.

Intermetallic Si alloys have been studied as anode materials since 1986[43-45]. In 1999, Kim and Moriga investigated the reaction mechanism of lithium insertion into the Mg_2Si alloy. They found that 1 mol Mg_2Si reacted with 3.9 mol Li, where an initial capacity of approximate 1370 mAh g^{-1} was achieved [46, 47]. In 2000, Wang used Si (325 mesh) and Ni (100 mesh) to prepare intermetallic NiSi alloy with HEMM[48]. The NiSi alloy exhibited a high initial discharge capacity of 1180 mAh g^{-1} at the current density of 80 μA cm^{-2}.

Si thin films emerged as potential LIB anodes during this period as well. Si thin films with the thickness of 1.2 μm were deposited on porous Ni substrates by CVD

[49]. The electrochemical performance exhibited capacities up to 1000 mAh g^{-1}. However, a severe capacity fading was observed after only a few cycles due to huge mechanical stress generated by a massive volume change of the thin film.

In a short summary, during the time range between 1990 and 2000, the research on Si-based anodes was still quite limited. Only a few research activities have been reported (**Table 1**). The pyrolysis of Si-containing polymer, Si/C composites, Si thin films and Si alloys were investigated. Particularly, capacity as high as 1000 mAh g^{-1} was achieved in some work. But the initial capacity and cyclic performance were generally rather limited. Nevertheless, these studies triggered great interest worldwide and were inspiring to the Si-based anode research for LIBs in the next decade.

4. Rise of the Si-based Anodes between 2001 and 2005

The unique features of the Si-based anodes are their high gravimetric and volumetric lithium storage capacities, and appropriate thermodynamic lithiation potentials of 1.0 V - 0.3 V (vs. Li/Li^+) instead of 0.2 V - 0.1 V for the lithiated graphite. However, the major drawback for the Si anodes is the poor cyclability originated from drastic volume expansion upon lithiation [43, 45]. Followed by the research work before 2000, this critical issue has been intensively tackled between the years 2001 and 2005. Various effective strategies including size reduction [41, 50-53] and compositing with active and/or inactive buffer matrix have been developed [51, 54-57]. These research activities have achieved great success in improving the electrochemical performance and understanding the fundamental mechanism of Si-based anode during this time range.

4.1 Si Alloys/Alloy Composites

Besides the Si alloys reported in the late 1990s[46, 48], many other types of Si alloys were synthesized and used as LIB anodes such as SiAg[58], Mg_2Si[59], $CaSi_2$[60]. However, these alloys exhibited inferior cyclic performance compared to graphite. Therefore, compositing with graphite was tried with mechanical milling technique to improve the cyclic stability. For example, $Fe_{20}Si_{80}$-graphite was prepared by directly ball milling the $Fe_{20}Si_{80}$ alloy with graphite. The composite showed a reversible capacity of 600 mAh g^{-1} and the capacities were retained above 400 mAh g^{-1} after 25 cycles. The improved cyclic stability was attributed to the *in situ* formation of the buffer matrix of $FeSi_2$ during ball milling[55]. Similar composites such as BaFeSi/graphite[54], FeSi/graphite[61] and SiNi/graphite[62] were also tested. These composites exhibited good reversible capacities above 420 mAh g^{-1}. Furthermore, improved capacity retention was achieved even after 50 cycles, where previous research only showed reasonable cyclic performance within 20 cycles. Generally, the formation of an inactive alloy buffer matrix ($FeSi_2$, $BaSi_2$, $NiSi_2$ and NiSi) and the incorporation of graphite contributed to the improved cyclic stability.

4.2 Si Films/Composite Films

Following the research work on micrometer thick Si film electrode, thin Si films with the thickness in the nanometer range were prepared and investigated as LIB anodes. In 2003, amorphous Si films (about 50 nm in thickness) prepared by CVD showed a maximum discharge capacity of 4000 mAh g^{-1} at a constant current of 100 mA cm^{-2} [63, 64]. Although this film electrode achieved exceptional capacity, its

cyclability was not very good because undesirable parasites and pores induced mechanical cracking upon cycling. Relative thick Si thin films (250 nm) deposited on Cu foil substrates were fabricated by radio-frequency (RF) magnetron sputtering. They yielded steady reversible capacity close to 3500 $mAhg^{-1}$ after 30 cycles at a current rate of 1680 mAg^{-1} [65]. Although the cyclic performance of these Si films has been significantly improved compared to previous work, the cyclic stability with even longer cycles was not mentioned. Takamura prepared a 77 nm thick Si film on a 30 μm thick Ni foil using a vacuum evaporation method[50]. The Si thin film had a capacity over 1500 mAh g^{-1} with stable cyclic performance over 700 cycles. After that work, they further improved the cyclic performance by decreasing the film thickness down to 50 nm and increasing the surface roughness of the current collector[66]. With this strategy, reversible capacities over 2000 mAh g^{-1} with a cycle lifetime as long as 1000 cycles were achieved. The surface roughness was identified as an important factor for improving the performance of thin film anodes. The rough foil effectively increased the contact area and enhanced the adhesion between the Si film and the current collector, which made the whole electrode more durable against volume change [66-69]. The concept of enhancing surface roughness was also working with micrometer thick Si film. For example, a 1.1 μm thick Si film deposited on the well-etched substrate maintained the specific capacity over 1500 mAh g^{-1} after 400 cycles with 1 C constant charge/discharge rate [69].

Inspired by the studies on bulk Si composites, composites based on Si films have also been utilized as LIB anodes. Qin found that the amorphous Si/TiN

nanocomposite film exhibited higher capacity and better capacity retention than that of the pure amorphous Si film electrode[70]. The nano-sized Si particles were embedded in the TiN matrix which helped to inhibit the pulverization process during Li-alloying/de-alloying. Lee studied the electrochemical characteristics of Fe/Si multilayer film. They found that the Fe layer effectively suppressed the volume expansion of the Si layer during cycling[71]. Besides, nanocrystalline Mg_2Si film of 30 nm in thickness was prepared with the pulsed laser deposition (PLD) technique. It showed a stable cycling behavior between 0.1 V and 1.0 V, yielding a reversible capacity of 2200 mAh g^{-1} for more than 100 cycles[52].

4.3 Zero-Dimension (0D) Si and their Composites

4.3.1 0D Silicon/Carbon Composites

Since 1990s, compositing Si with carbonaceous materials has been recognized as an effective strategy to stabilize electrode by absorbing stress generated by volume change. However, the choice of carbon source and mixing methods was quite limited at the early stage. The Si/C composites were mainly prepared by directly ball milling the mixture of Si and graphite powders. Between 2001 and 2005, more carbon precursors and compositing methods have been developed. Kumta and Kim chose polystyrene (PS) as the carbon source to synthesize Si/C nanocomposite [56]. The PS and Si powder (325 mesh) were mixed with HEMM followed by pyrolysis in inert atmosphere. EDX analysis on the nanocomposite showed that the content of Si was about 66 %. A reversible capacity of around 850 mAh g^{-1} with capacity retention of 98.9 %/cycle was achieved over 30 cycles with a current density of 100 μA cm^{-2}. Liu

used polyvinyl alcohol (PVA) as the carbon source to synthesize Si/C nanocomposite with a similar method[72]. The Si/C nanocomposite of 90 % PVA/10 % Si showed a high reversible capacity of 754 mAh g^{-1} within 20 cycles and an initial coulombic efficiency of 80.3 % at the current density of 50 mA g^{-1}. Poly (vinyl chloride) (PVC) was also used as the carbon precursor to synthesize Si/C nanocomposites [57, 73]. The composite with 40 wt% - 50 wt% of Si possessed a reversible capacity of around 900 mAh g^{-1} over 40 cycles at the current density of 0.3 mA cm^{-2} with an initial coulombic efficiency of 82 %. Furthermore, by introducing additional co-milling components (such as TiB_2 and TiN) into the Si/C composite, the rate and cyclic performance were improved, but with a slight capacity sacrifice due to the presence of inactive phase[73].

Apart from the carbon matrix derived from the thermoplastic polymer as mentioned above, thermosetting polymers were also used to generate carbon matrix to encapsulate Si powders. Si nanoparticles (80 nm) were homogeneously dispersed in the carbon aerogel by mixing the Si nanoparticles with the resorcinol-formaldehyde resin, followed by carbonization process[51]. The Si/C composites containing 40 wt% carbon showed a reversible capacity of 1450 mAh g^{-1} over 50 cycles at the current density of 200 mA g^{-1}. The good cyclic performance was attributed to the use of nanoscale Si particles and the homogeneous dispersion of the Si nanoparticles in the carbon matrix.

The meso carbon microbead (MCMB) was also used as a carbon matrix to disperse Si nanoparticles by ball milling. But the Si/MCMB composite suffered from

a relatively high fading rate[74]. Besides, graphite was still used as carbon source to composite with Si in this time range. Holzapfel prepared Si/graphite composite with nano-sized Si particles via thermal vapor deposition of silane on the surface of fine graphite particle [53, 75]. The Si/graphite composite with 20 % of Si showed an initial capacity of 1350 mAh g^{-1} whereas the discharge capacity for the following 100 cycles was maintained about 1000 mAh g^{-1} at a current density of 74 mA g^{-1} [53]. The relatively slow capacity loss upon cycling were attributed to the very small Si particle size (10 nm - 20 nm), good adherence to the graphite surface, and homogeneous distribution of the Si nanoparticles on the graphite surface.

Besides the strategy to disperse Si in carbon matrix, the concept to coating Si surface with carbon was also developed [76-78]. Yang prepared carbon-coated Si particles containing 27 % of carbon by mass[77]. The Si particles (*ca*. 3 μm) were coated with a carbon layer of around 500 nm in thickness. The carbon-coated Si particles achieved capacity as high as 1000 mAh g^{-1} with a constant current of 300 mA g^{-1}.

4.3.2 Other 0D Si composites

During this time range, metals were also tried to composite with Si in order to take advantage of their excellent electronic conductivity and good mechanical properties. For example, Si/Ag and Si/Cu composites were prepared by electroless plating of Ag and Cu particles on the surface of Si powder[79, 80]. The resulting anode materials exhibited improved cyclic performance due to introduction of metal coating. However, the long-term cyclability was not very impressive. The poor

interaction between metal and Si caused the detachment of metal from the Si surface due to severe volume change of the Si particles on cycling[80].

Conductive polymers such as polypyrrole (PPy) were also applied to composite with Si particles. Conductive polymers not only enhanced charge carrier transportation, but also acted as a buffer medium to inhibit the huge volumetric change. Guo synthesized Si/PPy composites using the HEMM technique. They found that PPy decreased the initial irreversible capacity loss due to reduced thickness of the solid electrolyte interface (SEI) layer[81]. The composite containing 50 wt% Si exhibited higher coulombic efficiency and better cyclic stability than bare Si.

4.5 Tentative Summary of the Progress between 2001 to 2005

In summary, a few tentative conclusions can be drawn to feature the new trend of the Si-based anode research work from the years 2001 to 2005 (**Table 2**). Firstly, nano-sized Si was widely used to tackle the volume change issue of the Si-based anode. Secondly, various materials have been employed in composites with Si to circumvent the adverse effect of the volume change, and provided other additional benefits as well. These included different types of carbon derived from various precursors, metals, and certain inactive components. Thirdly, the concept of using nano-sized Si and new compositing method were applied to different types of Si electrodes, such as Si alloys, films and particles. Moreover, the importance of roughness of the current collector was realized. By applying these strategies, the electrochemical performance of Si-based anodes has been significantly improved. The

specific reversible capacities can be normally lifted up to around 1500 mAh g^{-1} for hundreds of cycles.

5. Rapid Development of Si-based Anodes from 2006 to 2010

5.1 Si Alloys/Alloy Composites

The use of mechanical milling/alloying processes has continued to be an important technique to synthesize Si-based alloys. Furthermore, compositing Si-based alloys with other components have still been applied to tackle the critical volume expansion issue of Si. Si-based alloys/carbon composites such as Cu_5Si-Si/graphite[82], $FeSi_6$/graphite[83], SiNi/graphite[84, 85], and Mg_2Si/carbon[86] were reported in this period. However, their performance did not exhibit obvious improvements as compared to previous research work. Doh synthesized a ternary alloy comprising Fe, Cu and Si in conjunction with graphite through the HEMM technique [87]. The composite electrode exhibited an initial discharge and charge capacity of 809 mAh g^{-1} and 464 mAh g^{-1} respectively. A sustainable reversible capacity of more than 385 mAh g^{-1} was achieved at the 30th cycle and the coulombic efficiency of higher than 95% was maintained after the 4th cycle. $SiMo_x$ alloy was applied as anode coupled with the surface modified Cu foil current collector[88]. The rough Cu foil and the alloy component of Mo helped Si to overcome volume expansion. The $SiMo_{0.79}$ electrode gave an initial capacity of 1319 mAh g^{-1} and the capacity decreased to 1180 mAh g^{-1} after 100 cycles with capacity retention of 89.4 % at the current density of 714 μA g^{-1}.

In general, no significant performance breakthrough of the Si-based alloys was

made between 2006 and 2010. However, a new interesting concept on structure design of the Si-based alloys was reported. A core-shell structure composed of inactive ($NiSi_2$)/carbon@active (Si) was prepared by heating a mixture of Si powder and nickel phthalocyanine[89]. The nickel phthalocyanine was sublimed onto the Si surface, which was further decomposed to generate metallic nickel that diffused into the Si matrix to produce a core-shell Si/$NiSi_2$ composite. The nickel phthalocyanine also acted as a source for carbon, where a shell composed of $NiSi_2$ and carbon was coated on the surface of the Si particles. The cyclic performance of the composite was improved due to retarded formation of a crystalline lithiated phase ($Li_{15}Si_4$) phase by the inactive ($NiSi_2$) shell layer, which reduced the mechanical stress of lithiation. Nevertheless, the rate capability was poor because the charge carriers were partially blocked by the inactive phase.

5.2 Si Films/Composite Films

Through previous research work it was well recognized that Si thin film electrodes had the potential to exhibit good performance. In general, dense and thick Si film anodes are essential for practical applications, but dense and thick Si film anodes also generated much stress upon lithiation, leading to an inferior performance. It was also found that the mechanical pulverization process even occurred with thin Si film electrodes, which caused serious capacity fading along with cycling. Therefore, the poor electrochemical performance and structural stability of Si film anodes continued to be a critical problem. Mass loading density and strong adherence to the substrate of the thin film have been regarded as critical factors to determine the

electrochemical performance[90]. Different methods were developed to prepare Si film anodes with distinctly different mass loading density and interface adhesion during this time range[49, 67, 91].

For example, Park fabricated amorphous Si films with a thickness of 200 nm by RF magnetron sputtering[92]. The films exhibited excellent cycle ability with a specific capacity of around 3000 mAh g^{-1}. The good cyclic performance was attributed to the optimization between the strong adhesion force due to the Si/Cu interdiffusion and the film stress. Wang prepared Si-Al thin film on Cu foil by co-deposition from a Si target which was embedded in Al rods[93]. The film delivered a high reversible capacity of 2258 mAh g^{-1} and an initial columbic efficiency of 86 % at 0.05 C. The capacity retention of the Si-Al thin film was 80 % after 350 cycles, which was much better than that of Si thin films (67 %). The group also prepared 275 nm Si thin films on rough Cu foils by magnetron sputtering which exhibited a high capacity of 3134 mAh g^{-1} at 0.025 C rate[94]. The capacity retention was 61 % at 0.5 C for 500 cycles. The cycling performance was further improved by annealing the film at 300 °C, through which the interface adhesion between the Si thin film and copper foil was further enhanced.

Regarding thick Si films in the micrometer range, Takamura used a special recipe to enhance the adhesion between the Si film and the copper substrate. The Cu foil surface was modified by controlled electrolysis in $CuSO_4$ solution[68], through which agglomerated pyramid-like tiny hills of Cu were deposited on the Cu foil. This special structure feature enabled that the 3.6 μm thick Si film exhibited steady

capacities of about 2000 mAh g^{-1} over 50 cycles.

Because the commonly used heavy metal current collector for traditional Si film anode was heavier than the Si active material itself, it unavoidably increased the total mass of the Li-ion batteries. To resolve this problem, Cui designed a novel anode structure free of a heavy metal current collector by integrating a flexible, conductive carbon nanotube (CNT) network into a Si anode[95]. The CNT network functions as both mechanical support and electrical conductor. The CNT-Si films up to 4 μm in thickness showed a high specific charge storage capacity (2000 mAh g^{-1}) and a good cycling life. The performance was superior to pure sputtered-on Si films of similar thicknesses. The integrated structure effectively increased the specific capacity by 10 times on the anode side and the energy density was increased by 20 % with the full battery.

With the pioneering work on the synthesis of Si nanowires[96], researchers started to prepare Si films composed of Si nanowires. Zhu synthesized Si nanowire array film anodes by metal catalytic etching of Si wafers[97]. The films showed an initial discharge capacity of 3653 mAh g^{-1} and a stable reversible capacity of about 1000 mAh g^{-1} after 30 cycles at a rate of 150 mA g^{-1}. Si nanowire composite film anodes were reported by Wen, where eutectic Si-Au nanowires were synthesized and employed as anode through a special secondary deposition process based on vapor-liquid-solid (VLS) mechanism[98]. The initial coulombic efficiency of the composite Si film anode was up to 88 %, which was better than the anodes composed of isolated nanowires.

5.3 Zero-Dimension Si and their Composites

Previous studies have proved that the compositing Si particles with buffer matrix such as carbonaceous materials could effectively improve the cyclability of the Si-based anode compared to bare Si anode. From 2006 to 2010, the research on the Si composite anodes was featured by two characteristics: 1) The family of carbonaceous materials employed was expanded. 2) Hierarchical structures were designed beyond the simple compositing concept.

5.3.1 0D Silicon/Three-Dimensional (3D) Carbon Composites

Three-dimensional carbon matrixes originated from different sources were applied as buffer medium to stabilize the Si electrodes. Si particles were either homogeneously embedded in the carbon matrix or coated with carbon in a core-shell structure style. Kumta prepared Si/C composites through thermal treatment of mechanically milled powder, which contained Si, graphite (C), and poly(acrylonitrile) (PAN) powder with a nominal composition of C-17.5 wt.% Si-30 wt.% PAN[99]. PAN acted as a diffusion barrier for the interfacial diffusion between graphite and Si, which led to form the electrochemically inactive SiC during prolonged milling of graphite and Si. The resultant Si/C/PAN-C based composites exhibited a reversible capacity of 660 mAh g^{-1} with almost no capacity fading up to 30 cycles at a constant current of 160 mA g^{-1}. Liu pyrolyzed the blend of Si (60 nm) and poly (vinylidene fluoride) (PVDF) to prepare Si/C composites[100]. The porous composite exhibited a specific capacity of approximately 660 mAh g^{-1} with 75 % capacity retention after 50 cycles. Besides the embedding structure of the Si/C composites, various core-shell

structures of Si/C were also prepared. Liu fabricated spheroidal carbon-coated Si nanocomposite by low temperature spray pyrolysis of a mixture of Si particles (< 100 nm) and citric acid[13]. The anode showed a reversible capacity of 1450 mAh g^{-1}after 20 cycles at 100 mA g^{-1}. The carbon coating enhanced structural stability and prevented local capacity fading by maintaining electrical contact between the Si particles. Yin prepared a core/shell Si@carbon anode using poly (vinylidene fluoride) (PVDF) as carbon source[101]. The reversible capacity of the nanocomposite was 1290 mAh g^{-1} with capacity retention of 97 % at 50 mA g^{-1}. Furthermore, in order to enhance contact between the carbon layer and the Si particles, Kung established covalent bonding between Si particles and resorcinol-formaldehyde (RF) gel by hydrosilylation, followed by calcination[102]. The Si/C composite showed higher gravimetric capacity and coulombic efficiency than the corresponding samples prepared from a physical mixture of bare Si and RF polymer precursors.

5.3.2 0D Si/CNTs Composites

Besides the continuous 3D carbonaceous materials, low dimensional carbon species such as carbon nanotube (1D) and graphene (2D) have been applied to accommodate the volume expansion and corresponding mechanical stress of the Si. Compared to common carbon materials, carbon nanotubes (CNTs) have smaller diameter and high aspect ratio, which enables a higher degree of resiliency and a better electric conductivity. Thus, CNTs were exploited to build a conductive and ductile matrix to alleviate the adverse effect induced by the volume change of the Si [103, 104]. Li used CVD to grow CNTs directly on the surface of fine Si

nanoparticles[104]. Coiled CNTs with different lengths formed cage like structure to encapsulate the Si particles. This composite showed a reversible specific capacity of 940 mAh g^{-1} with an initial coulombic efficiency of 80 %. The performance improvement was ascribed to the good electronic contact maintaining among Si particles and forming a stable thick SEI film. Almost simultaneously, Oha reported their work using similar CVD method to prepare core/shell type Si/CNTs composite [103]. The performance of the Si/CNTs composite electrode was superior to that observed with bare Si and Si/CNTs mixed electrodes. It was supposed that the void space and the flexible characteristics of the CNTs buffer layer accommodated volume expansion of the Si core without severe electrode swelling. Similarly, Yang synthesized a novel Si/multi-walled carbon nanotube(MWNTs) nanocomposite by direct scattered growth of MWNTs on the surface of Si nanoparticles with CVD[105]. This composite presented a high reversible capacity of 1592 mAh g^{-1} and good cycling stability even at large current density of 500 mA g^{-1}. Another interesting concept was realized by Kumta, where two-step CVD method was applied to build vertically aligned multiwall CNTs (VACNTs), followed by deposition of nanoscale Si droplets on the VACNTs with clearly defined spacing[98] (**Figure 3**). This novel structure exhibited stable reversible capacity of 2050 mAh g^{-1} with little capacity fading of 0.15 % per cycle over 25 cycles. In general, the good performance of the Si/CNTs composites prepared by CVD originated from two reasons. Firstly, a good maintenance of the electronic conducting network was achieved due to the robust adherence of CNTs onto the Si particles. Secondly, the excellent flexibility of CNTs

helped to accommodate the severe volume change and absorbed the corresponding mechanical stress of Si upon lithium insertion and extraction.

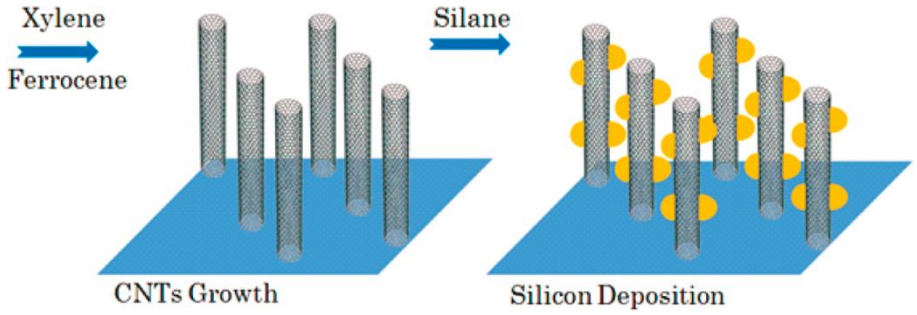

Figure 3. Schematic diagram for the fabrication of Si/carbon nanotube hybrid nanostructures. Reprinted with permission from Ref 98. Copyright 2010 American Chemical Society.

Besides the *in situ* growth of CNTs, direct mixing of Si and CNTs was also tried. The Si/CNTs composite prepared by ball milling showed a discharge capacity of 2274 mAh g^{-1} in the first cycle and retained a reversible capacity of 584 mAh g^{-1} after 20 cycles at a constant current of 35 mA g^{-1}, which was much higher than the Si/graphite composite[106]. It was also found that the Si/disordered carbon/CNTs composite anode prepared by pyrolyzing the mixture of Si, CNTs and PVC as carbon source showed a reversible capacity of 821 mAh g^{-1} after 20 cycles at a current density of 30 mA g^{-1} [107, 108].

5.3.3 0D Si/Graphene Composites

Graphene has a high surface area, good conductivity, and good mechanical properties[109]. It was firstly used to improve the performance of Si-based anodes in 2010[110]. Si/graphene composites were prepared by simple mixing in mortar in a manual way, which maintained a capacity of 1168 mAh g^{-1} and an average coulombic

efficiency of 93 % up to 30 cycles at a current density of 100 mA g^{-1} [110]. Si/graphene paper composites were also prepared by filtrating suspension of Si and graphene, followed by thermal reduction treatment. It showed a storage capacity of 2200 mA h g^{-1} after 50 cycles at a constant current of 100 mA g^{-1} and 1500 mA h g^{-1} after 200 cycles with a capacity retention of 99.5 % per cycle[111]. Similarly, self-supporting Si/reduced graphene oxide nanocomposite films were prepared, which showed a reversible specific capacity of 1040 mAh g^{-1} and a capacity retention of 94 % after 30 cycles at 50 mA g^{-1}[112].

5.3.4 Other 0D Si composites

Zhang fabricated nickel nanocone arrays (Ni NCAs) as a substrate for the deposition of Si[113] (**Figure 4**). The Ni NCAs facilitated charge collection and transportation, supporting the electrode structure, and acting as inactive buffer medium. The composite electrodes showed an impressive electrochemical performance with a capacity of around 2400 mAh g^{-1} over 100 cycles at a constant rate of 0.2 C and capacity retention of 99.8 % per cycle.

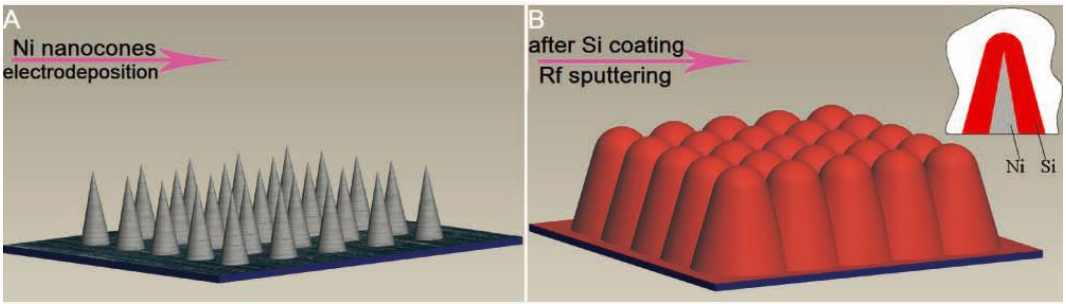

Figure 4. Schematic diagram illustrating the fabrication of a nickel nanocone-array supported Si anode architecture: A) Nickel nanocone-arrays before Si coating, B) after Si coating. Reprinted with permission from Ref 113. Copyright 2010

WILEY-VCH Verlag GmbH & Co. KGaA, Weinheim.

5.4 One-Dimension Si and their Composites

5.4.1 Si Nanowires and their composites

Although the synthesis of Si nanowires (SiNWs) by coupling laser ablation and VLS growth mechanism was pioneered as early as 1998, the use of the Si NWs as lithium-ion battery anode was rather rare until 2008[96]. The first paper dealing with the electrochemical lithiation of Si NWs was published in 1999[114]. One year later, the same group published a second paper within the context of LIB anodes, where they proved the amorphization process of crystalline Si NWs upon Li insertion[115]. Until 2001, the lithiation of Si NWs was well documented[116]. However, these three papers were quite unnoticed by the LIB researchers until 2008 when a few more papers appeared almost at the same time. In 2008, Cui reported their work using Si NWs with an average diameter of 89 nm as LIB anodes, which were grown directly onto stainless steel current collector by the VLS method[18] (**Figure 5**). The Si NWs anode achieved an exceptionally high charging capacity of 4277 mAh g^{-1} during the first charging cycle and maintained a discharge capacity close to 75 % of the maximum value during subsequent 10 cycles. Despite the large volume change, the Si NWs remained intact and did not break into small particles. The Si NWs released the mechanical stress induced by volume expansion by providing anisotropic route for volume expansion. Besides, the 1D Si NW structure features also facilitated charge transportation.

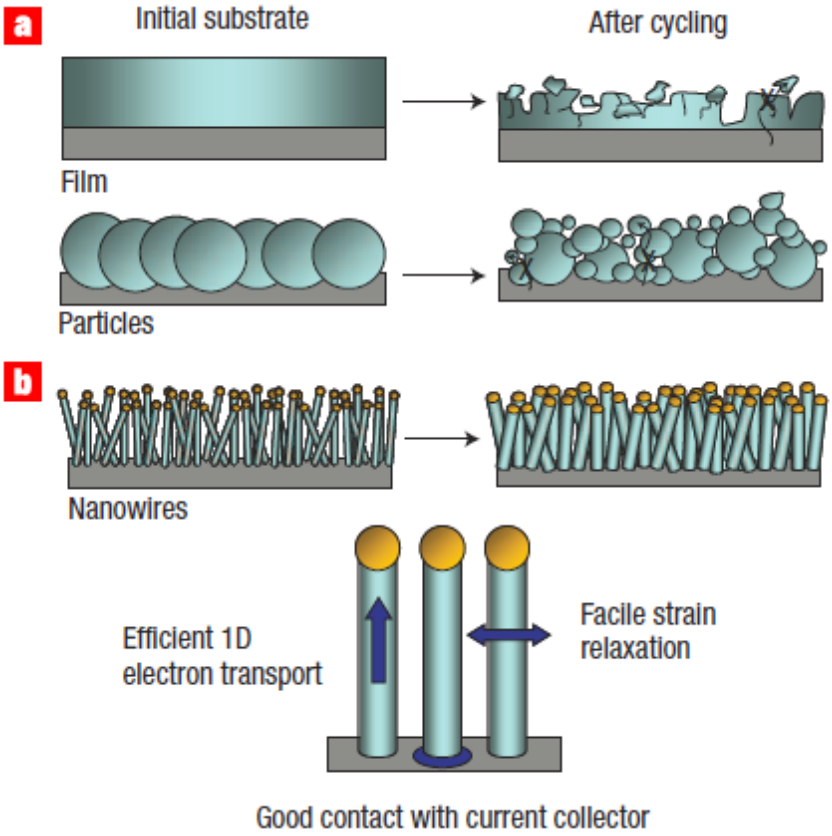

Figure 5. Scheme of morphological change occurring with different types of Si electrodes during electrochemical cycling. Reprinted with permission from Ref 18. Copyright 2008 Nature Publishing Group.

Concurrently, Lee fabricated wafer scale arrays of Si NWs via the aligned metal catalyzed electroless etching (MCEE) of Si wafer[117] (**Figure 6**). The MCEE Si NWs inherited the electrical characteristics of the original Si, which did not need additional doping to enhance electron conductivity. The MCEE Si NWs showed a discharge capacity of 0.5 mAh cm^{-2} and a longer cycling stability than bulk Si.

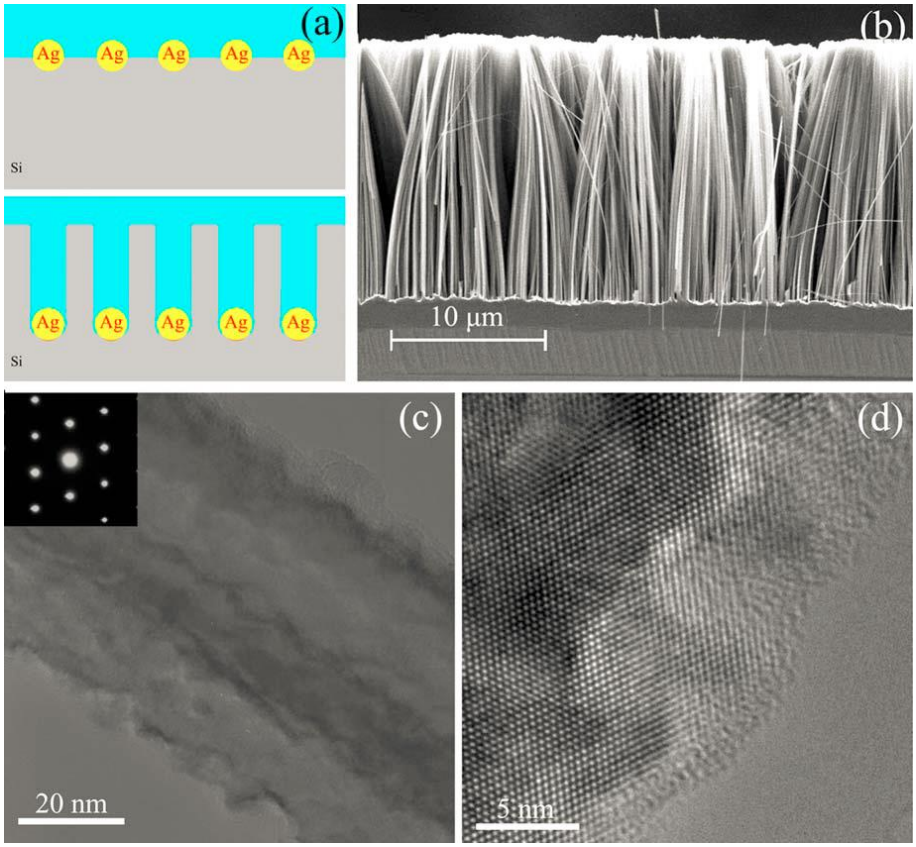

Figure 6. Scheme (a), SEM (b), TEM (c), and HRTEM (d) of the Si NWs fabricated by silver catalyzed electrochemical etching of Si wafer. Reprinted with permission from Ref 117. Copyright 2008 American Institute of Physics.

Choi prepared Si NWs by the conventional CVD method and got a reversible capacity of 2500 mAh g^{-1} for the first cycle [118]. Laik also studied the electrochemical characteristics of Si NWs as anodic material for LIBs[119]. All of the above work demonstrated the great potential and capability of using Si nanowires as LIB anode, which greatly promoted the research on the lithium-ion micro batteries.

Because the capacity of the bare Si NWs anodes degraded rapidly, Cui's group further developed hierarchical core-shell type Si NWs to improve the cyclic stability[120]. The amorphous Si shells and the crystalline Si cores possessed

different lithiation potential. Therefore, the crystalline Si core functioned as a stable mechanical support and an efficient electrical conducting pathway during the lithiation process of the amorphous Si shell. The core-shell NWs demonstrated a high capacity of around 800 mAh g^{-1} and showed little fading after 100 cycles at current density of 6800 mA g^{-1}. The same group also synthesized C-Si core-shell NWs by coating amorphous Si onto carbon nanofibers (CNFs) with CVD. These nanowires exhibited a capacity of around 2000 mAh g^{-1} with a high initial coulombic efficiency of 90 %[121].

Following the research work on the Si NWs based anodes, numerous studies have been carried out focusing on the electrochemical mechanism[118], structural transformation[122], formation of solid electrolyte interphase[14], impedance analysis[123], and maximum Li storage capability[124]. To comply with the practical electrode fabrication protocol, Cui used conventional slurry method to prepare the Si NWs electrodes. The Si NWs were synthesized with the supercritical fluid-liquid-solid (SFLS) growth technique, followed by carbon coating and using MCNTs as conductive agent for the slurry[125]. Reasonable capacity stability was achieved, where a reversible capacity of around 1500 mAh g^{-1} was observed for 30 cycles at the current of 210 mA g^{-1}. Further structure control of the Si NWs was tried to optimize the overall performance. Cho used SBA-15 as template to synthesize mesoporous Si@carbon core-shell nanowires with a diameter of 6.5 nm and well-ordered mesopores of 2.3 nm[126]. The well controlled inter-wire spacing generated uniform ordered mesopores to accommodate the volume expansion of the

Si. The as-synthesized nanowires demonstrated excellent first charge capacity of 3163 mAh g^{-1} with an initial coulombic efficiency of 86 % at a current density of 600 mA g^{-1}. After 80 cycles, the capacity retention was 87 %.

5.4.2 Si Nanotubes

Despite the great success of the Si NWs based anodes, Si NWs exhibited enhanced polarization at high rates and capacity faded over cycles. This could possibly be due to the limited surface area accessible to the electrolyte and the continuous growth of the SEI at the interface between the Si NWs and electrolyte. In order to increase the surface area, Si nanotubes (Si NTs) were synthesized by Cui through reductive decomposition of a Si precursor in the alumina template, followed by etching away the alumina template[127] (**Figure 7**). The first discharge and charge capacities of the Si NTs were 3648 and 3247 mAh g^{-1} at the current density of 600 mA g^{-1} (0.2 C). A Li-ion full cell consisting of $LiCoO_2$ cathode and Si NTs anode showed the initial capacity of above 3000 mAh g^{-1} at the rates of both 3 C and 5 C, and capacity retention of 89 % after 200 cycles at the rate of 1 C.

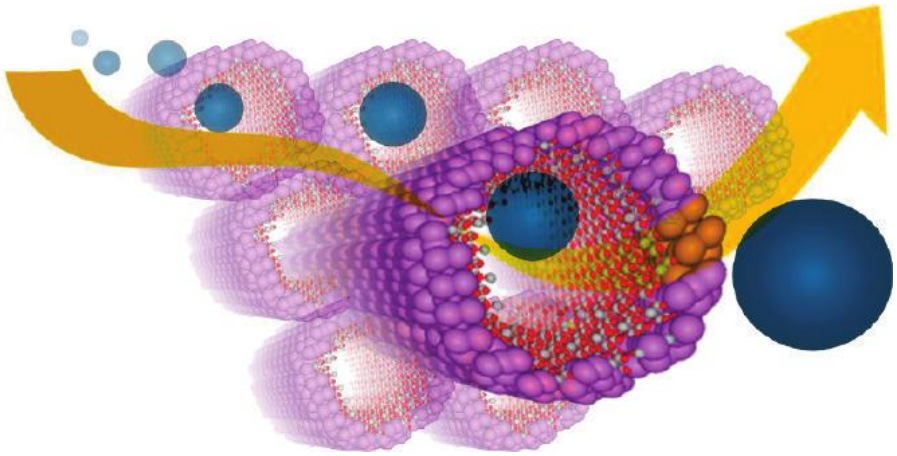

Figure 7. Schematic diagram of the Li-ion pathway in Si nanotubes. Reprinted with permission from Ref 127. Copyright 2009 American Chemical Society.

After Cui's work, Kim developed arrays of sealed Si NTs with a sacrificial template strategy[128]. The structures had an outer diameter of around 60 nm and inner diameter of around 30 nm, with a height of between 3 μm and 5 μm. At a rate of 0.2 C (1 C = 4200 mAg^{-1}), the Si NT array electrodes exhibited a discharge capacity of 2924 mAh g^{-1} and an initial columbic efficiency of 90 %. Their capacity retention was 82 % after 50 cycles. The performance was significantly better than that of the corresponding Si NWs systems. The inner space of the Si NTs provided additional room to accommodate the volume expansion of the Si. Besides, it also added specific surface area to improve the accessibility of the electrolyte. The experimental results showed that there was only around 35 % dimension change along the axial direction with respect to the nearly 400 % total volumetric expansion.

5.5 Three-Dimension Si and their Composites

The research on the Si NWs based anodes showed that the incorporation of pores provided additional space to effectively accommodate the drastic volume expansion and therefore reduced the generated mechanical stress. With this concept, the electrochemical performance of the Si NWs was significantly improved. However, the Si NWs had an intrinsic drawback of very low mass loading density, which limited the practical applications of the Si NWs based anodes. Therefore, constructing three-dimensional Si network incorporated with pores became an attractive strategy to resolve the problem of the Si NWs. Cho prepared three dimensional porous bulk Si particles by the thermal annealing and etching of physical composites obtained from butyl-capped Si gels and SiO_2[129] (**Figure 8**). The 3D porous Si showed

interconnected pores with a size of 200 nm and a wall thickness of approximately 40 nm. This unique structure effectively accommodated stress without pulverization after 100 cycles, and maintained charge capacity of more than 2800 mAh g^{-1} at 400 mA g^{-1}.

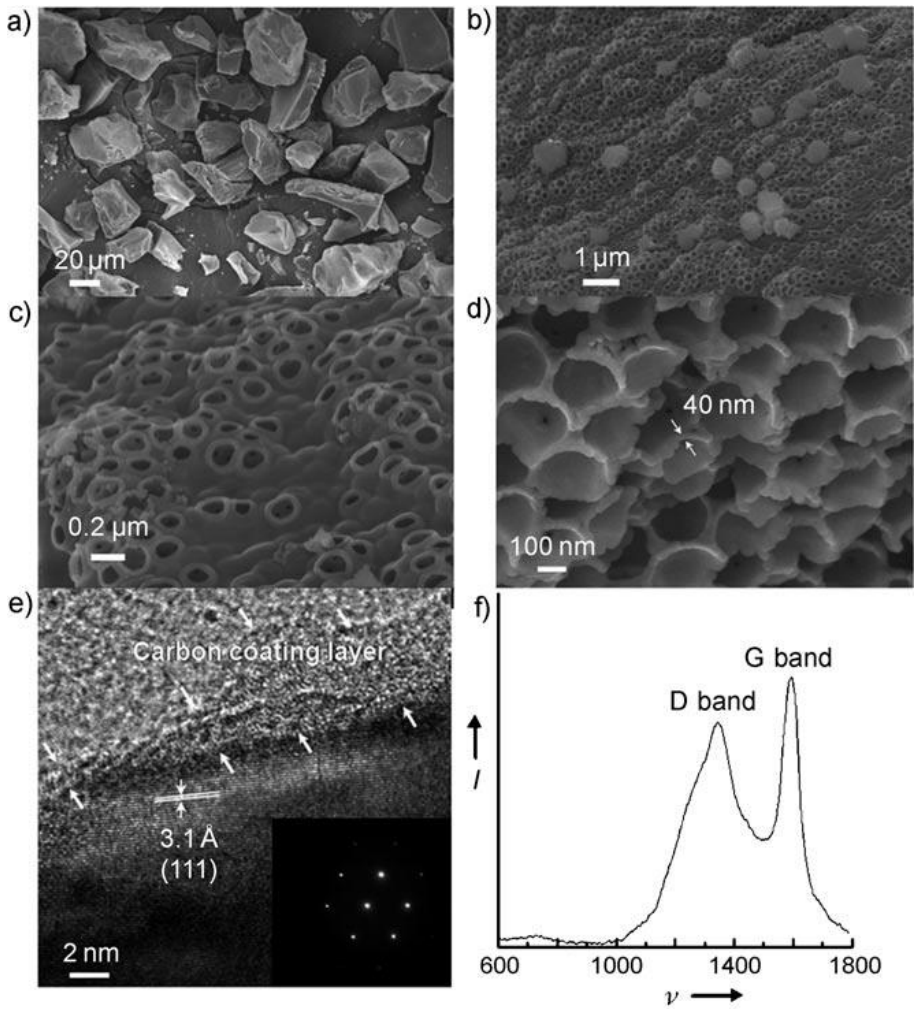

Figure 8. SEM (a, b, c, and d) and TEM (e) images, and Raman spectrum (f) of the 3D porous c-Si particles after etching. Reprinted with permission from Ref 129. Copyright 2008 Wiley-VCH Verlag GmbH & Co. KGaA, Weinheim.

In order to further improve the electrical conductivity of the porous Si anode, Yu synthesized a silver coated 3D macroporous Si with uniform macropores of about 200 nm in diameter through silver mirror reaction[21]. The macroporous Si coated with silver exhibited a discharge capacity of 3585 mAh g^{-1} with an initial coulombic

efficiency of 81 % and improved capacity retention of 82 % after 100 cycles at 100 mA g^{-1}. It was also shown that an enhanced rate capability of 2122 mAh g^{-1} at 500 mA g^{-1} was achieved. Chen prepared nest-like Si particles composed of hollow Si spheres through solvothermal reaction[17]. The nest-like Si spheres displayed an initial specific capacity of 3052 mAh g^{-1} at the current density of 2000 mA g^{-1}, and retained 1095 mAh g^{-1} after cycling up to 48 cycles.

5.6 Summary of the Progress from 2006 to 2010

From 2006 to 2010, the research on the Si-based anode has been expanded from the previous bulk alloys, 0D particles and 2D thin films to new 1D nanowires, 1D nanotubes and 3D porous structures (**Table 3**). With the newly developed 1D Si nanowires and nanotubes, and 3D Si porous structures, big performance improvements have been achieved. Si nanowires exhibited very high initial capacity with moderate capacity retention. Therefore, incorporation of pores into low-dimensional Si (nanowire, nanotubes) has been developed to further improve the performance. Furthermore, due to the low mass loading density of the Si NWs based anode, three-dimensional porous Si has been designed and synthesized to tackle this issue while still keeping good cyclic stability.

6. Explosive Progress of the Si-Based Anodes Research from 2011 to 2015

6.1 Si Alloys/Alloy Composites

The structure design and preparation methods of Si alloys and alloy composites were further diversified in recent years. Core-shell structures and porous structures

were introduced into the alloy composites to improve their performance.

Mg_2Si anode materials synthesized by hydrogen-driven chemical reaction delivered an initial capacity of about 1095 mAh g^{-1} at 100 mA g^{-1} with an initial coulombic efficiency of 92 %[130]. The discharge capacity stayed at 406 mAh g^{-1} after 60 cycles, which was much better than that of the commercial Mg_2Si anode and previously reported Mg_2Si anodes synthesized by mechanical alloying[59]. The authors found that the dissociation and irreversible lithiation of Mg was the critical factor for capacity fading of the Mg_2Si anodes. As previous study indicated, the cyclic stability of the Si-based alloys could be improved by compositing with carbon [83, 85, 86]. Yang synthesized Mg_2Si/C composites with an uniform carbon coating layer by *in situ* decomposition of C_2H_2 gas onto the surface of the pre-synthesized Mg_2Si[131]. The composites with a carbon content of 1.19 % delivered a first discharge capacity of 1405 mAh g^{-1} at 100 mA g^{-1}. It maintained a capacity of 320 mAh g^{-1} after 100 cycles with a stable coulombic efficiency over 95 % after the first cycle, which was better than the bare Mg_2Si anode. Ai prepared a $FeSi_2$/Si@C composite by a two-step ball milling of Fe, Si powders and graphite. The composite showed not only a stable reversible capacity of 1010 mAh g^{-1} with 94 % capacity retention after 200 cycles, but also a good rate capability with more than700 mAh g^{-1} at 1000 mA g^{-1} [132].

During this time frame, compositing silicon alloys with other matrix to build hierarchical structures was also developed to improve the performance. Kim synthesized multicomponent nanocomposites of $FeSi_2$@Si@graphene via the

magnesiothermic reduction of core-shell Fe_3O_4@SiO_2 nanoparticles with graphene oxide shell[133]. Inactive $FeSi_2$ domains in relieving the severe change of volume while the coating of graphene layer inhibited pulverization and enhanced electrical conductivity of the active Si core. The specific discharge capacity of the nanocomposites was estimated to be 2806 mAh g^{-1} for the initial cycle and 510 mAh g^{-1} for the 100^{th} cycle at 100 mAg^{-1}. Winter created porous structures within the $NiSi_2$/Si/carbon composite by using LiCl as porogen material[134]. The well-dispersed mesopores with an average size of about 22 nm and the inactive $NiSi_2$ phase effectively accommodated the volume expansion of Si. As a result, a stable specific capacity of 1272 mAh g^{-1} was realized for 200 cycles at 1 C (1C = 2034 mA g^{-1}) and a good rate capability with 740 mAh g^{-1} at 5 C was achieved as well.

Recently, lithium-free cathode materials have attracted great interests due to their very high capacities [135, 136]. The lithium-free cathodes need to be used in combination with the lithium-rich anodes as a full cell. Nishihara developed a Li-rich Li-Si alloy anode which showed a high initial lithium-extraction capacity of 1000 mAh g^{-1} [137]. Upon delithiation, the Li-Si particles turned into porous structure, whereas the original particle size remained unchanged. Since the Li-Si alloy was free from severe contraction/expansion upon delithiation/lithiation, it showed much better cyclability than the bare Si.

Besides the binary alloys, tertiary alloys were also investigated in this time range. Some researchers tried to utilize super-elastic nickel titanium (NiTi) alloys (nitinol) as inactive matrix to accommodate the stress generated by the Si volume change[138].

Jung reported that ultra-fine sized Si embedded in the NiTi matrix phase showed reversible capacity of 907 mAh g^{-1} and capacity retention of 77 % for 50 cycles at 100 mA g^{-1} [139]. Son successfully embedded Si nanoparticles into a matrix of $Ti_4Ni_4Si_7$ with a melt spinning method. The electrode delivered an initial discharge capacity of 1325 mAh g^{-1} with an initial coulombic efficiency of 87 %, and capacity retention of 78 % after 50 cycles[140]. A two-stage HEMM method was also applied to embed nanocrystalline Si into the NiTi matrix. The composite showed a capacity of 553 mAh g^{-1} after the 52^{nd} cycle at 2.5 mA cm^{-2} [141]. However, several challenges existed for the practical use of the Si/NiTi composite anodes. Various native oxides, such as SiO_x, TiO_x and NiO_x, were likely formed on the surface of Si/NiTi particles, which further induced large irreversible capacity and poor rate capability[139, 140]. Besides Si/NiTi, $FeSi_2Ti$ has also been explored as LIB anode. Kang fabricated a core-shell structure of nano-Si/$FeSi_2Ti$ with a traditional scalable melt-spinning technique[142]. The nano-Si/FeSi2Ti hetero-structure showed a discharge capacity of 780 mAh g^{-1} at 0.1 C. It maintained about 70 % of its initial capacity at 0.2 C after cycling at 5 C.

6.2 Si Films/Composite Films

Several types of Si-based film anodes have been investigated including pure Si films, binary Si films and ternary Si films. For each type of Si film anode, both compositing and constructing hierarchical structures have been identified as effective strategies to alleviate the problem of the volume expansion of Si.

During the time frame 2011 to 2015, binary films with unusual structures were synthesized. Mg-Si thin films with various elemental compositions in $Mg_xSi_{(1-x)}$ were

obtained via combinatorial magnetron sputter deposition of Si and Mg. The Si was embedded in an active Mg-Si matrix[143]. With the Mg content below the Mg_2Si stoichiometry ratio, capacity of 1000 mAh g^{-1} was exhibited with capacity retention of 96 % after 400 cycles.

Current collectors with special structure design were used to convert the feature of the Si film into three-dimensional architecture. Sun deposited Si film on Ni foam by electrodeposition[144]. The Si film supported by the 3D conductive frame work accommodated the volume change of the Si effectively. It displayed a high reversible specific capacity over 2800 $mAhg^{-1}$ for 80 cycles at 360 mA g^{-1} and a good rate capability of 870 $mAhg^{-1}$ at the current density of 18 A g^{-1}. Liu studied the impact of different types of copper current collectors on the electrochemical performance of porous Si-Al films[145]. The Si-Al film deposited on the copper foam showed higher capacity, capacity retention, and longer cycle life in comparison to the Si-Al films deposited on expanded copper mesh and flat copper mesh grid. The performance improvement was attributed to the unique 3D macroporous structure. The 3D macroporous copper substrate facilitated Si/electrolyte contact, improved anode/current collector adhesion, lowered down electrical resistance, and alleviated stress. All of these effects contributed to the accommodation of the volume expansion of the Si. CNT was also used as current collector for the Si film anode as mentioned previously[95]. Similarly，micron carbon-fibers (MCFs) was applied as the current collector to ease the mechanical stress to improve the cyclic stability[146]. With sputtering, Si was deposited onto the surface of the MCFs. The three-dimensional

structures the Si/MCFs electrodes exhibited capacity of 1087 $mAhg^{-1}$ after 200 cycles with a fading rate of 0.3 % per cycle.

Besides the work employing current collector with special structure design, fabrication of 3D Si film anodes was also reported. Patterned Si film anodes coated with alumina were fabricated by combining photolithography and reactive-ion etching technology[147] (**Figure 9**). The electrode showed significantly improved cycling performance compared to uncoated Si anode. The initial charge capacity was 1125 mAh g^{-1} and the capacity maintained at 1100 mAh g^{-1} after 100 cycles at the current density of 3750 mA g^{-1}. The alumina layer acted as a protective layer to inhibit the side reactions between the electrode and electrolyte. Simultaneously, the alumina layer also increased the fracture resistance of the patterned Si anode to improve the robustness of the Si anode.

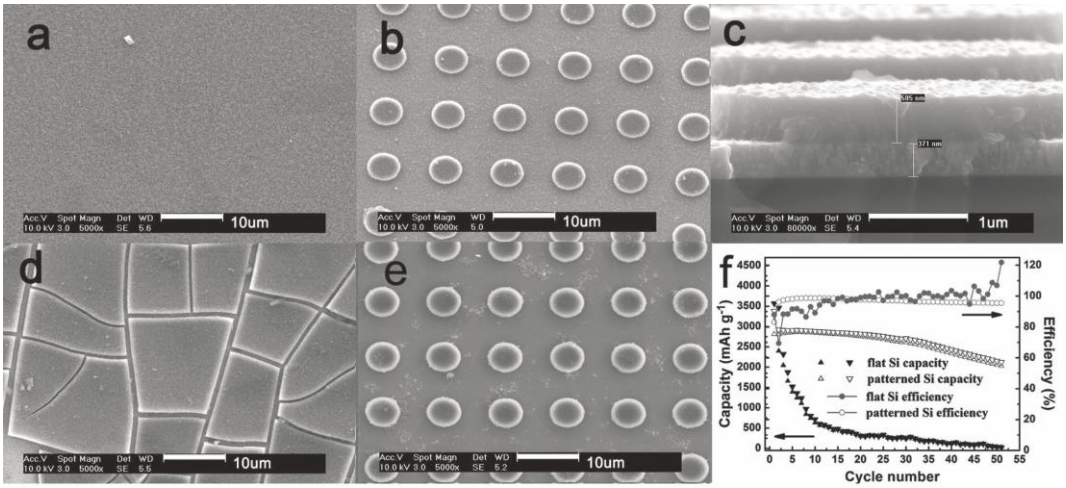

Figure 9. SEM images of the unetched (a) and patterned (b) Si thin film electrode, cross-section of the patterned Si thin film electrode (c), SEM image of the unetched (d) and patterned (e) of the Si thin film electrode after the first charge to 2 V, and the cycling performance and coulombic efficiency of the unetched and patterned Si

thin-film electrode. Reprinted with permission from Ref 147. Copyright 2011 WILEY-VCH Verlag GmbH & Co. KGaA, Weinheim.

One-dimensional non-Si nanowires or nanotubes were introduced into the 2D film structure to generate voids to accommodate volume expansion. Huang fabricated Si-Cu-Ti thin films by depositing Cu_3Si nanowires on the substrate surface by magnetron sputtering to generate voids within the Cu layer, followed by atomic layer deposition (ALD) of alumina[148]. The films showed excellent capacity retention of more than 900 mAh g^{-1} at the current density of 20 μA cm^{-2} after 100 cycles. The improvement of the electrochemical performance of the Si-Cu-Ti thin film electrodes was attributed to the presence of the Cu_3Si nanowires. The nanowires reduced polarization and inhomogeneous lithiation by forming surface conductive network. Furthermore, the voids within the Cu layer helped to alleviate the mechanical stress induced by the volume expansion of the Si. Paul et al. investigated self-organized anodic titania nanotube arrays with silicon coating[149]. Si-coated TiO_2 nanotubes delivers an additional 166 mAh g^{-1} to the 194 mAh g^{-1} of the TiO_2 nanotubes without Si.

Park fabricated a self-supported MWCNTs film embedded with Si nanoparticles (Si NPs) via CVD and spin coating process[150]. The void spaces between the MWCNTs were densely filled with a considerable amount of Si NPs with a diameter of around 50 nm. The electrodes showed 2900 mAh g^{-1} and 1510 mAh g^{-1} after 10 and 100 cycles respectively at a current density of 840 mA g^{-1}.

Porous or hollow structures were also introduced into the 2D films in order to

maintain structural integrity of the electrodes. Li prepared a binder-free composite film anode with alternatively stacked Si-porous carbon layers and graphene layers (Si-C/G) using the electrostatic spray deposition (ESD) technique followed by heat treatment[151]. The porous carbon framework produced by the pyrolysis of poly (vinyl pyrrolidone) (PVP) not only buffered the volume change of the Si NPs, but also effectively inhibited the agglomeration of the Si NPs. The flexible graphene layer facilitated the electron transfer and maintained the structural integrity of the electrode. The obtained layer-by-layer Si-C/G electrode showed a maximum reversible capacity of 1020 mAh g^{-1} with 75 % capacity retention after 100 cycles at a current density of 200 mA g^{-1}. Lee designed a core-shell type nanostructured film composed of hollow carbon nano spheres/Si/alumina (CNS/Si/Al_2O_3)[152]. The hollow CNS film acted as a 3D conductive substrate and provided void space. In this approach, the Al_2O_3 thin layer was beneficial to reduce the formation of the SEI. Moreover, the structure held robust surface-to-surface contact between Si and CNSs, which promoted fast electron transportation. As a result, the electrode exhibited a high specific capacity of 1560 mAh g^{-1} with the capacity retention of 85 % after 100 cycles at a current density of 1000 mA g^{-1}.

In addition to 2D Si film, 2D Si nanosheets (Si NSs) started to be utilized as anode materials in LIBs since 2011. 2D Si nanosheets exhibited many advantages such as easy accessibility of lithium ions, compatibility with other materials, and small volume expansion from ultrathin sheet structure.

In 2011, Yan synthesized ultrathin Si nanosheets with different sizes by using

graphene oxide nanosheets as sacrificial templates[153]. The Si nanosheet electrodes maintained a discharge capacity of 600 mAh g^{-1} with a coulombic efficiency of 96.2 % during the 100th cycle at a current density of 0.1 C, which is better than that of 50 nm Si nanoparticles. In 2013, Ng and Malyi separately employed the first-principle density functional theory to prove that Si NSs could be a potential anode material for Li-ion batteries [154, 155]. One year later, Xue fabricated ultrathin 2D Si NSs with a scalable DC arc-discharge plasma method and employed it as LIBs anode[156]. The size of the obtained Si NSs was 20 nm in 2D direction and 2.4 nm in thickness which was about 8 atomic layers. The discharge and charge capacities of the Si sheets were 2553 and 1242 mAh g^{-1} respectively, with an initial coulombic efficiency of 49 %. After 40 cycles, the charge capacity was 442 mAh g^{-1} at a current density of 100 mA g^{-1}. Meanwhile, Hong synthesized the Si NSs from natural sand by scalable magnesiothermic reduction[157]. The initial discharge and charge capacities of the Si NSs were 3563 mAh g^{-1} and 2431 mAh g^{-1}, corresponding to the initial coulombic efficiency of 70 %. After encapsulation by RGO, the cycle performance was improved with capacity above 1000 mAh g^{-1} after 50cycles at a current density of 200 mA g^{-1}. The rate capability of the RGO-encapsulated Si nanosheet electrode exhibited a capacity of 1113 mAh g^{-1} even at a high current density of 3000 mA g^{-1}.

In order to enhance the binding between the active Si films and current collector, Zhang synthesized 2D Ni-Si nanosheet on Ni foam by integrating Si film with an interconnected Ni nanosheet[158] (**Figure 10**). This unique composite anode possessed large pores between the nanosheets and exhibited high conductivity and

robust adhesion to the current collector as well. As a result, high specific capacity of 2038 mAh g^{-1} at 0.2 C (1 C = 4200 mA g^{-1}) after 100 cycles was achieved with a remarkable cycling stability of 655 mAh g^{-1} at 2 C over 1000 cycles.

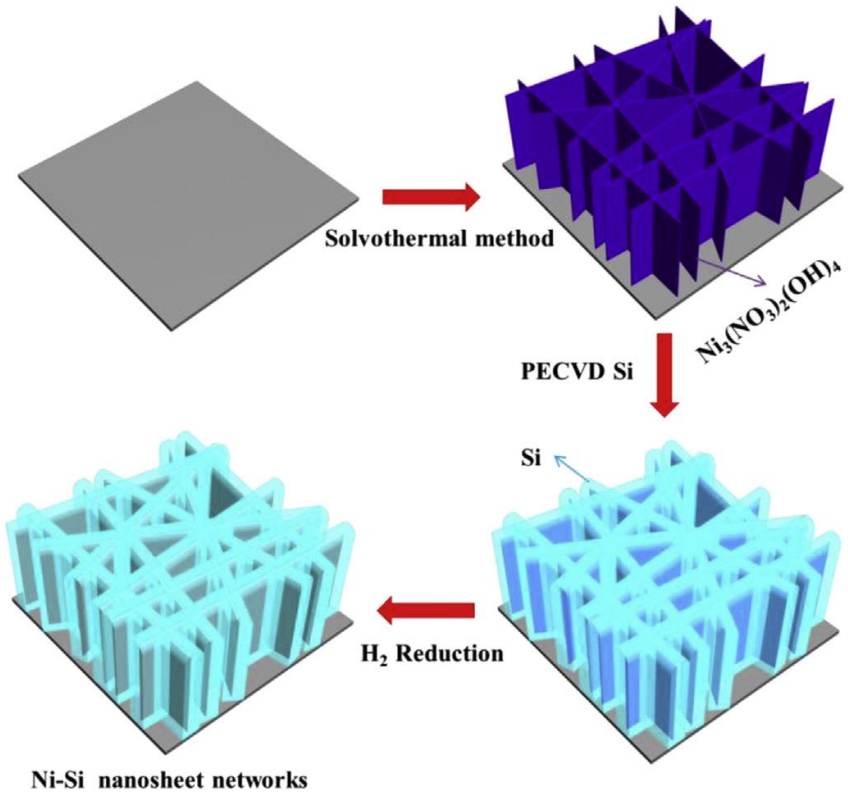

Figure 10. Scheme for the fabrication of Ni-Si nano sheet network. Reprinted with permission from Ref 158. Copyright 2015 Elsevier B.V.

Recently, Park prepared Si nanosheets utilizing inexpensive natural clays via a one-step simultaneous molten salt-induced exfoliation and chemical reduction process[159]. This approach produced 5 nm-thick high purity mesoporous Si nanosheets with high yield. Carbon-coated Si nanosheet anodes exhibited excellent electrochemical performances including a high specific capacity (865 mAh g^{-1} at 0.5 C), outstanding cycling stability (capacity retention of 92.3 % after 500 cycles at a rate of 0.5 C), excellent rate capability (a capacity of 60 % at 20 C compared to 2 C), and remarkably suppressed volume expansion (42 % after 200 cycles at a rate of 0.2

C).

6.3 Zero-Dimension (0D) Si and their Composites

It has been found that composting Si particles with different matrixes as buffer medium can effectively improve the performance by accommodating the volume expansion and releasing the mechanical stress[160]. Particularly, carbonaceous materials such as graphite, pyrolyzed carbon, carbon nanotubes and graphene, have been widely exploited as matrixes. Therefore, the research work about the Si particle/carbon composites will be mainly addressed in this section. While the work on other matrixes such as metal, metal oxide and polymer will be discussed only briefly.

6.3.1 Embedding Type 0D Si/C Composites

The embedding type Si/C composites meant that Si particles were embedded in a continuous carbon matrix. Normally, Si particles were embedded in a continuous dense carbon matrix. However, the diffusion of lithium ions within the composite might be retarded because the Si particles were well buried inside the carbon matrix. The research at this time frame found that the performance of the Si-based anode could be significantly improved by tuning the structure and morphology of the carbon matrix. Different types of carbon matrixes have been developed to embed the Si particles, which provided efficient electron transportation routes, appropriate porosity for electrolyte wetting, and space for volume expansion accommodation. Porous Si/C composites provided an alternative route to tackle the problem of the dense Si/C composites. Wang synthesized mesoporous Si/C composite via evaporation induced

self-assembly process (EISA) of a triblock copolymer in resorcinol-formaldehyde resin[161]. The Si nanoparticles (< 100 nm) were uniformly dispersed in the well-defined mesoporous carbon matrix, which offered void space and mechanical support to accommodate large volume change and release mechanical stress. The composite (76 % Si) delivered a reversible capacity of 1410 mAh g^{-1} in the first cycle and retained a capacity of 1018 mAh g^{-1} after 100 cycles at the current density of 500 mA g^{-1}, which was much higher than that of the bare nano-Si anodes (59 mAh g^{-1}). Similarly, Park reported a one-step synthesis to trap Si nanoparticles in ordered mesoporous carbon composite through an EISA process[8]. The composite showed a reversible capacity above 700 mAh g^{-1} over 50 cycles at 2000 mA g^{-1}. Zhao prepared mesoporous Si/C nanocomposites with ultrasmall, uniform Si nanoparticles (*ca*. 3 nm) embedded in a rigid mesoporous carbon framework by a magnesiothermic reduction approach[160] (**Figure 11**). The large pores of the main channels and small pores inside the carbon frameworks promoted electrolyte wetting and facilitated lithium ion diffusion at the interface between the electrolyte and Si nanoparticles. The composites showed excellent performance with a high reversible capacity of 1790 mAh g^{-1} (close to the theoretical capacity), excellent coulombic efficiency (*ca*. 99.5 % each cycle) and rate capability, outstanding cycle stability (capacity remains as high as 1480 mAh g^{-1} after 1000 cycles at a high current density of 2000 mA g^{-1}).

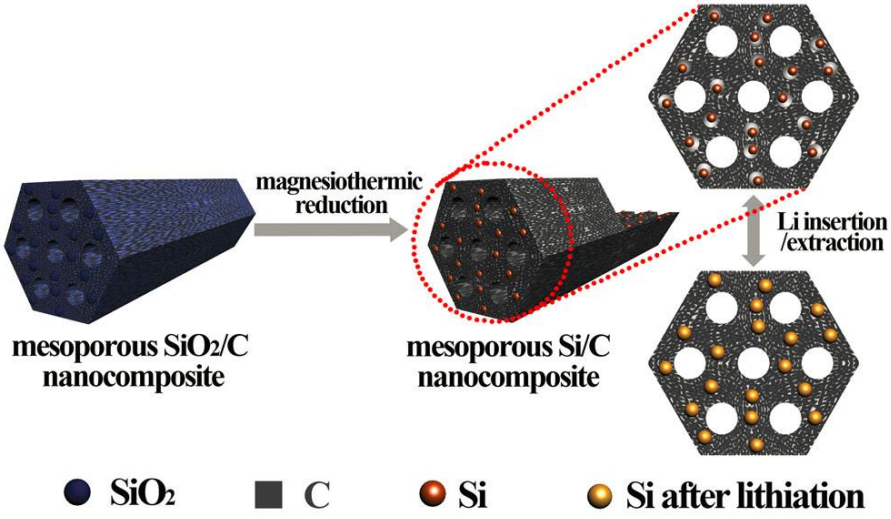

Figure 11. Scheme of the mesoporous Si/C nanocomposite prepared by the magnesiothermic reduction approach. Reprinted with permission from Ref 160. Copyright 2014 WILEY-VCH Verlag GmbH & Co. KGaA, Weinheim.

Zhang prepared a porous Si/C composite with buffering voids by co-assembling phenol-formaldehyde resin, SiO_2 and Si nanoparticles, followed by a carbonization and subsequent removal of SiO_2 [162]. The Si nanoparticles were coated with a layer of porous carbon shell with rationally designed void in between. The Si/void/porous carbon composite showed a stable reversible capacity of 980 mAh g^{-1}over 80 cycles at a current density of 100 mA g^{-1}. Besides the porous carbon matrix, dendritic carbon structures were also developed to embed Si nanoparticles through a hierarchical bottom-up self-assembly process. The specific reversible capacity of the composite with an estimated 50 wt% of Si reached 1950 mAh g^{-1} at C/20. Particularly, a good specific capacity at high discharge rates of 1 C and 8 C (2.98 A g^{-1}) were as high as 1590 and 870 mAh g^{-1} respectively[163] (**Figure 12**).

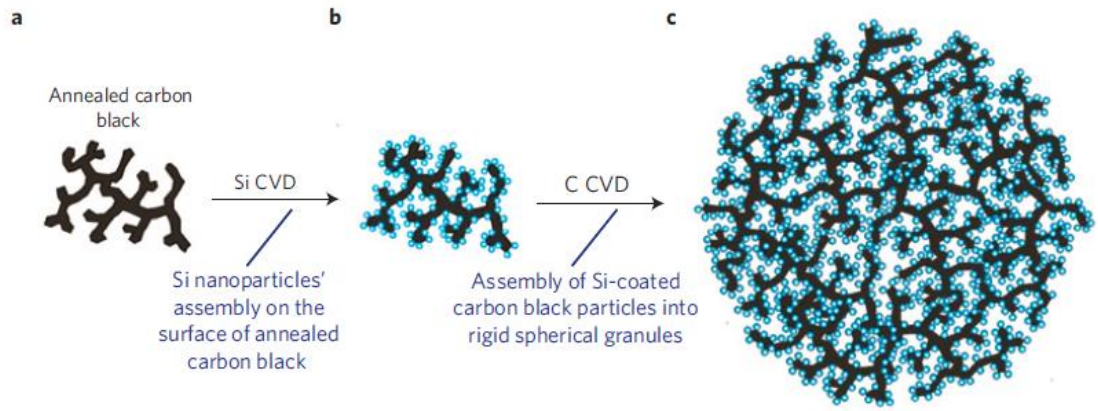

Figure 12. Scheme of the fabrication of Si/C hierarchical nanocomposite granule through hierarchical bottom-up assembly. Reprinted with permission from Ref 163. Copyright 2010 Nature Publishing Group.

6.3.2 Core-Shell Si/C Composites

Besides the embedding type of 0D Si/C composites, core-shell Si/C composites including solid core-shell and hollow core-shell structures with Si core and carbon shell were also synthesized and utilized as LIB anodes. Compared to the embedding type Si/C composites, the electrochemical kinetics of the core-shell type Si/C composites was enhanced because the Si particles were only surrounded with limited carbon layer. Meanwhile, the carbon shell still provided mechanical support to accommodate the volume expansion.

Solid core-shell Si/C anodes prepared through substrate induced coagulation process showed a reversible capacity of 1800 mAh g^{-1} at the current density of 100 mA g^{-1} over 50 cycles, with good rate capability and cycle retention.[164] Core-shell Si/C nanofibers were also prepared with a dual nozzle electrospinning method[165] (**Figure 13**). The composite nanofiber anodes exhibited a capacity of 721 mAh g^{-1} after 300 cycles with 99 % capacity retention at the current density of 2750 mA g^{-1}.

The unique 1D core-shell type structure helped to release the mechanical stress induced by volume change and enhanced the vulnerable contacts between Si and carbon shell, and stabilized the SEI layer as well.

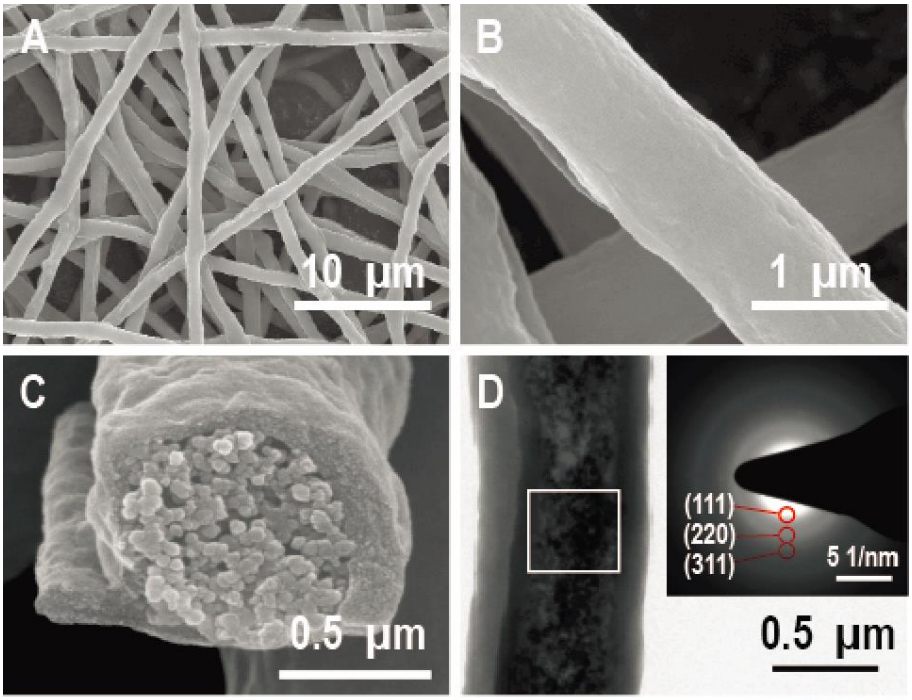

Figure 13. SEM (a, b), SEM cross section (c), and TEM (d) of the SiNP@C core-shell 1D nanofiber. Reproduced with permission from Ref 165. Copyright 2012 American Chemical Society.

Compared to solid core-shell structure, hollow core-shell structure provided additional internal void space to accommodate Si volume expansion. Cui designed and fabricated a "yolk-shell" type Si/C composite electrode[166] (**Figure 14**). The yolk-shell structure consisted of Si particles completely protected by a thin, conformal, and self-supporting carbon shell. This structure showed excellent capacity (2833 mAh g^{-1} at 400 mA g^{-1}), cycle life (1000 cycles with 74 % capacity retention), and coulombic efficiency (99.84 %).

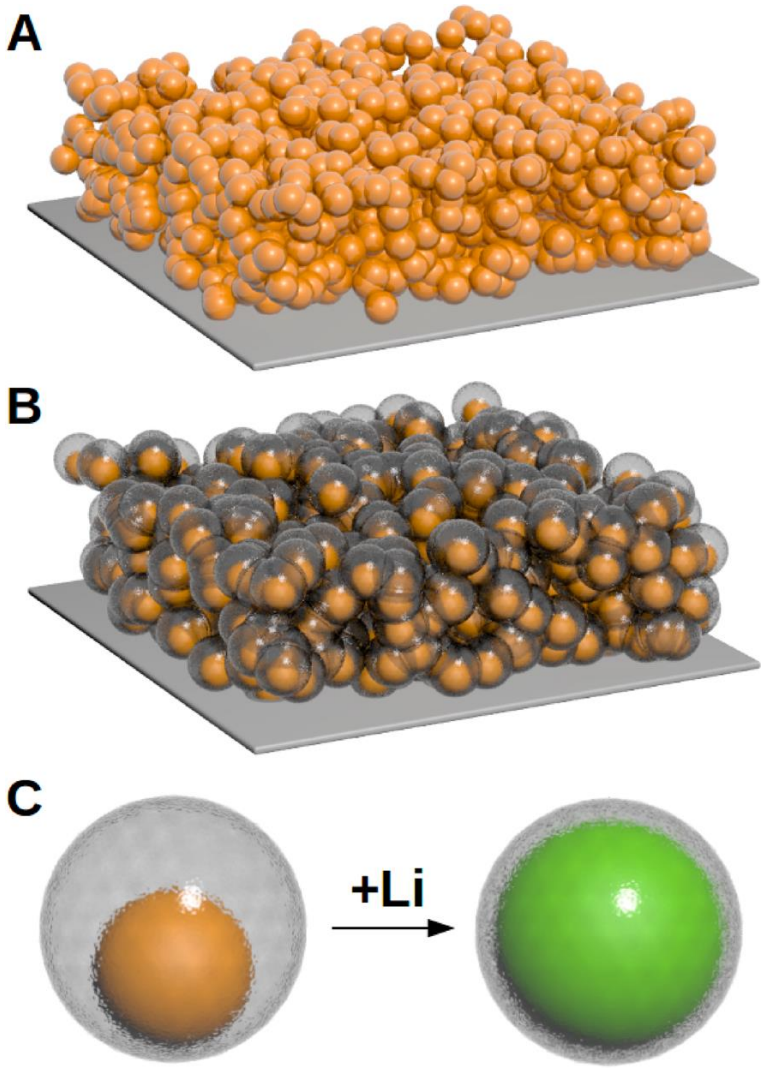

Figure 14. Scheme of the yolk-shell Si/C hierarchical structure design. (A) Conventional slurry coated Si NP electrode. (B) Si@void@C electrode with voids between each Si NP. (C) Magnified schematic of an individual Si@void@C particle. Reprinted with permission from Ref 166. Copyright 2012 American Chemical Society.

Based on this work, the Cui's group further designed a pomegranate like structure to improve the tap density and volumetric capacity[19] (**Figure 15**).

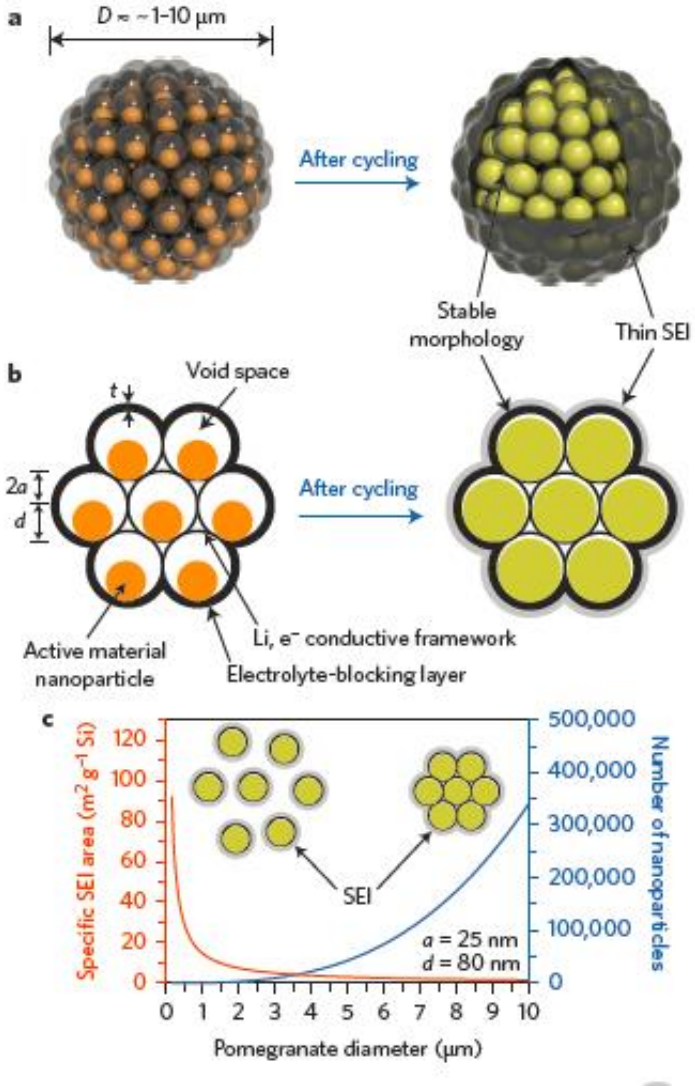

Figure 15. Scheme of the pomegranate Si/C hierarchical structure. Three dimensional (a) and cross-sectional (b) of the pomegranate Si/C structure before and after cycling, and calculated surface area in contact with electrolyte (specific SEI area) and the number of primary nanoparticles in one pomegranate particle versus its diameter (c). Reprinted with permission from Ref 19. Copyright 2014 Macmillan Publishers Limited.

The individual Si nanoparticles were encapsulated by a carbon shell that left enough room for accommodating volume expansion. These hybrid “yolk-shell” composite particles were then further assembled together and encapsulated by thick carbon layer

to form micrometer-sized pouch. This hierarchical Si/C composite showed superior cyclic stability (97 % capacity retention after 1000 cycles), high coulombic efficiency (99.87 %) and volumetric capacity (1270 mAh cm^{-3}). The voids inside the "yolk-shell" structures provided an effective way to accommodate the volume expansion. Due to the presence of the voids, the generation of the mechanical stress induced by volume expansion was quite limited. As a result, the stability of the carbon shell and SEI layer was significantly enhanced. Furthermore, the pomegranate microstructures not only lifted the tap density and volumetric capacity, but also reduced the electrode–electrolyte contact area, resulting in improved coulombic efficiency.

Li prepared hollow core-shell structures based on a low cost scalable approach. Firstly, the Si nanoparticles were coated with a SiO_2 and carbon layer in sequence, followed by etching away the middle SiO_2 layer with HF[167]. The porous Si/C composite exhibited a high capacity of 760 mAh g^{-1} after activation cycles. 86 % capacity retention was achieved after 100 cycles at a current density of 1000 mA g^{-1}. In another similar work, hollow core-shell Si/C nanocomposite with 37 wt% of Si exhibited initial discharge capacity of 1370 mAh g^{-1} with a capacity retention of 98 % after 100 cycles at 100 mA g^{-1} [168]. Recently, Liu prepared a novel Si/void/SiO_2/void/C nanostructures by selective etching away of SiO_2 within the Si/SiO_2/C structures by HF[169] (**Figure 16**). In the dual yolk-shell structure, the carbon layer enhanced conductivity; while the SiO_2 layer acted as mechanically strong support. The two internal void spaces played multiple roles by confining and accommodating volume expansion of the Si during lithiation. Therefore, these

specially designed dual yolk-shell structures exhibited a stable and high capacity of 956 mA h g^{-1} after 430 cycles with capacity retention of 83 % at a current density of 460 mA g^{-1}.

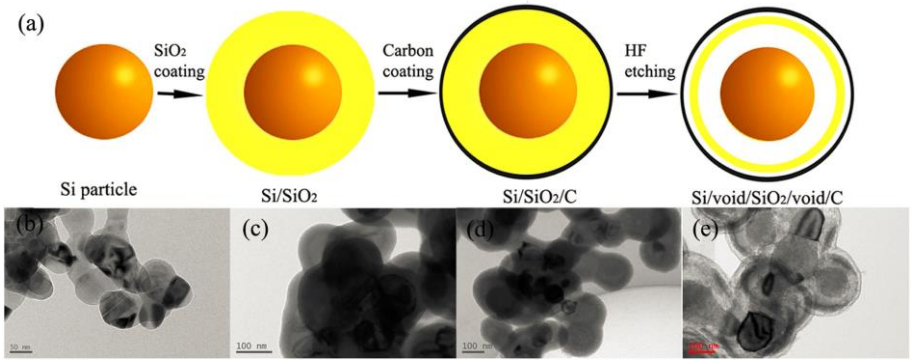

Figure 16. Scheme of the dual yolk-shell structure fabrication (a), TEM images of Si, Si/SiO_2, $Si/SiO_2/C$, and $Si/void/SiO_2/void/C$ spheres. Reprinted with permission from Ref 169. Copyright 2015 Nature Publishing group.

6.3.3 0D Si/CNT Composites

As shown by previous research work, CNTs could be used as good ductile host matrix to improve the electrochemical performance of the Si anodes due to its superior mechanical strength, excellent electrical conductivity, large aspect ratio, and structural flexibility[12]. Several groups found that the addition of CNTs in the electrospun Si/C composite nanofibers helped to enhance the high rate capabilities [170, 171]. In 2012，Lak investigated the electrochemical performance of the Si decorated with vertically aligned CNTs, which were directly grown onto metal foil via a two-step CVD process[172]. The performance test showed a capacity of 3000 mAh g^{-1} at 1.3 C, a capacity of 1900 mAh g^{-1} at 5 C and 760 mAh g^{-1} at 15 C (1.3 C = 0.77 mA cm^{-2}) . The key factors for good cycling properties were found to be the perfect adhesion between CNTs directly connected to the current collector and Si

particles, which facilitated electron and lithium ion transportation. With similar concept, Kumta demonstrated the fabrication of binder-less Si/MWCNT LIB electrodes[173]. This Si/MWCNT electrode exhibited a first discharge capacity of 3112 mAh g^{-1} at 300 mA g^{-1} and retained 76 % of capacity after 50 cycles. The enhanced electrochemical performance was attributed to the strong interface between CNT and Si leading to reduced volume change and good electrical conductivity. Recently, Du fabricated MWCNT@Si composites by magnesiothermic reduction of pre-synthesized MWCNTs@SiO_2 nanocables[174]. The MWCNT@Si anode exhibited a discharge capacity of 520 mAh g^{-1} after 70 cycles at a current density of 400 mA g^{-1}. Mangolini dispersed liquid dispersion containing Si quantum dots, CNTs and poly (vinyl pyrrolidone) (PVP) onto copper foil, followed by annealing under inert atmosphere. With this method, the Si quantum dots were well dispersed within the CNTs and heterojunctions were formed between Si and CNTs [175]. Specific charge capacity of approximately 1000 mAh g^{-1} was maintained after 200 cycles with a coulombic efficiency of 99.8 %.

6.3.4 0D Si/ Graphene Composites

Besides carbon nanotubes, graphene was continued to be used to composite with Si due to its excellent properties[176]. Particularly, because of the 2D structure feature of graphene, special hierarchical Si/graphene composites including encapsulation and sandwich structures were constructed. The graphene provided skeleton support to buffer the mechanical stress and enhanced lithium ion transportation and electrochemical reaction as well.

Xia prepared Si/graphene composite by magnesiothermic reduction of the *in situ* generated SiO_2 particles on graphene sheets[177]. The composite delivered an initial reversible capacity of 1750 mAh g^{-1} at a current rate of 100 mA g^{-1} and exhibited an excellent cycling stability with a capacity of 1374 mAh g^{-1} over 120 cycles. Wang synthesized a unique Si/graphene composite, where the Si particles were covalently bonded to the graphene oxide[178]. The composite delivered a specific charge capacity of 2250 mAh g^{-1} at 100 mA g^{-1} and retained 85 % of its initial capacity after 120 cycles. The bonding between the Si particles and graphene made significant contributions to the good performance. Cho fabricated a nanocomposite constructed by amorphous Si nanoparticles and backboned-graphene to improve the kinetics and cyclic stability of the Si anodes[179] (**Figure 17**). Due to the amorphous nature of the nano Si (particle size < 10 nm) and partially exposed graphene surface, the anodes showed a remarkable initial coulombic efficiency of 92.5 % with a high specific reversible capacity of 2858 mAh g^{-1} at a current density of 56 mA g^{-1}. After 1000 cycles, the capacity was still retained at around 1103 mA h g^{-1}.

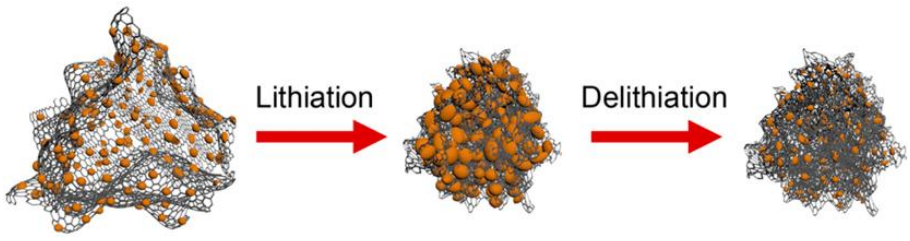

Figure 17. Schematic illustration of the Si backboned-graphene nanocomposites before and after electrochemical cycling. Reprinted with permission from Ref 179. Copyright 2014 American Chemical society.

Ruoff prepared a 3D Si/graphene/ultrathin graphite foam (UGF) electrode by

drop-casting a slurry of Si nanoparticles coated with graphene on ultrathin-graphite foam (UGF)[180]. The UGF had a very low mass density with a very high specific surface area owing to the porous 3D structure. Thus, the mass loading density of the Si on UGF could be increased while maintaining the electrode thickness still comparable to the one on flat metal foil. The gravimetric capacity with respect to the mass of the whole electrode was 983 mAh g^{-1} on the first cycle and retained 370 mAh g^{-1} after 100 cycles. The capacity was much higher than that of the graphite electrode used in a commercial 18650 cell (244 mAh g^{-1}), and an order of magnitude higher than that of Si directly loaded on a metal foil.

To further improve the electronic conductivity and structural stability of the Si/graphene composite anode, Guan developed a double protection strategy to fabricate graphene/Si/amorphous carbon hybrid anodes[181]. The graphene and the amorphous carbon coating layers worked together to effectively accommodate the volume expansion, and suppress the aggregation and destruction of the Si particles as well. As a result, a discharge capacity of 902 mAh g^{-1} was retained after 100 cycles at a current density of 300 mA g^{-1}. Xie modified the Si nanoparticles by surface grafting with polyaniline, followed by an assembly process between the polyaniline-grafted-Si nanoparticles and graphene oxide triggered by π–π interaction and electrostatic interaction. The composite was further treated by carbonization to form the Si/C/G hybrid[182]. The composites exhibited a reversible specific capacity of 1500 mAh g^{-1} at 50 mA g^{-1} and more than 900 mAh g^{-1} at 2000 mA g^{-1}. After 300 cycles at 2000 mA g^{-1}, the composites still retained about 70 % of the initial capacity. Guo employed

a 3D conductive network built by carbon particles and graphene sheets to composite with Si[183]. They synthesized the Si/G/C composite from a homogeneous suspension of Si nanoparticles and graphene oxide in aqueous PEO solution by electrospinning and subsequent pyrolysis. Such Si/G/C composites showed a discharge capacity of 1521 mAh g^{-1} after 200 cycles at a current density of 840 mA g^{-1}.

6.3.5 Other 0D Si composites

Besides carbonaceous materials, various other materials have been exploited to composite with Si nanoparticles including metal, metal oxide, electron conductive polymers to improve the electrochemical performance of the Si-based anode. For example, Korgel prepared copper-coated amorphous Si particles as an anode material with a polyol reduction method[184]. The copper coated a-Si:H particles exhibited 7 fold improvement of the lithium storage capacity over pristine a-Si:H particles. The presence of Cu helped to suppress electrolyte decomposition and enhanced electrical wiring between the Si particles. Zhang synthesized a unique core-shell structure of Si@TiO_2 composite with Si nanoparticles encapsulated in TiO_2 hollow spheres by a simple hydrolysis method combined with magnesiothermic reduction method[185]. Reversible capacities of 1911 and 795 mAh g^{-1} were reached at 0.05 C and 1 C respectively. After 100 cycles at 0.1 C, the composite electrode still maintained a capacity of 804 mAh g^{-1}. Jeong synthesized a core-shell structured Si nanoparticles@TiO_{2-x}/C mesoporous microfiber composite by electrospinning[186]. The composite consisted of a porous assembly of Si nanoparticles as the core and the

mesoporous wall of TiO_{2-x}/C nanocomposite as the shell. The core-shell composite exhibited initial discharge capacity of 1710 mAh g^{-1} with an initial coulombic efficiency of 74 %, and capacity retention of 90 % after 50 cycles. With the current density of 12000 mA g^{-1}, the capacity still reached 939 mAh g^{-1}. Furthermore, it showed remarkable suppression of exothermic process, which prevented possible thermal runaway to ensure operation safety of the cells. Yoo prepared a ternary nanocomposite of Si/Ti_2O_3/reduced graphene oxide (RGO) by mechanical blending, followed by subsequent thermal treatment of the Si, TiO_2 nanoparticles, and RGO nano sheets[187]. The obtained ternary nanocomposite exhibited a specific capacity of 985 mA h g^{-1} after 100 cycles at 100 mA g^{-1}. Metal-organic frameworks (MOFs) were also used as precursor for carbon and metal oxide to composite with the Si nanoparticles. Wang developed a one-pot strategy to grow MOFs on the surface of Si nanoparticles via *in situ* mechano-chemical synthesis [188]. After pyrolysis, the obtained composite showed a capacity up to 1050 mAh g^{-1} at 200 mA g^{-1} and maintained a reversible capacity of 830 mA h g^{-1} after 500 cycles. Finally, Wang embedded Si nanoparticles into a lithium-ion conductive polymer to form a Si/polymer composite with core-shell structure by ball milling the mixture of Si nanoparticles and N-doped poly (para-phenylene) (PPP) polymer[189]. The Si/PPP composites demonstrated a capacity of 3184 mA h g^{-1} with an initial coulombic efficiency of 78 %, a capability of 1670 mA h g^{-1} at 16 A g^{-1}, and a long term cyclability with 60 % capacity retention over more than 400 cycles.

6.4 One-Dimension Si and their Composites

6.4.1 Si Nanowires

Previous studies have shown that the Si nanowires (Si NWs) possessed exceptional capacities and stable cycling life, with reversible capacities reaching 3100 mAh g^{-1} [18]. Based on the research work between 2008 and 2010, new synthesis methods of Si NWs have been developed. For example, Si NWs were prepared by a scalable SFLS method with a relatively low cost [190]. These solution-based Si NWs were coated with carbon, and demonstrated reversible capacities of 1800 mAh g^{-1} after 100 cycles at the current density of 358 mA g^{-1}. Yang synthesized Si NWs on stainless steel foil by a Cu-catalyzed CVD method showing an initial coulombic efficiency of 89 % with a specific capacity of over 2000 mAh g^{-1} in several dozens of cycles[191]. Emma developed a high boiling point solvent-vapor-growth (SVG) system catalyzed by tin to achieve high density Si NW growth[192]. The Si NWs remained excellent capacities of 1078 mAh g^{-1} after 50 cycles at 1245 mA g^{-1}. Besides, Si NWs were also fabricated by metal-assisted chemical (MAC) etching of single crystal Si wafer[193]. The Si NWs exhibited the specific capacity above 1800 mAh g^{-1} prior to the 6^{th} cycle.

Porous structures and voids were tried to be incorporated into the Si NWs anode to provide additional space to accommodate volume expansion. Zhou synthesized porous Si nanowires by direct etching boron-doped Si wafers[194]. The nanowires were highly porous at the surface, with pore diameter and wall thickness both around 8 nm. The capacity remained stable above 2000 mAh g^{-1}, 1600 mAh g^{-1}, and 1100

mAh g^{-1} after 250 cycles at the current densities of 2000 mA g^{-1}, 4000 mA g^{-1}, and 18000 mA g^{-1}, respectively. The exceptional performance originated from the high porosity and electron conductivity of the porous doped Si nanowires. Jiang synthesized Si nanowire arrays (n-SNWAs) with a coral-like surface on Cu foam via a one-step CVD method, where the Cu foam acted as both catalyst and current collector[195]. The as-prepared n-SNWAs on Cu foam were directly applied as electrode, exhibiting a reversible capacity of 2745 mAh g^{-1} at 200 mA g^{-1} and 884 mAh g^{-1} at 3200 mA g^{-1} respectively. The capacities were much higher than that of the conventional SNWAs (127 mAh g^{-1} at 3200 mA g^{-1}). Meanwhile, an improved cycling stability was also observed (2178 mAh g^{-1} at 400 mA g^{-1} after 50 cycles). Korgel reported a non-woven fabric composed of Si nanowires with about 90 % of the fabric volume belonging to void space[196]. The self-supporting, mechanically flexible anodes showed capacities of more than 800 mAh g^{-1} without the addition of conductive carbon or binder.

6.4.2 Si Nanowires Composites

It is well-recognized that Si NWs can minimize the volume expansion due to strain relaxation and provide efficient electronic pathways as well [120, 197]. Nevertheless, in practice, the drastic volume expansion still likely causes fracture of the Si nanowires, resulting in capacity losses. To further reduce the capacity fading of the Si NWs, several approaches have been developed including coating carbon or metal on the surface of the Si NWs. By coating Si NWs with a conductive carbon skin, the Si NWs electrodes exhibited capacities of over 2000 mAh g^{-1} for 100 cycles when

cycled at C/10 and over 1200 mAh g^{-1} when cycled at 1 C (1 C = 2617 mA g^{-1})[198]. Coating Si NWs with a conductive polymer of poly(3,4-ethylenedioxythiophene) (PEDOT) generated capacities of 2510 mAh g^{-1} for 100 cycles at 840 mA g^{-1} [199]. The capacity retention was increased from 30 % to 80 % after 100 cycles compared to bare NWs. By coating Si NWs with copper, the electrode exhibited a discharge capacity of 2700 mAh g^{-1} with the initial coulombic efficiency of 90.3 % at 210 mA g^{-1} [200]. The copper-coated Si NWs showed a better cycling performance compared with the pristine and carbon-coated Si NWs. Similarly, The Ag-coated Si NWs also showed a higher reversible capacity than the bare Si NWs[201]. When employed lithium-active Sn as coating layer, the Si NWs electrode maintained a reversible capacity of 1865 mAh g^{-1} after 100 cycles at 0.1 C (359-314 mA g^{-1}), which was almost double to the capacity of the bare Si NWs[202]. Kalisvaart studied the electrochemical properties and microstructural evolution of the bare Si NWs and Si NWs coated with Mg and Mg_2Si [203]. Both, Mg- and Mg_2Si-coated Si NWs, showed significant improvement in coulombic efficiency during cycling compared to bare Si NWs. The XPS measurements revealed a passivating effect of the coating layer towards electrolyte decomposition.

Zhi developed a new strategy to composite the Si NWs with one-dimensional carbon matrix. They synthesized a novel Si/C anode nanohybrid where the Si NWs dwelled in the hollow graphitic tubes (GT) [204]. This 1D Si/1D carbon hybrid structure (Si NW-d-GT) held robust line-to-line contact between Si and C, which created efficient channels for fast transportation of both electrons and lithium ions.

Combined with the built-in void space and the line-to-line contact mode, the Si NW-d-GT exhibited good rate capability and remarkable cycling stability (*ca*. 1100 mAh g^{-1} at 4200 mA g^{-1} over 1000 cycles). Park prepared Si-SiOx core-shell nanowires ranging from 10 to 30 nm in diameter by heat treatment of Si monoxide and control of substrate temperatures without any catalyst [205]. Reversible capacities of 2000 mAh g^{-1} at a 0.2 C and 1000 mAh g^{-1} at 50 C over 100 cycles were achieved (1 C = 3700 mA g^{-1}).

2D graphene was also used to composite with the Si NWs. Graphene not only facilitated effective charge transfer between the Si NWs and the electrolyte, but also helped to maintain reliable electrical contact between Si and current collector. Hng synthesized Si NWs in graphene papers using the SFLS process[206]. This Si/graphene electrodes maintained reversible capacities of 1400 mAh g^{-1} after 30 cycles at 420 mA g^{-1}, which was much better compared to that of pure Si nanowire. Wang fabricated graphene-wrapped Si NWs (GNS@Si NWs) as a core/shell anode by electrostatic self-assembly[207]. The as-prepared GNS@Si NWs delivered a reversible capacity of 1648 mAh g^{-1} with an initial coulombic efficiency of 80 %. Moreover, the capacity remained at 1335 mAh g^{-1} after 80 cycles at 200 mA g^{-1}, showing significantly improved electrochemical performance. Zhang also prepared a novel hierarchical Si NWs/RGO composite through solvothermal reaction followed by CVD[208]. Uniform sized [111]-oriented Si NWs were well dispersed both on the RGO surface and in between RGO sheets. The performance test showed that the Si NWs/RGO composite electrode exhibited a stable cycling retention over 100 cycles

with a specific capacity of 2300 mAh g^{-1}. Ren decorated the SiC nanofiber with Si NWs, followed by encapsulation with graphene shell [209]. The core-shell SiC/Si/G electrode was capable of serving over 500 cycles in half cell with a lithium storage capacity of 1650 mAh g^{-1} at 800 mA g^{-1}. The graphene shell provided a highly conductive path and prevented direct exposure of Si NWs to electrolytes; while the SiC nanocrystals might act as a rigid backbone to retain the integrity of the Si NWs during its deformation process.

6.4.3 Si Nanotubes and their Composites

As indicated by previous research, the Si nanotubes (Si NTs) exhibited better lithium storage performance than the Si NWs because the nanotubular structures provide larger access area for electrolyte, additional space for volume expansion accommodation.

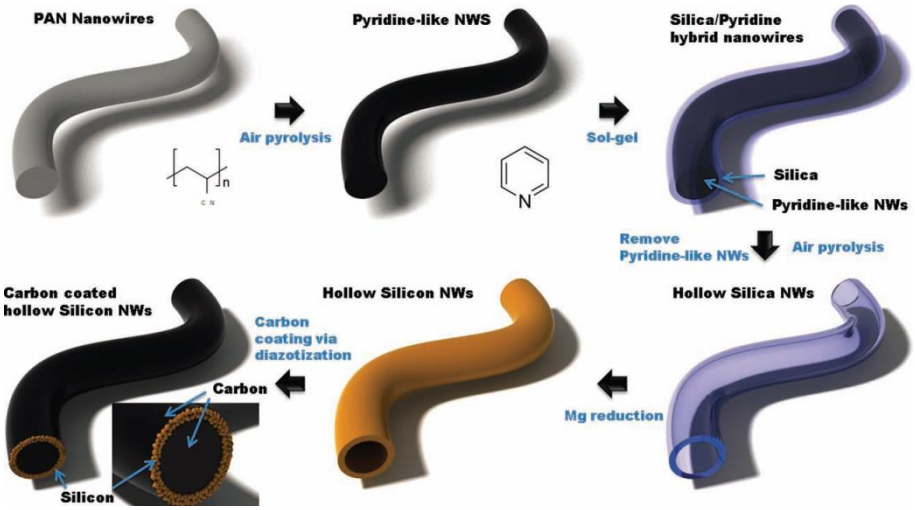

Figure 18. Scheme of the synthesis of carbon coated Si nanotubes. Reprinted with permission from Ref 210. Copyright 2012 WILEY-VCH Verlag GmbH & Co. KGaA, Weinheim.

Jung fabricated carbon coated Si NTs through surface sol-gel reaction on organic

nanowires, followed by magnesiothermic reduction[210] (**Figure 18**). The Si NTs showed a capacity of about 1900 mAh g^{-1} at 400 mA g^{-1} with a coulombic efficiency of nearly 100 % during cycling. Chen synthesized Si NTs by magnesiothermic thermal reduction of silica nanotubes, which were prepared using rod-like NiN_2H_4 as a template[211]. The Si NTs showed significantly improved rate capability and long-term cycling performance compared to commercial Si meshes. A capacity of 1000 mAh g^{-1} was retained after 90 cycles at 0.5 C. Coffer fabricated porous Si NTs with defined porous sidewalls based on sacrificial ZnO nanowire template[212]. The porous Si NTs showed a discharge capacity of 3095 mAh g^{-1} with a coulombic efficiency of 63 % at 210 mA g^{-1}. Stable reversible capacity of 1670 mAh g^{-1} was achieved after 30 cycles.

Si NTs composites were also fabricated to further improve the electrochemical performance. Lu tried to decorate the Si NTs with carbon through a CVD process[213]. The C@Si NTs anode delivered a capacity of 2085 mAh g^{-1} at 840 mA g^{-1}, and capacity retention of 95 % after 200 cycles relative to the capacity value of the 10^{th} cycle. Hertzberg successful controlled the SEI growth on Si NTs with rigid CNT outer shell[214]. The rigid outer shell of CNT on the Si NTs exhibited capacity of 800 mAh g^{-1} after 250 cycles at 1700 mA g^{-1}. Braun presented a carbon-Si-carbon (C@Si@C) nanotube sandwich structure to address the mechanical and chemical stability issues[215]. The C@Si@C nanotube array exhibited a capacity of 2200 mAh g^{-1} and a nearly constant coulombic efficiency of 98 % over 60 cycles. The enhanced electrochemical performance was attributed to the stable SEI formation due to the

existence of carbon layer at inner and outer shell of the Si NTs. Free standing and binder-free copper/Si core–shell nanotube arrays were fabricated by Zhang using Si NW arrays as the template[216]. The cone-shaped copper nanotube arrays acted as both the supporter and current collector for Si. The electrode maintained excellent structure stability after 400 cycles with a specific capacity of 1506 mAh g^{-1} at the current density of 840 mA g^{-1}.

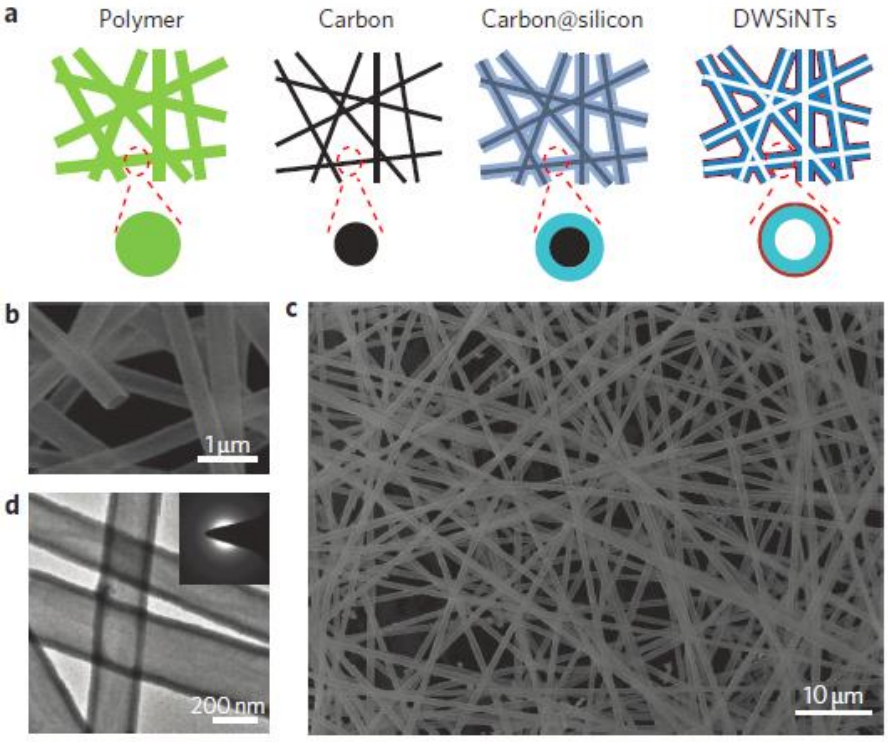

Figure 19. Scheme for the fabrication of double-walled Si-SiO_x nanotube (a), SEM (b, c), and TEM (d) of the Si-SiOx nanotube. Reprinted with permission from Ref 217. Copyright 2012 Macmillan Publishers Limited.

In order to address the SEI stability issue, Cui's group designed a novel double-walled Si-SiO_x nanotube (DWSiNT) anode, in which the inner wall was active Si and the outer wall was confining SiO_x, which still allowed lithium ions to pass through[217] (**Figure 19**). The outer surface of the Si NT was prevented from

expansion by the oxide shell. The expanding inner surface was not exposed to the electrolyte. This specific structure design helped to stabilize the solid electrolyte interphase. The Si NT anode exhibited high specific charge capacity (1780 mAh g^{-1} at 1/5 C, 600 mAh g^{-1} at 12 C) and a capacity retention of around 600 mAh g^{-1} after an 6000 cycles at 12 C rate (1 C = 2000 mA g^{-1}).

In a short summary, like the development trend of Si alloys and Si films, the structure design and synthesis methods of Si NWs and Si NTs composites were also further diversified in recent few years. Porous, sandwich, core–shell and coating structures were introduced to modify the 1D Si materials. The electrodes demonstrated very good electrochemical performance. The results suggested that combining porous structures and/or compositing with buffer medium to the one-dimensional Si further improved the electrochemical performance. However, one of the drawbacks for 1D Si is that their electrode making process is different from the current powder-based electrode making process used commercially. As a result, new electrode making processes at low cost need to be developed for the emerging materials. Besides, increasing the areal “mass loading” and decreasing the material costs are the two main challenges of Si NWs anodes for industrialization manufacture[218].

6.5 Three-Dimension Si and their Composites

As pointed out early in this review article, low-dimension Si inherited the major drawback of low mass loading density. Therefore, three-dimensional porous Si has attracted considerable attention from both academia and industry because they hold

great promise for practical applications. Cho prepared three-dimensional nanoporous Si by depositing Si particles onto SiO_2 nanoporous templates. This structure exhibited high capacity of over 2800 mAh g^{-1} without significant degradation up to 100 cycles at a current density of 400 mA g^{-1} [219]. Despite the promising performance from the porous Si-based electrodes, the synthesis generally required several complicated experimental steps, which were expensive, time consuming, and difficult to scale up. Therefore, synthesis of three-dimensional porous Si from cheap source with scalable method has been one of the major issues in this time range. Yuan synthesized 3D porous micrometer sized Si particles embedded with silver based on mesoporous silica powder via a facile and low cost metal-assisted chemical etching process[220]. The silver-coated macroporous Si electrode exhibited capacity of around 2500 mAh g^{-1} at 0.2 C after 100 cycles, which was higher than that of the non-coated 3D macroporous Si electrodes. The high conductive silver nanoparticles encapsulated in the matrix of porous Si acted as conductive additives, which improved the cycling performance of the Si-based electrodes. Park synthesized multi-dimensional Si electrodes composed of porous nanowires and micro-sized cores with nano-sized pores from commercially available bulk Si powder by combining a metal deposition and metal-assisted chemical etching process[221](**Figure 20**). The synthetic route was simple, scalable (high yield of 40 % - 50 %), and cost effective. Carbon-coated multi-dimensional Si electrodes showed a high reversible charge capacity of 2410 mAh g^{-1} at a rate of 0.1 C with coulombic efficiency of 91 % and stable capacity retention of 95 % after 70 cycles at a rate of 0.2 C. However, the mesopores existing

in the as-synthesized bulk Si particles affected the morphologies of the original Si particles after a few cycles. Thereafter, 3D macroporous silicon particles were further synthesized from commercially available bulk silicon powders via a galvanic displacement reaction and metal-assisted chemical etching process [222]. The carbon-coated 3D macroporous bulk Si exhibited a high storage capacity of 2050 mAh g^{-1} at a rate of 0.2 C (1 C = 2000 mA g^{-1}) with remarkable coulombic efficiency of 94.4 % and stable cycling retention of 87 % after 50 cycles.

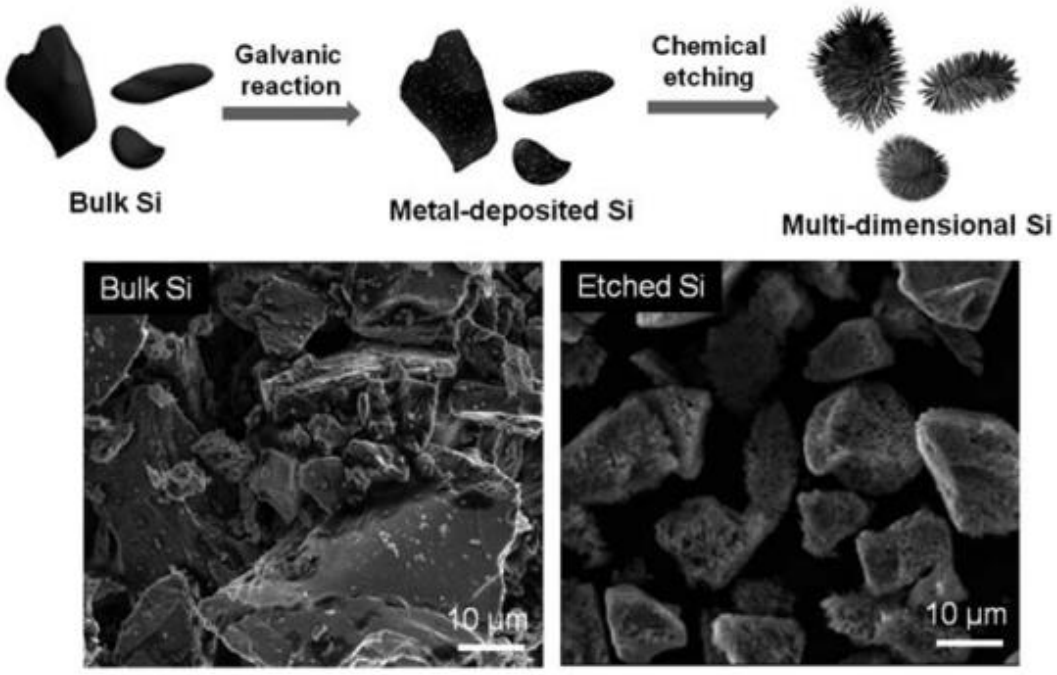

Figure 20. Schematic of the synthetic route of multi-dimensional Si powder. Reprinted with permission from Ref 220. Copyright 2011 Elsevier. B.V.

Wada prepared freestanding bulk 3D nanoporous Si using a top-down process which allowed for mass production[223]. The electrode had an initial capacity of around 3550 mAh g^{-1} and remained over 1500 mAh g^{-1} after 500 cycles at the current density of 1800 mA g^{-1}. By further adjusting the lithiation capacity below the volume

accommodation limit, the bulk 3D Si electrode exhibited even longer cycle lifetime and higher coulombic efficiencies than the nanoparticle-based Si electrodes. Zhang fabricated nanoporous Si networks with controllable porosity and thickness by a simple and scalable electrochemical process[224]. The nanoporous Si networks showed an initial discharge capacity of 2570 mAh g^{-1} at 0.1 C and around 1000 mA h g^{-1} at 1 C after 200 cycles without any electrolyte additives. Zhou prepared porous Si nanoparticles using a scalable and cost-effective method by combining boron doping and electroless etching together [225]. The anode achieved capacities of around 1400 mAh g^{-1} at 1000 mA g^{-1}, and 1000 mAh g^{-1} at 2000 mA g^{-1}. Additionally, it showed a stable cycling up to 200 cycles when combined with reduced graphene oxide. The same group also fabricated nanoporous Si particles from metallurgical Si through ball milling and stain-etching[226] (**Figure 21**). The nanoporous Si coated with carbon and graphene oxide showed a reversible capacity of 2900 mAh g^{-1} at 400 mA g^{-1} and a stable capacity above 1100 mAh g^{-1} for 600 cycles at 2000 mA g^{-1}.

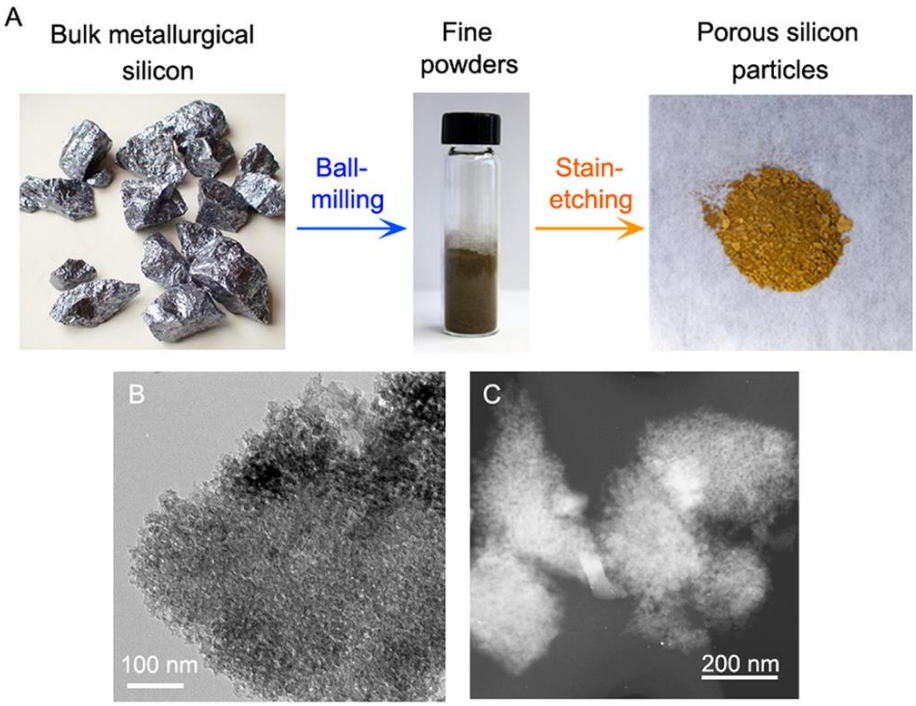

Figure 21. Schematic diagram of the synthesis and morphology of porous Si particles. Reprinted with permission from Ref 227. Copyright 2014 American Chemical Society.

Jiang applied acid etching on the Al/Si alloy powder to obtain porous Si powder[227]. The porous Si electrodes showed the first charge and discharge capacities of 3450 mAh g^{-1} and 2072 mAh g^{-1} respectively at current density of 100 mA g^{-1}. The discharge capacity retained 66 % after 258 cycles. Based on this work, the group also modified the porous Si powder by coating with nano-Cu through acid-etching Al/Si alloy powder followed by electroless plating of Cu[228]. The porous Si coated with copper showed a capacity of 1651 mAh g^{-1} at 200 mA g^{-1} after 150 cycles. Similarly, Han prepared micro-sized porous Si materials from Fe/Si alloy by acid etching. It showed an initial coulombic efficiency of 88.1 % and exhibited a good cycling stability of 1250 mAh g^{-1} at 500 mA g^{-1} after 100 cycles[229]. The same

group also synthesized micro-sized Si/C composites consisting of 20 nm carbon-coated Si particles starting from low cost Al/Si alloy through acid etching, ball-milling and carbonization procedure. The unique nano-porous Si/C composite provided a capacity of 1200 mAh g^{-1} at a current density of 50 mA g^{-1}, and maintained 86.8 % of initial capacity after 300 cycles at the current density of 500 mA g^{-1}, with an average loss of only 0.044 % per cycle[230]. Feng further prepared porous Si/RGO nanocomposites by one-pot acid etching Al/Si eutectic and in-situ reduced graphene oxide. The as-prepared porous Si/RGO electrode delivered a reversible initial capacity of 2280 mAh g^{-1} and capacity retention of 85 % even after 100 cycles and a capacity as high as 1521 mAh g^{-1} at 4000 mA g^{-1} [231]. It can be seen that the simple, low-cost and scalable acid etching method is a promising route for a large-scale production of Si-based anode materials.

Inspired by the peanut shell structure, Chen synthesized carbon coated porous Si through ball milling and carbonization processes[232]. The peanut shell structured Si/C electrode exhibited good reversible capacity (1179 mAh g^{-1} at 0.1 C over 120 cycles and 432 mAh g^{-1} at 0.3 C over 400 cycles) as well as good rate performance (493 mAh g^{-1}at 4 C) , (1C = 1880 mA g^{-1}). The enhanced electrochemical performance was due to the formation of C-SiO_2 layer and the improved interfacial contact brought by the void space of the peanut shell structure.

Besides the above mentioned studies, porous Si was also synthesized from silica through magnesiothermic reduction, which was amenable to scale-up[233]. Cui recovered nanoporous Si from rice husks as a sustainable source for nanostructured Si

through the magnesiothermic reduction process[234]. The porous Si electrode exhibited an initial reversible capacity of 2790 mAh g^{-1} and capacity retention of 86 % after 300 cycles at the current density of 2100 mA g^{-1}. The enhanced performance was attributed to the accommodation of a large volume change of Si without rupturing the SEI at the outer surface during cycling. Zhan synthesized nano-sized mesoporous Si by magnesiothermic reduction of Stöber silica, followed by HF etching[235]. The final product delivered a capacity of 1867 mAh g^{-1} at the current rate of 400 mA g^{-1}. After 100 cycles, the capacity was retained at 1444 mAh g^{-1}. Ozkan carried out surface protected magnesiothermic reduction of 200 nm sized Stöber silica sphere to obtain highly monodisperse porous Si nanospheres (MPSSs) [236]. The spherical nature of the MPSSs (*ca*. 200 nm in diameter) allowed a homogenous stress-strain distribution within the sphere during lithiation and delithiation, which dramatically improved the electrochemical stability. The LIB anodes based on MPSSs demonstrated a high reversible capacity of 3105 mAh g^{-1} and the capacities were maintained above 1500 $mAhg^{-1}$ after 500 cycles at 1789 mA g^{-1}.

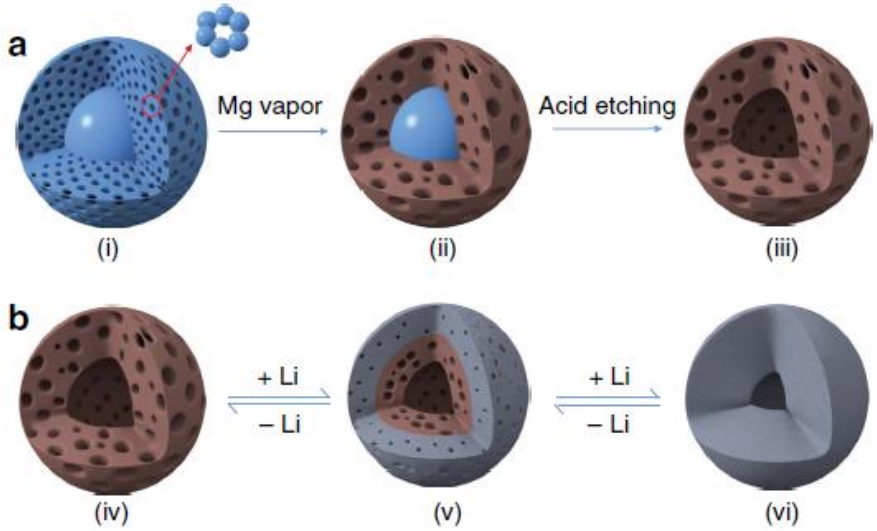

Figure 22. Scheme of the synthesis method and lithiation/delithiation process for hp-SiNSs. Reprinted with permission from Ref 23. Copyright 2015 Macmillan Publishers Limited.

Xiao reported the synthesis of hierarchical porous Si nanospheres composed of porous shell and hollow core (hp-SiNSs) from solid core/mesoporous shell SiO_2 spheres[23] (**Figure 22**). On cycling, the hp-SiNSs accommodated the volume change through reversible inward Li breathing with negligible particle-level outward expansion. The reversible specific capacity reached 1850 mAh g^{-1} at 0.1 C (1 C = 3600 mA g^{-1}) and maintained above 1800 mAh g^{-1} after 200 cycles at C/20. Lee reported the facile synthesis of porous Si via magnesiothermic reduction of Stöber SiO_2 followed by coating with $TiSi_2$[237]. This combination of porous structure and highly conductive $TiSi_2$ coating provided a synergistic effect to improve the electrochemical performance. The coated porous Si electrode exhibited a discharge capacity of 1577 mAh g^{-1} at 400 mA g^{-1} after 50 cycles whereas the uncoated electrode exhibited capacity of only 651 mAh g^{-1}. The enhanced cyclic stability of composites might be caused by the $TiSi_2$ coating layer, which maintained the structure and restrained the continuous growth of SEI layer. Yin fabricated 3D interconnected porous Si/carbon (Si/C) hybrid architectures via a controllable reduction route from silica aerogels[238]. The 3D porous Si/C hybrids showed a reversible capacity of 1552 mAh g^{-1} after 200 cycles at 200 mA g^{-1}. With the current density of 2000 mA g^{-1}, the reversible capacity was still maintained at 1057 mAh g^{-1} after 50 cycles. Fan prepared ordered porous Si@C nanorods through magnesiothermic reduction of

well-ordered hexagonal mesoporous silica (SBA-15)[239]. The obtained porous Si@C nanorods demonstrated a reversible specific capacity approaching 627 mAh g^{-1} after 220 cycles at 100 mA g^{-1} as well as improved cycling stability and excellent rate capacity. The same group also prepared porous Si/C composites through magnesiothermic reduction of diatomite, followed by impregnation and carbonization of phenolic resin[240]. The obtained composites consisted of porous Si coated with a 15 nm thick amorphous carbon layer. The porous Si/C composite containing 33 % of carbon exhibited a reversible capacity of about 1628 mAh g^{-1} and maintained 759 mAh g^{-1}after 30 cycles at 50 mA g^{-1}. Zhou synthesized carbon-coated micro/nano porous Si with a wet chemical etching method[241]. The anodes with 11.3 nm mean pore diameter exhibited almost no capacity fading after 50 cycles when cycled at a given discharge capacity of 1500 mAh g^{-1}. This work pointed out that it was the porous structure, rather than the particle size, played a more important role in determining the performance of the Si.

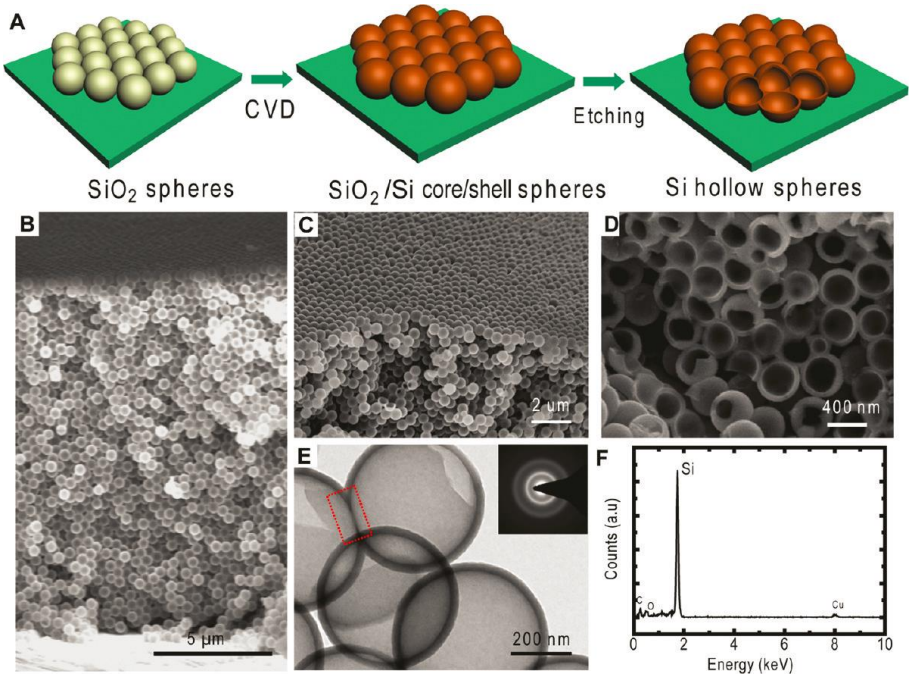

Figure 23. Scheme of the synthesis of Si hollow spheres, SEM of SiO2 spheres(A) and SiO@/Si core-shell spheres (C), SEM (D) and TEM (E) , and Energy dispersive X-ray spectroscopy of Si hollow spheres. Reprinted with permission from Ref 242. Copyright 2011 American Chemical Society.

Besides the conventional porous structures, nanostructured hollow Si was also designed and synthesized. Cui fabricated hollow Si nanospheres using solid silica nanospheres as template[242] (**Figure 23**). The interconnected Si hollow nanospheres exhibited initial discharge capacity of 2725 mA g^{-1} with less than 8 % capacity degradation every hundred cycles for total 700 cycles at 220 mA g^{-1}. The well-designed nanoparticles with a free volume in the hollow particle interior and the porosity in the shell effectively cushioned the volume change and consequently improved the electrochemical performance. Xie also fabricated hollow porous Si (HPSi) nanocomposite coated with silver nanoparticles by magnesiothermic reduction of hollow porous SiO_2 nanoparticles[243] (**Figure 24**). The HPSi coated with silver showed a reversible specific capacity of 3762 mAh g^{-1}, capacity retention of 93 % after 99 cycles, and capacity of over 2000 mAh g^{-1} at 4000 mA g^{-1}. Conductive polymer was also applied to improve the electrochemical kinetics of Si.

Figure 24. Scheme for synthesis of hollow porous Si (HPSi) nanoparticles. Reprinted with permission from Ref 243. Copyright 2012 Wiley-VCH Verlag GmbH & Co.

KGaA, Weinheim.

Wang prepared ploypyrrole@porous Si hollow spheres (PPy@PHSi) nanocomposite using the magnesiothermic reduction of mesoporous silica hollow nanospheres, followed by *in situ* chemical polymerization of PPy on the PHSi surface[244]. The PPy@PHSi electrode demonstrated a reversible capacity of above 2000 mAh g^{-1} and capacity retention of 88 % capacity after 250 cycles with respect to the capacity value of the 2^{nd} cycle. Unlike the methods mentioned above, Chen used carbonates as templates to synthesize hollow Si with tunable morphology including hollow cubes, spheres, tubes, flowers and other shapes[245]. The as-prepared hollow Si showed outstanding cyclic performance. In particular, the flower-like Si anode delivered a capacity of 814 mAh g^{-1} at a current density of 4800 mA g^{-1} and retained 80 % of its reversible capacity after 700 cycles.

6.6 Summary of the Progress from 2011 to 2015

During the period from 2011 to 2015, an explosive development of the Si-based anode has happened. The research work on Si-based anodes continued to be on the Si alloy, 0D Si particles, 1D Si nanowires and nanotubes, 2D Si films and nanosheets, and 3D porous Si. Significant progress has been made in improving the electrochemical performance of Si-based anodes through size reduction, incorporation of a buffer matrix, and hierarchical structure construction **(Table 4**). Particularly, introducing voids into the nanostructured Si has been recognized as an effective way to accommodate the volume expansion and release corresponding mechanical stress. By applying this concept, the overall performance of Si-based anodes has been

significantly improved compared to previous research. Meanwhile, researchers also started to address the issue of low cost synthesis of high performance Si-based anodes, which would be of high level interest in practical applications.

7. Si-based Multicomponent Systems

In addition to the 0D Si particles, 1D Si nanowires and nanotubes, 2D Si films and nanosheets, and 3D porous Si, Si-based multicomponent materials have also been exploited as LIBs anodes since 2006 (**Table 5**). The Si-based multicomponent systems exhibit reasonable tap densities, which is crucial for applications where volumetric energy density is vital. Besides, the synthetic routes of the Si-based multicomponent systems are normally simple, scalable, low-cost, and safe, which makes the Si-based multicomponent systems particularly promising for practical applications.

Morita prepared Si nanocluster-SiO_x-C composites based on the disproportionation of SiO and the polymerization of furfuryl alcohol to improve cyclability of the silicon composite[246]. The nanosilicon composite anode exhibited a capacity of 700 mAh g^{-1} after 200 cycles at 1 mA cm^{-2}. Park reported the synthesis of nano-Si/SiO_x/graphite composite in 2010 by thermally treating the commercial SiO at 1000 °C, followed by HEMM with graphite[247]. It was found that the heat treatment generated well-developed Si nanoparticles uniformly dispersed within an amorphous SiOx matrix. The composite showed high discharge and charge capacities of 1516 mAh g^{-1} and 1002 mAh g^{-1} respectively after 100 cycles at 100 mA g^{-1}, with a cyclic retention of above 70 %. Meanwhile, The same group also prepared 3D porous Si-based multicomponent system with core (Si dispersed in amorphous silicon

suboxides) and shell (crystalline silica) by chemical-assisted thermal disproportionation of porous SiO[248]. The system exhibited a high reversible capacity (*ca.*1600 mAh g^{-1}) and a stable retention over 100 cycles at 0.1 C. They also synthesized Si-SiO-SiO_2 multicomponent particles, consisting of an active Si/SiO core and a SiO_2 buffer shell, from a commercially available solid SiO particle via a high-temperature annealing process in the presence of sodium hydroxide[249]. This material exhibited a high reversible capacity of 1280 mAh g^{-1} at the 0.1 C and excellent cycle retention of 99.5 % at 0.2 C after 200 cycles. The good electrochemical properties of the Si-based multicomponents were ascribed to the combination of high specific capacity of Si and highly stable cycling performance of SiO. Recently, the same group also synthesized nanotube-type Si-based multicomponents consisting of Si, Al_2O_3 and Ti_xSi_y by combining a coaxial electrospinning technique and subsequent metallothermic reduction reaction[250]. The anode showed stable cycling property (765 mAh g^{-1} after 280 cycles at 0.5 C) and high rate capability (483 mAh g^{-1} at 10 C), and significantly reduced volume change (electrode expansion of 14 %). Based on their previous work, the group further developed a novel Si-based multicomponent using a simple sol-gel process. The Si core was covered with multifunctional shell layers consisting of lithium silicate and lithium titanate[251]. The multifunctional coating layers not only increased electronic conductivity to enhance rate capability but also promoted the formation of a stable SEI layer on the Si electrode surface to enhance the cycling property. The resulting multicomponent anode delivered a high capacity of around

1000 mAh g^{-1}, a stable cycling retention (65 % after 1000 cycles at 1 C), an excellent rate capability (800 mAh g^{-1} at 10 C), and a remarkably suppressed volume expansion (12 % after 100 cycles).

Du systematically investigated the impact of the nickel composition on the structure and electrochemical performance of the $NixSi_{1-x}$ ($0 \leq x \leq 0.5$) alloy anodes[252]. It was found that nanocrystalline $Si/NiSi_2$ phases were formed with $x \leq 0.25$; while NiSi phase was observed with higher Ni content. The increasing Ni content gradually lowered the lithiation voltage, and did not affect the delithiation voltage for $x \leq 0.25$. The nanocrystalline $NiSi_2$ phase exhibited moderate activity toward lithiation; while the NiSi phase did not contribute to capacity. The best cycling performance of Ni_xSi_{1-x} alloys was obtained for x = 0.20 with 94 % capacity retention after 50 cycles.

Chae successfully synthesized Fe-Cu-Si ternary composite (FeCuSi) by scalable spray drying and facile heat treatment with high tap density[253]. FeCuSi possessed a porous silicon secondary structure where numerous nano-sized metal silicides were embedded. The porous secondary structure effectively accommodated the volume expansion of Si to relieve mechanical stress. As a result, the FeCuSi composite exhibited remarkable initial coulombic efficiency of 91 % and specific capacity of 1287 mAh g^{-1} and capacity retention of 98 % after 50 cycles at 210 mA g^{-1}.

8. Latest Progress of the Si-Based Anodes Research in 2016

Most research work on the Si-based LIBs anode reported in 2016 focused on the silicon/graphene composites as a continuation from the previous time range

between 2011 and 2015 (**Table 6**). Duh designed a Si-graphene hybrid composite by inserting Si ultra-nano particles (SiUP) into nitrogen-doped graphene nanosheets(N-GNSs) with facile top-down dispersion and bottom-up synthesis strategies[254]. The anode exhibited an initial specific capacity above 1200 mAh g^{-1} at 500 mA g^{-1} and outstanding long cycling performance of 600 cycles with a capacity fading of less than *ca*. 0.09 % per cycle. The intrinsic structure of the SiUP together with the mechanical feature of the sheet-by-sheet coverage from the N-GNSs helped to reduce the stress from the lithiation/delithiation processes to extend the cycling lifetime. Kim synthesized an rGO-Si hybrid using Si NPs of less than 10 nm derived from sol-gel reaction and magnesiothermic reduction[255]. The uniform distribution of the silicon nanoparticles on the surface of rGO nanosheets through covalent bonding resulted in stable cycling performance and superior rate capability. The rGO-Si delivered an initial discharge capacity of 1338 mAh g^{-1} with capacity retention of 87.1 % after the 100th cycle at 2100 mA g^{-1}. Ding fabricated nano-sized Si-based composites coated with monolayer graphene (mGra) through a melting self-assembly route. The Cu film acted as catalyst for deposition of graphene monolayer and sacrificial layer to create void space between Si and graphene as well (**Figure 25**) [256]. The composite demonstrated an initial coulombic efficiency exceeding 85 % with a discharge capacity of 3100 $mAhg^{-1}$ at current density of 100 mA g^{-1}. At 500 mA g^{-1}, the capacity was retained as high as 1287 $mAhg^{-1}$ and capacity retention of 89 % were achieved over 500 cycles. The monolayer graphene and the void space between Si and graphene not only effectively accommodated the

volume change during the lithiation process, but also provide preferential pathways for Li-ion diffusion.

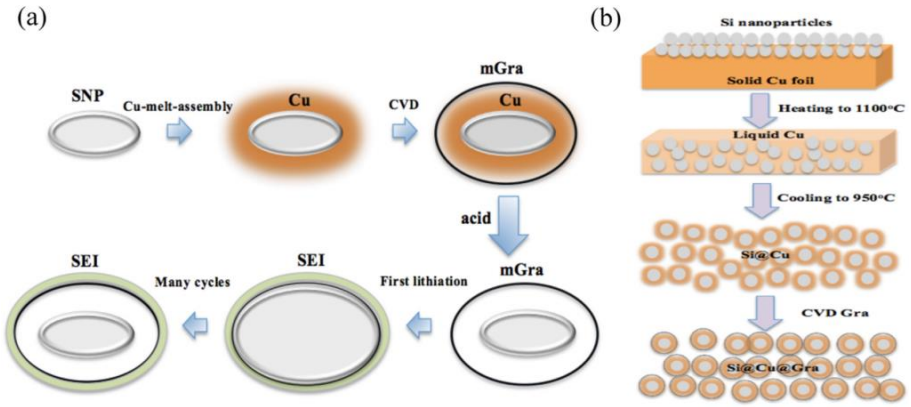

Figure 25. Scheme for synthesis of melt-self-assembly of Si@void@mGra composite. Reprinted with permission from Ref 256. Copyright 2016. Elsevier. B.V.

Kang prepared a novel Si NP-carbon-graphene (Si@C-rGO) composite with the sandwich structure assembled by commercial Si NPs, dopamine hydrochloride, and GO solutions through simple stirring and vacuum filtration[257]. A high gravimetric capacity (1001 mAh g^{-1} at a current density of 300 mA $g^{-1.}$) and a long cycle life (93 % over 400 cycles) were simultaneously achieved with the Si@C-rGO composite. Excellent volume suppression was also recorded with less than 10 % volume change. The dopamine carbon coating firmly anchored the Si onto the rGO sheets and elastically cushioned the volume expansion of Si. Furthermore, the unique sandwich structure helped to suppress the huge volume change of Si. Ma employed the H-bonding effect from sodium carboxymethyl cellulose (Na-CMC) polymer to bridge the monolithic graphene foam (GF) protective sheath and Si NPs in a complete encapsulation arrangement through freeze-drying[258]. The highly oriented GF monolith was engineered to fully encapsulate the Si NPs. It served not only as a

robust framework with the well-accessible thoroughfares for electrolyte percolation but also a physical blocking layer to restrain Si from direct exposure to the electrolyte. In return, the pillar effect of Si NPs prevents the graphene sheets from restacking while preserving the highly efficient electron/Li^+ transport channels. The GF/Si (mass ratio of silicon to GO is 1:1) electrode exhibited stable capacity of 1295 mAh g^{-1} after total 180 cycles at the current density of 500 mA g^{-1}. Upon cycling at the high current density of 1000 mA g^{-1}, the GF/Si electrode only suffered from a capacity loss of 0.005 % per cycle. And a reversible capacity of 1170 mAh g^{-1} was retained after 1200 cycles.

To avoid the use of expensive silicon nanoparticles with low tap density, micrometer-sized silicon particles emerged as a new family of lithium-ion battery anodes. Li encapsulated Si microparticles (1 μm - 3 μm) with an *in situ* synthesized graphene cage (**Figure 26**)[259]. The graphene cage acted as a mechanically strong and flexible buffer during deep galvanostatic cycling. It allowed the microparticles to expand and fracture within the cage to retain electrical connectivity at the levels of both particle and electrode. The chemically inert graphene cage also formed a stable solid electrolyte interface to minimize irreversible consumption of lithium ions and rapidly increased the columbic efficiency in the early cycles. The reversible capacity reached 3300 mAh g^{-1} at 210 mA g^{-1} and capacity retention of 85 % after 300 cycles at 2100 mA g^{-1}. Besides, the anode exhibited an initial coulombic efficiency of 93.2 %, which increased to 99.5 % within the first five cycles and reached 99.9 % after ten cycles. When the Si/graphene hybrid was tested in a full-cell configuration,

90 % of capacity retention was achieved after 100 cycles.

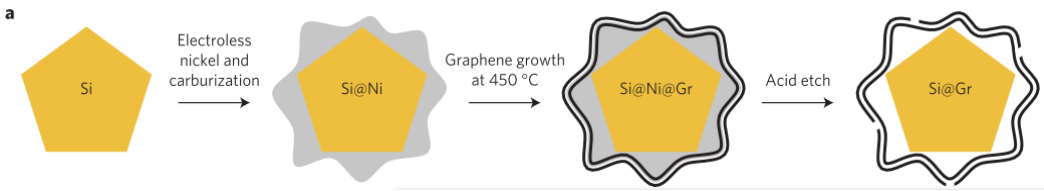

Figure 26. Scheme of the fabrication of the silicon caged with *in situ* synthesized graphene. Reprinted with permission from Ref 259. Copyright 2016 Nature Publishing Group.

Recently, Cui's group demonstrated the feasibility of a next-generation hybrid anode by synthesizing Si-nanolayer-embedded graphite/carbon hybrids (SGC) based on a CVD process in a scalable furnace[260]. The anode achieved a reversible capacity of 517 mAh g^{-1} with high initial columbic efficiency of 92 % at 0.5 C, where 96 % of capacity was retained after 100 cycles. This hybrid effectively overcame the electrode expansion problem even with high electrode density (>1.6 g cm^{-3}) and areal capacity loading of more than 3.3 mAh cm^{-2}. Besides, a full cell exploiting $LiCoO_2$ as cathode demonstrated a higher energy density (1043 Wh L^{-1}) than the full cell based on routine graphite anode. Dou prepared granadilla-like silicon via a green, facile and scalable templating method using calcium carbonate as a sacrificial agent and acetylene as a carbon precursor[261]. Silicon granadillas with 30 % silicon content delivered a reversible capacity of around 1100 mAh g^{-1} at a current density of 250 mA g^{-1} after 200 cycles. Besides, this composite exhibited 830 mAh g^{-1} and 700 mAh g^{-1} at the current densities of 1000 mA g^{-1} and 2000 mA g^{-1} respectively.

9. Perspective of the Si-Based Anodes for Real Battery Applications

Although the Si-based electrodes with good performance including high capacity and long cycle life have been extensively reported, the wide application of the silicon-based anodes has not been realized in real batteries. Several critical concerns including the coulombic efficiency (CE), mass loading density, and cost need to be addressed for real applications.

Firstly, the coulombic efficiency is crucial for practical battery applications. Tiny change of the CE can drive the capacity of the full cells to fade into unacceptable level rapidly[262]. Normally, the initial CE of the Si-based anode is typically in the range of 65 % - 85 %, which is far below that of commercial graphite anodes (90 % - 94 %). The later-cycle CE of the Si-based anodes is usually 98 % - 99.7 %. But it still needs further improvement to reach 99.9 %, which is suitable for practical applications. It seems that only very few reported work satisfied this rigorous requirement[259].

Secondly, reasonable areal mass loading of the Si-based electrode has been gradually recognized as an important issue to realize decent energy output in real battery applications[263]. However, in many publications only specific capacity values normalized to the mass of the active materials were reported. And the real mass loading density was normally not high enough for practical applications. Recently, a few work demonstrated the possibility to improve the mass loading density while retaining reasonable specific capacity and cyclic stability [251, 264].

Thirdly, cost will inevitably become one of the critical issues influencing the commercialization of the Si-based anodes. Because typical nano-sized silicon is quite expensive, the exploitation of micrometer sized silicon has attracted attention from both academia and industry. Developing low cost synthesis and processing methods and exploiting non-expensive materials are essential for the practical applications of the Si-based anodes[265].

Due to the critical factors mentioned above, it seems that the wide application of the Si-based anode in real batteries has not emerged yet. However, there have been a few reports about the commercialization of the Si-based lithium-ion battery anodes. Nexeon patented two types of silicon anode materials with capacities up to 1000 mAh g^{-1} and 3600 mAh g^{-1} respectively[266]. 3M developed silicon anode powders with twice the energy density of the conventional graphite anodes with excellent cycling property (70 % retention at 500 cycles)[267]. Amprius Inc. recently demonstrated a new protocol for the production of silicon nanowire anodes. With the Si nanowires anode, high energy density (800 WhL^{-1} - 1000 WhL^{-1}) was achieved[268]. XG Sciences, Inc. (XGS) announced silicon-graphene anode material which is reported to be available immediately at commercial scale[269]. Hitachi Maxell Ltd. achieved an energy density of 335 Wh/kg with silicon based anode[270]. BTR New Energy Materials Inc. developed SiO based composite anode and high capacity Si based composite material[271].

10. Conclusion and Outlook

Silicon is recognized as one of the most promising candidates for next generation

lithium-ion battery anode to replace the conventional carbon-based anode due to its high theoretical capacity, proper discharge potential and reliable operation safety. However, the critical drawback of huge volume expansion upon lithiation causes series of adverse consequences, leading to very poor cyclic stability. It has been one of the central issues to improve the cyclic performance of the Si-based anode for real practical applications. By systematically reviewing the academic research on the Si-based anodes in a chronical perspective from early 1990s to 2016, the evolution of the structure design and surface modification of the Si-based anodes are clearly presented.

(1) 0D Si nanoparticles with sufficiently small sizes are able to undergo large volumetric strains without mechanical fracture. However, the large surface area of Si NPs promotes the side reactions and SEI formation, which leads to poor cycling life and short calendar life. Besides, repetitive volume changes result the electrical disconnection between the particles and the current collector. Many surface modification strategies have been developed to address the problems. Compositing Si with various types of carbonaceous materials has been widely used throughout the time range addressed in this review. Particularly, tuning the structure and morphology of the carbon matrix and construction of hierarchical structures has been increasingly reported since 2010.

(2) 1D Si nanowires and nanotubes are considered to be superior to 0D nanoparticles due to continuous 1D electronic pathway to facilitate efficient charge transport. Moreover, the 1D Si has the possibility to grow directly on a current

collector to avoid the use of binders and conductive fillers. Meanwhile, 1D Si has the advantage of allowing the expansion of silicon radially to minimize the cracking propensity. The use of the Si NWs and Si NTs as lithium-ion battery anode was initiated in 2008. From 2008 to 2010, the research work was mainly focused on the development of new synthetic methods and understanding the electrochemical mechanism. Although the Si NWs could realize the theoretical charge capacity of silicon, capacity degrades rapidly after a few cycles. Additionally, the electrical contact of 1D Si with the current collector or with the conducting particles limits carrier injection and consequently the rate performance. Similar to the development of the 0D Si，porous structure, core-shell structure, surface coating, and compositing with carbon matrix were also developed to modify the 1D Si since 2011. The results suggested that these surface modification strategies improved the electrochemical performance of the 1D Si.

(3) 2D Si thin films may be more robust than bulk Si over repeated cycles of Lithium ion insertion and extraction owing to their thin and uniform structure feature. Si thin films minimize volume variation and retain structural integrity, leading to improved cycle stability and rate capabilities. Meanwhile, it is possible to get rid of conductive additives and/or binders when the Si thin film anodes are exploited. The Si thin films emerged as potential LIB anodes in 1999 with capacities up to 1000 mAh g^{-1}, but the capacity faded severely after only a few cycles. Decreasing the thickness to nanometer range and increasing the surface roughness of the current collector were used to improve the cycle performance during 2000-2005. Several concepts including

improvement of the adherence force between the Si film and current collector, avoiding the use of current collector, and compositing with metal or carbon materials were developed since 2006. Recently, the strategies of fabricating current collectors with special structure feature, exploiting Si alloy film, and Si NWs film, porous or hollow structures were also introduced to maintain structural integrity and enhance the performance of the 2D Si film. Besides the Si thin film anodes, 2D Si nanosheets were also utilized as anode materials since 2011 due to easy accessibility of lithium ions, compatibility with other materials, and small volume expansion.

(4) Low-dimension Si materials inherit the major drawback of low tap density, which is not good to achieve decent volumetric energy density. On the contrary, 3D porous Si has attracted considerable attention due to their special structure feature and great promise for practical applications. The porous structure accommodates volume change during cycling without losing the structural integrity of the electrode. Meanwhile, the existing pores are helpful for electrolyte wetting, charge carrier transportation. The research on 3D porous Si was seen reported from 2011. Developing scalable synthetic methods based on sustainable source has been one of the major focuses in this area. Metal-assisted chemical etching process, top-down process, acid etching and magnesiothermic reduction have been developed. With this various methods, unique 3D porous silicon including hierarchical porous Si, hollow porous Si, and porous Si composites have been synthesized to achieve outstanding cyclic performance.

(5) In addition to the 0D Si, 1D Si, 2D Si and 3D Si, Si-based alloys and

Si-based multicomponent systems have also been widely studied as LIB anode due to their reasonable tap densities. Similarly, composting with matrix and hierarchical structure construction are adopted to improve the cyclic performance.

The systematic review elaborated in this manuscript tells that the main development trend for the silicon-based anode is evolving from nano-sized Si material to composite materials, and then to hierarchical structured materials. Nowadays, the combination of three strategies to fabricate the Si-based composites containing voids has become the mainstream. As a result, the major failure mechanisms responsible for rapid capacity fading of silicon materials can be inhibited, leading to enhanced cyclic performance. Nevertheless, delicate structure design is still mandatory to achieve outstanding performance. In future, further improvements will probably be achieved by simultaneously introducing new concepts of materials synthesis and hierarchical structure construction. We believe that improvements in the battery performance and the real applications of Si-based lithium-ion battery anode are on the near horizon.

Table 1. Si-based lithium-ion battery anodes between 1990 and 2000

1990 - 2000	Anode	Synthesis method	Cycling stability			Ref.
			Discharge capacity [mA h g^{-1}]	After n^{th} cycle	Current density [mA g^{-1}]	
SiOC	Si_zC_1-z	pyrolysis of siloxane polymers	near 600	1	18.6	29
	$C_{1-y-z}Si_zO_y$	pyrolysis of epoxy-silane composites	770	1	18.6	30
	Si-O-C	pyrolysis of pitch-polysilane blends	364-640	1	18.6	33
	Si-C-O	pyrolysis of Polysiloxanes	600-900	1	18.6	31
	Si-O-C	pyrolysis of pitch-polysilane blends	Over 600	1	18.6	32
Si/C nanocomposites	Si/C	nano Si on graphitic carbon by CVD	600	1	-	35
	Si/graphite composite($C_{0.8}Si_{0.2}$)	ball milling the mixture of Si (325 mesh) and graphite	794	20	45	40
	Si/C composite	manual grinding 78 nm Si with carbon black	1700	10	100μA cm^{-2}	41
Si/TiN Nanocomposites	Si/TiN Nanocomposite	HEMM Si and TiN	300	20	250 μA cm^{-2}	42
alloys	Mg_2Si	directly used	1370	1	10	46
	NiSi	HEMM NiSi powders	1180	1	80 μA cm^{-2}	48
Si films	Si film (1.2 μm)	CVD on porous Ni substrates	(1000)200	20	-	49

Table 2. Si-based lithium-ion battery anodes between 2001 and 2005

2001-2005	Development trend	Anode	Synthesis method	Cycling stability			Ref.
				Discharge capacity [mA h g^{-1}]	After n^{th} cycle	Current density [mA g^{-1}]	
alloys	pure alloys	SiAg	HEMM of Ag and Si powders	280	50	0.2 mA cm^{-2}	58
		Mg_2Si	milling of Mg and Si powders	100	25	15	59
		$CaSi_2$	HEMM of $CaSi_2$ powders	220	50	20μA cm^{-2}	60
	Alloy-graphite composites	$Fe_{20}Si_{80}$-graphite	ball milling the $Fe_{20}Si_{80}$ alloy with graphite	(600)400	25	-	55
		BaFeSi/graphite	ball milling of Ba–Fe–Si alloy and graphite powder	420	25	100	54
		FeSi/graphite	ball milling of Fe–Si alloy and graphite powder	500	15	100	61
		SiNi/graphite	HEMM of Si/Ni alloy and graphite	780	50	0.1C	62
Si Films/ Composite Films	Si Films	Si film (250 nm)	radio-frequency magnetron sputtering	3500	30	1680	65
		Si film(77 nm)	vacuum evaporation method	1500	700	2c	50
		Si film (50 nm)	vacuum deposited on a Ni foil	2000	1000	12c	66
		Si film (1.1 μm)	vacuum deposited on a Ni foil	1500	400	1c	69
	Composite Films	Si/TiN composite film	pulsed laser deposition	1000	40	5 μA cm^{-2}	70
		Fe/Si multilayer film	electron-beam evaporation method	3000 mAh cm^{-3}	300	30 μA cm^{-2}	71
		Mg_2Si film (30 nm)	pulsed laser deposition	2200	100	35 μA cm^{-2}	52
Si/C composites		Si/C nanocomposite	HEMM and pyrolysis of PS and Si powder	850	30	100 μA cm^{-2}	56
			HEMM and pyrolysis of PVA and Si	750	20	50	72

		powder				
		HEMM and pyrolysis of PVC and Si powder	900	40	300 μA cm^{-2}	93,73
		pyrolysis of carbon aerogel embedded with nano Si	1450	50	200	51
		CVD silane on the surface of graphite	1000	100	74	53
Other Si composites	Si/Ag composites	electroless plating	-	-	-	79
	Si/Cu composites	electroless plating	>1000	5	100	80
	Si/PPy composites	HEMM Si and PPy	~700	10	250 μA cm^{-2}	81

Table 3. Si-based lithium-ion battery anodes between 2006 and 2010

2006-2010	Development trend	Anode	Synthesis method	Cycling stability			Ref.
				Discharge capacity [mA h g^{-1}]	After n^{th} cycle	Current rate [mA g^{-1}]	
Si Alloy Composites	Alloy Composites	Cu_5Si–Si/graphite	HEMM of Cu–Si alloy and graphite powder	455	40	200 μA cm^{-2}	82
		$FeSi_6$/graphite	ball milling $FeSi_6$ alloy and graphite powder	615	50	100	83
		SiNi/graphite	arc-melting followed by HEMM	800	28	-	84,85
		Mg_2Si/C	ball-milling of Si and CNTs or CMS	400	30	50	86
		Fe–Cu–Si/C	HEMM of Fe, Cu, Si and graphite	385	30	253μA cm^{-2}	87
		SiMox-alloy	RF magnetron sputtering	1180	100	714 μAcm^{-2}	88
	Alloy Composites + Structure Design	Core-shell structure $NiSi_2$/carbon@active Si composite	heat-treatment on a mixture of Si powder and nickel phthalocyanine	~600	50	100	89
Si Films/ Composite Films	Si Films	Si films (200 nm)	RF magnetron sputtering	Over 1000	200	2100	92
		Si films (275nm)	magnetron sputtering	1910	500	0.5c	94
		Si films(3.6μm)	vacuum deposition on a well-etched Ni foil	Over 2000	50	1C	68
	Composite Films + Structure Design	Si nanowire array films (90μm)	metal catalytic etching of Si wafers	1000	30	150	96
		CNT-Si films (4 μm)	CVD deposition of a-Si on CNT film	~2000	100	1200	95
		Si-Al thin film	co-deposition from Si target	1800	350	0.05C	93

			embedded with Al rods				
0D Silicon/ 3D Carbon Composites	Si/porous C composite		mechanical mill and thermal treatment of Si, graphite, and PAN powder	660	30	160	99
			pyrolysis blends of Si and PVDF	660	50	180	100
			pyrolysis of composite gel of Si and RF	~800	10	100	102
	core/shell Si/C composite		spray pyrolysis of a mixture of Si powder and citric acid in ethanol	1450	20	100	13
			pyrolysis of a mixture of Si and PVDF in DMF	1290	30	50	101
0D Silicon/ 1D Carbon Composites	0D Si/CNTs Composites	Si/CNTs composite with a cage structure	CVD	940	20	156μA cm^{-2}	104
		core/shell type Si/CNTs composite	CVD	Over 1000	12	100	103
		Si/MWNTs nanocomposite	CVD	700	40	500	105
		Si/VACNTs composite	CVD	~1000	100	100	62
		Si/CNTs composite	ball milling Si and CNTs	584	20	35	106
		Si/CNTs/C composite	pyrolyzing the mixture of Si, CNTs and PVC	821	20	30	107
0D Si/2D C Composites	Si/Graphene Composites	Si/Graphene Composite	manual mixing Si and Graphene	1168	30	100	109
		Si/Graphene paper Composite	Filtrating suspension of Si and graphene, followed by thermal reduction treatment.	1500	200	100	111
		self-supporting	filtrate suspension of Si and RGO,	1040	30	50	112

		Si/RGO composite film	followed by thermal reduction treatment				
Si NWs and composites	Si NWs	Si NWs 89 nm	VLS	~3000	10	C/20	116
		Si NWs	MCEE	0.5 mAh cm^{-2}	3	200μA cm^{-2}	117
		Si NWs < 100 nm,	CVD	2500	1	50	118
	Si NWs composites + structure design	core-shell Si NWs	CVD	800	100	6800	120
		C-Si core-shell NWs	CVD	1300	50	120	121
		carbon coating Si NWs	SFLS	1500	30	210	125
		mesoporous Si@carbon core-shell nanowire	template	2750	80	600	126
Si NTs	Si NTs	Si Nanotubes	template	3648	1	600	127
		sealed Si Nanotubes	template	2397	50	2100	128
3D Si and composites	3D Si	porous bulk Si	thermal annealing and etching	2800	100	400	129
		nest-like Si particles	solvothermal reaction	1095	48	2000	17
	3D Si composites	silver coated 3D macroporous Si	magnesiothermic reduction reaction and silver mirror reaction	2900	100	100	21

Table 4. Si-based lithium-ion battery anodes from 2011 to 2015

2011-2015	Development trend	Anode	Synthesis method	Cycling stability			Ref.
				Discharge capacity [mA h g^{-1}]	After n^{th} cycle	Current rate [mA g^{-1}]	
Si Alloys/Alloy Composites	Alloy Composites	Mg_2Si	hydrogen-driven chemical reaction	406	60	100	130
		Mg_2Si/C composites	situ decomposition of C_2H_2 gas on Mg_2Si	320	100	100	131
		$FeSi_2$/Si@C composite	ball milling	940	200	100	132
		Si/NiTi	arc melting and rapid quenching	698	50	100	139
		$Si/Ti_4Ni_4Si_7$	melt spinning	1000	50	100	140
		Si/NiTi composite	HEMM	553	52	2.5 mA cm^{-2}	141
		$Si/FeSi_2Ti$	melt-spinning	~620	50	0.1c	142
	Alloy Composites + 3D structure	Core-shell $FeSi_2$@Si@graphene	magnesiothermic reduction	510	100	100	133
		porous $NiSi_2$/Si/Carbon composite	template	1272	200	2034	134
Si Films/Composite Films	Composite Film	Mg-Si film	magnetron sputter deposition	1400	400	3.2C	143
		Si film	electrodeposition on Ni foam	2800	80	360	144
	Composite Film + 3D structure	porous Si-Al film	magnetron sputtering (co-sputtering) on Cu foam	1268	50	50 μA cm^{-2}	145
		3D Si/MCFs film	TCVD	1087	200	750 μA cm^{-2}	146
		Patterned Si	atomic layer deposition (ALD)	1100	100	3750	147
		Si-Cu-Ti thin films with Cu_3Si nanowires	magnetron sputtering and ALD	900	100	20 μA cm^{-2}	148
		Si/MWCNTs film	CVD and spin coating process	1510	100	840	150

		Si-porous carbon layers and graphene layers (Si-C/G)	ESD and heat treatment	760	100	200	151
		CNS/Si/Al_2O_3 core-shell film	plasma enhanced chemical vapour deposition (PECVD) and ALD	1560	100	1000	152
Si NSs/ composites	Si NSs	ultrathin Si NSs	template	600	100	0.1C	153
		ultrathin Si NSs	DC arc-discharge plasma	441	40	100	156
	Si NSs composite	Si NSs/RGO	magnesiothermic reduction	1000	50	200	157
		Ni-Si NSs	solvothermal method, PECVD and H_2 reduction process	655	1000	8400	158
		Carbon-coated Si NSs	molten salt-induced exfoliation and chemical reduction	798	500	0.5C	159
0D Si/3D C Composites	Embedding Type 0D Si/ 3D C Composites	Si/ mesoporous C composite	solvent evaporation induced self-assembly (EISA)	1018	100	500	161
		Si/ mesoporous C composite	EISA	700	50	2000	8
		Si/ mesoporous C composite	magnesiothermic reduction	1480	1000	2000	160
		Si/void/porous carbon composite	template	980	80	100	162
		Si/dendritic C nanocomposite	a hierarchical bottom-up self-assembly process	~1500	100	372	163
	Solid core–shell structured 0D Si/ 3D C Composites	Solid core–shell structured Si/C	substrate induced coagulation method	1800	50	100	164
		Si/C nanofibers	electrospinning	721	300	2750	165
	hollow core-shell	yolk-shell type Si/C	template	1110	1000	400	166

	structured 0D Si/ 3D C Composites	composite					
		Si pomegranates	Evaporation-driven self-assembly + template	1160	1000	400	11c
		hollow core-shell Si/C composite	template (etching SiO_2)	650	100	1000	167
		hollow core-shell Si/C composite	template (etching SiO_2)	1340	100	100	168
		Si/void/SiO_2/void/C nanostructures	template (etching SiO_2)	956	430	460	169
0D Si/1D C Composites	0D Si/CNT Composites	Si decorated with vertically aligned CNTs	two-step CVD	800	100	5.9mA cm^{-2}	172
		Si/MWCNT composite	a manual scribing action of VASCNTs on a copper foil	2365	50	300	173
		Si/MWCNT composite	magnesiothermic reduction	520	70	400	174
		Si/CNTs composite	drop-casting and annealing	925	200	0.1 C	175
0D Si/2D C Composites	0D Si/ Graphene Composites	Si/graphene composite	magnesiothermic reduction	1374	120	100	177
		Si/graphene composite	aerosol spraying	1800	120	100	178
		Si backboned-graphene composite	decomposition	1103	1000	56	179
		3D Si/graphene/graphite foam	drop-casting	370	100	400	180
		graphene/Si/carbon composites	hybrid electrostatic assembly and carbon coating	902	100	300	181
		graphene/Si/carbon composites	assembly	1050	300	2000	182
		graphene/Si/carbon	electrospinning and pyrolysis	1521	200	840	183

		composites					
Other 0D Si composites	Si/metal oxide composite	$Si@TiO_2$ composite	hydrolysis combined with magnesiothermic reduction	804	100	0.1c	185
		Si $@TiO_{2-x}$/C mesoporous microfiber composite	electrospinning	~800	50	1000	186
		Si/Ti_2O_3/reduced graphene oxide (rGO)	mechanical blending and thermal treatment	985	100	100	187
	Si/MOFs composite	MOFs	*in situ* mechano-chemical synthesis	830	500	200	188
	Si/conductive polymer composite	Si/PPP composites	ball milling	1600	400	300	189
Si NWs	Si NWs	Tin-Seeded Si NWs (50 nm)	SFLS	1800	100	358	190
		Si NWs(50-100nm)	Cu-catalyzed CVD	>1000	100	840	191
		Tin Catalyzed Si NWs (105 ±30 nm)	SVG	1078	50	1245	192
		Si NWs(80-150 nm)	MAC	-	-	-	193
	Si NWs + structure design	porous Si NWs	etching Si wafers	2000	250	2000	194
		Si nanowire arrays (n-SNWAs)	CVD	2178	50	400	195
		Si NWs fabric	SFLS	800	20	179	197
Si NWs Composites	Coated Si NWs	Carbon coated Si NWs	SFLS and pyrolysis	2000	100	260	198
		PEDOT coated Si NWs	electropolymerization processes	2510	100	840	199
		Cu coated Si NWs	CVD and magnetron sputtering	2562	15	210	200
		Ag-coated Si NWs	MACE and redox processes	707	30	0.5C	201
		Sn-coated Si NWs	VLS and CVD	1865	100	0.1C	202

		Mg and Mg_2Si coated Si NWs	VLS and RF magnetron sputtering	~800	100	0.1C	203
	core-shell structured Si NWs	Si NWs dwelled in the hollow graphitic tubes	VLS, CVD and HF etching	1100	1000	4200	204
		Si-SiOx core-shell nanowires	heat treatment	2000	100	740	205
	Si NWs /graphene Composites	Si NWs/graphene papers	SFLS	1400	30	420	206
		graphene-wrapped Si NWs (core/shell)	electrostatic self-assembly	1335	80	200	207
		Si NWs/rGO composite	solvothermal synthesis and CVD	2300	100	300	208
		core-shell SiC/Si/ graphene	electrochemical etching techniques and MPCVD	1560	500	800	209
Si NTs and their Composites	Si NTs	Si NTs	magnesiothermic thermal reduction	1000	90	0.5C	211
	Si NTs Composites	carbon coated Si NTs	surface sol-gel reaction and magnesiothermic reduction	~800	90	400	210
		C@SiNTs	CVD	2085	200	840	213
		CNT on the Si NTs	template	800	250	1700	214
	Si NTs + structure design	porous Si NTs	template	1670	30	210	212
		C@Si@C nanotube sandwich structure	CVD and etching	2200	60	0.07 C	215
		copper/Si core–shell nanotube arrays	template	1506	400	840	216
		double-walled Si-SiO_x nanotube	electrospinning and CVD	600	6000	24000	217
3D Si and their Composites	3D Si	nanoporous Si	Template synthesis + HF etching	2800	100	400	219
	3D Si composite	Ag coated 3D porous Si	metal-assisted chemical etching	2500	100	0.2C	220

			process				
		Carbon-coated multi-dimensional Si	metal-assisted chemical etching process	2083	70	0.2C	221
		Carbon-coated 3D macroporous silicon	Electroless metal deposition and metal-assisted chemical etching process	1683	50	400	222
	3D Si with cheap source and scalable method	Bulk-nanoporous-Si	a top-down process	1500	500	1800	223
		nanoporous Si networks	electrochemical process	1000	200	1c	224
		porous Si NPs with RGO	boron doping and electroless etching	1400	200	0.25c	225
		nanoporous Si coated with C and RGO	ball milling and stain-etching	1100	600	2000	226
		porous Si	etching on the Al/Si alloy	2277	258	100	227
		Cu coated porous Si	acid-etching Al/Si alloy followed by electroless plating	1651	150	200	228
		micro-sized porous Si	acid-etching Fe/Si alloy	1250	100	500	229
		Carbon coated micro-sized porous Si	acid etching, ball-milling and carbonization	1041	300	500	230
		porous Si/RGO nanocomposites	acid etching Al/Si eutectic and in-situ reduced graphene oxide	1521	100	4000	231
		peanut shell structured carbon coated porous Si	electrochemical process	1179	120	188	232
	3D Si originated from magnesiothermic reduction of SiO_2	mesoporous Si	magnesiothermic reduction of Stöber SiO_2	1444	100	400	234
		monodisperse porous Si nanospheres	magnesiothermic reduction of Stöber SiO_2	1500	500	1789	236
		porous Si nanospheres	magnesiothermic reduction of solid	1800	200	180	23

		composed of porous shell and hollow core	core/mesoporous shell SiO_2 spheres				
		$TiSi_2$ coated porous Si	magnesiothermic reduction of Stöber SiO_2 followed by coating with $TiSi_2$	1577	50	400	237
		3D interconnected porous Si/carbon	magnesiothermic reduction of silica aerogels	1552	200	200	238
		ordered porous Si@C nanorods	magnesiothermic reduction of SBA-15	627	220	100	239
		porous Si/C composites	magnesiothermic reduction of diatomite	759	30	50	241
	hollow Si spheres	hollow Si nanospheres	template +HF etch	2500	700	220	242
		Ag coated hollow porous Si	magnesiothermic reduction of hollow porous SiO_2	3400	100	500	243
		PPy@porous Si hollow spheres nanocomposite	magnesiothermic reduction and *in situ* chemical polymerization	2000	250	1000	244

Table 5. Si based multicomponent lithium-ion battery anodes

	Anode	Synthesis method	Cycling stability			
			Discharge capacity [mA h g^{-1}]	After n^{th} cycle	Current rate [mA g^{-1}]	Ref.
Si-based multicomponent systems	Si nanocluster-SiO_x-C composites	disproportionation of SiO and the polymerization of furfuryl alcohol	700	200	1mA cm^{-2}	246
	nano-Si/SiO_x/graphite composite	disproportionation of SiO and HEMM with graphite	1061	100	100	247
	3D porous Si-based multicomponent	chemical-assisted thermal disproportionation of porous SiO	1600	100	0.1C	248
	Si-SiO-SiO_2 multicomponent	high-temperature annealing process	1280	200	0.2C	249
	nanotube-type Si-based multicomponents	coaxial electrospinning technique and subsequent metallothermic reduction reaction	765	280	0.5C	250
	Si-based multicomponent	sol-gel process	~650	1000	1C	251
	Fe-Cu-Si ternary composite	scalable spray drying and facile heat treatment	1261	50	210	252

Table 6. Si-based lithium-ion battery anodes in 2016

2016	**Anode**	**Synthesis method**	**Cycling stability**			
			Discharge capacity [mA h g^{-1}]	**After n^{th} cycle**	**Current rate [mA g^{-1}]**	**Ref.**
0D Si NPs	Si NPs/graphene composite.	top-down dispersion and bottom-up synthesis	>1200	600	500	254
0D Si NPs	Si NPs/ rGO- hybrid	sol-gel reaction followed by magnesiothermic reduction	1165	100	2100	255
0D Si NPs	SNPs@void@ mGra	melting self-assembly route	1287	500	500	256
0D Si NPs	Si@C-rGO	stirring and vacuum filtration	930	400	300	257
0D Si NPs	Si NPs/graphene foam	freeze-drying method	1295	180	500	258
0D Si NPs	Si-nanolayer-embedded graphite/carbon hybrids	CVD	496	100	0.5C	260
Si microparticles (1–3μm)	graphene cages/um silicon	using a dual-purpose Ni template	2805	300	210	259
3D Si	granadilla-like silicon/carbon composite	templating method	1100	200	250	261

Acknowledgements

This research is funded by the open project of the Beijing National Laboratory for Molecular Science (20140138), CAS-EU S&T cooperation partner program (174433KYSB20150013), and Ningbo Key Laboratory of Polymer Materials. The authors thank Shanshan Yin for helping with manuscript polish.

References

[1] J.M. Tarascon, M. Armand, Nature 414 (2001) 359-367.

[2] B. Scrosati, J. Garche, J. Power Sources 195 (2010) 2419-2430.

[3] M. Armand, J.-M. Tarascon, Nature 451 (2008) 652-657.

[4] P. Roy, S.K. Srivastava, J. Mater. Chem. A 3 (2015) 2454-2484.

[5] W.J. Zhang, J. Power Sources 196 (2011) 13-24.

[6] K.M. Abraham, J. Phys. Chem. Lett. (2015) 830-844.

[7] B.A. Boukamp, G.C. Lesh, R.A. Huggins, J. Electrochem. Soc. 128 (1981) 725-729.

[8] B. Liang, Y. Liu, Y. Xu, J. Power Sources 267 (2014) 469-490.

[9] H. Wu, Y. Cui, Nano Today 7 (2012) 414-429.

[10] L.Y. Beaulieu, K.W. Eberman, R.L. Turner, L.J. Krause, J.R. Dahn, Electrochem. Solid-State Lett. 4 (2001) A137-A140.

[11] J.H. Ryu, J.W. Kim, Y.-E. Sung, S.M. Oh, Electrochem. Solid-State Lett. 7 (2004) A306-A309.

[12] M.A. Rahman, G. Song, A.I. Bhatt, Y.C. Wong, C. Wen, Adv. Funct. Mater. 26 (2016) 647-678.

[13] S.H. Ng, J. Wang, D. Wexler, K. Konstantinov, Z.P. Guo, H.K. Liu, Angew. Chem. 45 (2006) 6896-6899.

[14] C.K. Chan, R. Ruffo, S.S. Hong, Y. Cui, J. Power Sources 189 (2009) 1132-1140.

[15] Y. Oumellal, N. Delpuech, D. Mazouzi, N. Dupre, J. Gaubicher, P. Moreau, P. Soudan, B. Lestriez, D. Guyomard, J. Mater. Chem. 21 (2011) 6201-6208.

[16] M. Ashuri, Q. He, L.L. Shaw, Nanoscale 8 (2016) 74-103.

[17] H. Ma, F. Cheng, J.Y. Chen, J.Z. Zhao, C.S. Li, Z.L. Tao, J. Liang, Adv. Mater. 19 (2007) 4067-4070.

[18] C.K. Chan, H. Peng, G. Liu, K. McIlwrath, X.F. Zhang, R.A. Huggins, Y. Cui, Nat. Nanotechnol. 3 (2008) 31-35.

[19] N. Liu, Z. Lu, J. Zhao, M.T. McDowell, H.W. Lee, W. Zhao, Y. Cui, Nat. Nanotechnol. 9 (2014) 187-192.

[20] L. Baggetto, D. Danilov, P.H. Notten, Adv. Mater. 23 (2011) 1563-1566.

[21] Y. Yu, L. Gu, C. Zhu, S. Tsukimoto, P.A. van Aken, J. Maier, Adv. Mater. 22 (2010) 2247-2250.

[22] X. Li, M. Gu, S. Hu, R. Kennard, P. Yan, X. Chen, C. Wang, M.J. Sailor, J.-G. Zhang, J. Liu, Nat. Commun. 5 (2014)4105.

[23] Q. Xiao, M. Gu, H. Yang, B. Li, C. Zhang, Y. Liu, F. Liu, F. Dai, L. Yang, Z. Liu, X. Xiao, G. Liu, P. Zhao, S. Zhang, C. Wang, Y. Lu, M. Cai, Nat. Commun. 6 (2015)8844.

[24] D.L. Ma, Z.Y. Cao, A.M. Hu, Nano-Micro Lett. 6 (2014) 347-358.

[25] A.N. Dey, J. Electrochem. Soc. 118 (1971) 1547-1549.

[26] R.A. Sharma, R.N. Seefurth, J. Electrochem. Soc. 123 (1976) 1763-1768.

[27] R.N. Seefurth, R.A. Sharma, J. Electrochem. Soc. 124 (1977) 1207-1214.

[28] C. van der Marel, G.J.B. Vinke, W. van der Lugt, Solid State Commun. 54 (1985) 917-919.

[29] A.M. Wilson, J.N. Reimers, E.W. Fuller, J.R. Dahn, Solid State Ionics 74 (1994) 249-254.

[30] J.S. Xue, K. Myrtle, J.R. Dahn, J. Electrochem. Soc. 142 (1995) 2927-2935.

[31] W.B. Xing, A.M. Wilson, K. Eguchi, G. Zank, J.R. Dahn, J. Electrochem. Soc. 144 (1997) 2410-2416.

[32] W.B. Xing, A.M. Wilson, G. Zank, J.R. Dahn, Solid State Ionics 93 (1997) 239-244.

[33] A.M. Wilson, W. Xing, G. Zank, B. Yates, J.R. Dahn, Solid State Ionics 100 (1997) 259-266.

[34] A.M. Wilson, B.M. Way, J.R. Dahn, T. van Buuren, J. Appl. Phys. 77 (1995) 2363-2369.

[35] P. Colombo, G. Mera, R. Riedel, G.D. Soraru, J. Am. Ceram. Soc. 93 (2010) 1805-1837.

[36] A.M. Wilson, G. Zank, K. Eguchi, W. Xing, J.R. Dahn, J. Power Sources 68 (1997) 195-200.
[37] J.S. Xue, K. Myrtle, J.R. Dahn, J. Electrochem. Soc. 142 (1995) 2927-2935.
[38] D. Larcher, C. Mudalige, A.E. George, V. Porter, M. Gharghouri, J.R. Dahn, Solid State Ionics 122 (1999) 71-83.
[39] A.M. Wilson, W.B. Xing, G. Zank, B. Yates, J.R. Dahn, Solid State Ionics 100 (1997) 259-266.
[40] C.S. Wang, G.T. Wu, X.B. Zhang, Z.F. Qi, W.Z. Li, J. Electrochem. Soc. 145 (1998) 2751-2758.
[41] H. Li, X.J. Huang, L.Q. Chen, Z.G. Wu, Y. Liang, Electrochem. Solid-State Lett. 2 (1999) 547-549.
[42] I. Kim, P.N. Kumta, G.E. Blomgren, Electrochem. Solid-State Lett. 3 (2000) 493-496.
[43] J.O. Besenhard, P. Komenda, A. Paxinos, E. Wudy, M. Josowicz, Solid State Ionics 18–19 (1986) 823-827.
[44] O. Mao, R.A. Dunlap, J.R. Dahn, J. Electrochem. Soc. 146 (1999) 405-413.
[45] J.O. Besenhard, M. Hess, P. Komenda, Solid State Ionics 40–41 (1990) 525-529.
[46] H. Kim, J. Choi, H.J. Sohn, T. Kang, J. Electrochem. Soc. 146 (1999) 4401-4405.
[47] T. Moriga, K. Watanabe, D. Tsuji, S. Massaki, I. Nakabayashi, J. Solid State Chem. 153 (2000) 386-390.
[48] G.X. Wang, L. Sun, D.H. Bradhurst, S. Zhong, S.X. Dou, H.K. Liu, J. Alloys Compd. 306 (2000) 249-252.
[49] S. Bourderau, T. Brousse, D.M. Schleich, J. Power Sources 81 (1999) 233-236.
[50] S. Ohara, J. Suzuki, K. Sekine, T. Takamura, J. Power Sources 119-121 (2003) 591-596.
[51] G.X. Wang, J.H. Ahn, J. Yao, S. Bewlay, H.K. Liu, Electrochem. Commun. 6 (2004) 689-692.
[52] S.W. Song, K.A. Striebel, R.P. Reade, G.A. Roberts, E.J. Cairns, J. Electrochem. Soc. 150 (2003) A121-A127.
[53] M. Holzapfel, H. Buqa, W. Scheifele, P. Novak, F.-M. Petrat, Chem. Commun. 12(2005) 1566-1568.
[54] H. Dong, X.P. Ai, H.X. Yang, Electrochem. Commun. 5 (2003) 952-957.
[55] H.Y. Lee, S.M. Lee, J. Power Sources 112 (2002) 649-654.
[56] I.-S. Kim, P.N. Kumta, J. Power Sources 136 (2004) 145-149.
[57] Y. Liu, K. Hanai, J. Yang, N. Imanishi, A. Hirano, Y. Takeda, Electrochem. Solid-State Lett. 7 (2004) A369.
[58] S.-M. Hwang, H.-Y. Lee, S.-W. Jang, S.-M. Lee, S.-J. Lee, H.-K. Baik, J.-Y. Lee, Electrochem. Solid-State Lett. 4 (2001) A97-A100.
[59] G.A. Roberts, E.J. Cairns, J.A. Reimer, J. Power Sources 110 (2002) 424-429.
[60] J. Wolfenstine, J. Power Sources 124 (2003) 241-245.
[61] H. Dong, R.X. Feng, X.P. Ai, Y.L. Cao, H.X. Yang, Electrochim. Acta 49 (2004) 5217-5222.
[62] M.S. Park, Y.J. Lee, S. Rajendran, M.S. Song, H.S. Kim, J.Y. Lee, Electrochim. Acta 50 (2005) 5561-5567.
[63] H. Jung, M. Park, S.H. Han, H. Lim, S.-K. Joo, Solid State Commun. 125 (2003) 387-390.
[64] H. Jung, M. Park, Y.-G. Yoon, G.-B. Kim, S.-K. Joo, J. Power Sources 115 (2003) 346-351.
[65] J.P. Maranchi, A.F. Hepp, P.N. Kumta, Electrochem. Solid-State Lett. 6 (2003) A198-A201.
[66] T. Takamura, S. Ohara, M. Uehara, J. Suzuki, K. Sekine, J. Power Sources 129 (2004) 96-100.
[67] K.-L. Lee, J.-Y. Jung, S.-W. Lee, H.-S. Moon, J.-W. Park, J. Power Sources 129 (2004) 270-274.
[68] T. Takamura, M. Uehara, J. Suzuki, K. Sekine, K. Tamura, J. Power Sources 158 (2006) 1401-1404.
[69] M. Uehara, J. Suzuki, K. Tamura, K. Sekine, T. Takamura, J. Power Sources 146 (2005) 441-444.
[70] Y. Zhang, Z.-W. Fu, Q.-Z. Qin, Electrochem. Commun. 6 (2004) 484-491.
[71] J.-B. Kim, H.-Y. Lee, K.-S. Lee, S.-H. Lim, S.-M. Lee, Electrochem. Commun. 5 (2003) 544-548.

[72] Z.P. Guo, E. Milin, J.Z. Wang, J. Chen, H.K. Liu, J. Electrochem. Soc. 152 (2005) A2211-A2216.
[73] K. Hanai, Y. Liu, N. Imanishi, A. Hirano, M. Matsumura, T. Ichikawa, Y. Takeda, J. Power Sources 146 (2005) 156-160.
[74] G.X. Wang, J. Yao, H.K. Liu, Electrochem. Solid-State Lett. 7 (2004) A250-A253.
[75] M. Holzapfel, H. Buqa, F. Krumeich, P. Novák, F.M. Petrat, C. Veit, Electrochem. Solid-State Lett. 8 (2005) A516-A520.
[76] N. Dimov, K. Fukuda, T. Umeno, S. Kugino, M. Yoshio, J. Power Sources 114 (2003) 88-95.
[77] W.-R. Liu, J.-H. Wang, H.-C. Wu, D.-T. Shieh, M.-H. Yang, N.-L. Wu, J. Electrochem. Soc. 152 (2005) A1719-A1725.
[78] M. Yoshio, H. Wang, K. Fukuda, T. Umeno, N. Dimov, Z. Ogumi, J. Electrochem. Soc. 149 (2002) A1598-A1603.
[79] X. Wu, Z. Wang, L. Chen, X. Huang, Electrochem. Commun. 5 (2003) 935-939.
[80] J.W. Kim, J.H. Ryu, K.T. Lee, S.M. Oh, J. Power Sources 147 (2005) 227-233.
[81] Z.P. Guo, J.Z. Wang, H.K. Liu, S.X. Dou, J. Power Sources 146 (2005) 448-451.
[82] Y. NuLi, B. Wang, J. Yang, X. Yuan, Z. Ma, J. Power Sources 153 (2006) 371-374.
[83] T. Li, Y.L. Cao, X.P. Ai, H.X. Yang, J. Power Sources 184 (2008) 473-476.
[84] H.-Y. Lee, Y.-L. Kim, M.-K. Hong, S.-M. Lee, J. Power Sources 141 (2005) 159-162.
[85] M.-S. Park, S. Rajendran, Y.-M. Kang, K.-S. Han, Y.-S. Han, J.-Y. Lee, J. Power Sources 158 (2006) 650-653.
[86] J.M. Yan, H.Z. Huang, J. Zhang, Y. Yang, J. Power Sources 175 (2008) 547-552.
[87] C.H. Doh, H.M. Shin, D.H. Kim, Y.D. Jeong, S.I. Moon, B.S. Jin, H.S. Kim, K.W. Kim, D.H. Oh, A. Veluchamy, J. Alloys Compd. 461 (2008) 321-325.
[88] C.-M. Hwang, C.-H. Lim, J.-H. Yang, J.-W. Park, J. Power Sources 194 (2009) 1061-1067.
[89] T. Kim, S. Park, S.M. Oh, Electrochem. Commun. 8 (2006) 1461-1467.
[90] M.S. Park, G.X. Wang, H.K. Liu, S.X. Dou, Electrochim. Acta 51 (2006) 5246-5249.
[91] T.D. Hatchard, J.M. Topple, M.D. Fleischauer, J.R. Dahn, Electrochem. Solid-State Lett. 6 (2003) A129-A132.
[92] T. Moon, C. Kim, B. Park, J. Power Sources 155 (2006) 391-394.
[93] L.B. Chen, J.Y. Xie, H.C. Yu, T.H. Wang, Electrochim. Acta 53 (2008) 8149-8153.
[94] L.B. Chen, J.Y. Xie, H.C. Yu, T.H. Wang, J. Appl. Electrochem. 39 (2009) 1157-1162.
[95] L.-F. Cui, L. Hu, J.W. Choi, Y. Cui, Acs Nano 4 (2010) 3671-3678.
[96] A.M. Morales, C.M. Lieber, Science 279 (1998) 208-211.
[97] R. Huang, J. Zhu, Mater. Chem. Phys. 121 (2010) 519-522.
[98] W. Wang, P.N. Kumta, Acs Nano 4 (2010) 2233-2241.
[99] M.K. Datta, P.N. Kumta, J. Power Sources 158 (2006) 557-563.
[100] Y. Liu, Z.Y. Wen, X.Y. Wang, A. Hirano, N. Imanishi, Y. Takeda, J. Power Sources 189 (2009) 733-737.
[101] Y. Xu, G. Yin, Y. Ma, P. Zuo, X. Cheng, J. Mater. Chem. 20 (2010) 3216-3220.
[102] K.M.C. Lee J K, Trahey L, Missaghi M N, Kung H H. Chem. Mater. 2 (2009) 6-8.
[103] T. Kim, Y.H. Mo, K.S. Nahm, S.M. Oh, J. Power Sources 162 (2006) 1275-1281.
[104] J. Shu, H. Li, R.Z. Yang, Y. Shi, X.J. Huang, Electrochem. Commun. 8 (2006) 51-54.
[105] P.F. Gao, Y. Nuli, Y.S. He, J.Z. Wang, A.I. Minett, J. Yang, J. Chen, Chem. Commun. 46 (2010) 9149-9151.
[106] Y. Zhang, X.G. Zhang, H.L. Zhang, Z.G. Zhao, F. Li, C. Liu, H.M. Cheng, Electrochim. Acta 51 (2006)

4994-5000.
[107] Z. Zhou, Y. Xu, M. Hojamberdiev, W. Liu, J. Wang, J. Alloys Compd. 507 (2010) 309-311.
[108] Z. Zhou, Y. Xu, W. Liu, L. Niu, J. Alloys Compd. 493 (2010) 636-639.
[109] S. Park, R.S. Ruoff, Nat. Nanotechnol. 4 (2009) 217-224.
[110] S.-L. Chou, J.-Z. Wang, M. Choucair, H.-K. Liu, J.A. Stride, S.-X. Dou, Electrochem. Commun. 12 (2010) 303-306.
[111] J.K. Lee, K.B. Smith, C.M. Hayner, H.H. Kung, Chem. Commun. 46 (2010) 2025-2027.
[112] H.-C. Tao, L.-Z. Fan, Y. Mei, X. Qu, Electrochem. Commun. 13 (2011) 1332-1335.
[113] S.C. Zhang, Z.J. Du, R.X. Lin, T. Jiang, G.R. Liu, X.M. Wu, D.S. Weng, Adv. Mater. 22 (2010) 5378-5382.
[114] G.W. Zhou, H. Li, H.P. Sun, D.P. Yu, Y.Q. Wang, X.J. Huang, L.Q. Chen, Z. Zhang, Appl. Phys. Lett. 75 (1999) 2447-2449.
[115] H. Li, X. Huang, L. Chen, G. Zhou, Z. Zhang, D. Yu, Y. Jun Mo, N. Pei, Solid State Ionics 135 (2000) 181-191.
[116] B. Gao, S. Sinha, L. Fleming, O. Zhou, Adv. Mater. 13 (2001) 816-819.
[117] K. Peng, J. Jie, W. Zhang, S.-T. Lee, Appl. Phys. Lett. 93 (2008) 033105.
[118] H.K. Seong, M.H. Kim, H.J. Choi, Y.J. Choi, J.G. Park, Met. Mater. Int. 14 (2008) 477-480.
[119] B. Laïk, L. Eude, J.-P. Pereira-Ramos, C.S. Cojocaru, D. Pribat, E. Rouvière, Electrochim. Acta 53 (2008) 5528-5532.
[120] L.-F. Cui, R. Ruffo, C.K. Chan, H. Peng, Y. Cui, Nano Lett. 9 (2009) 491-495.
[121] L.F. Cui, Y. Yang, C.M. Hsu, Y. Cui, Nano Lett. 9 (2009) 3370-3374.
[122] C.K. Chan, R. Ruffo, S.S. Hong, R.A. Huggins, Y. Cui, J. Power Sources 189 (2009) 34-39.
[123] R. Ruffo, S.S. Hong, C.K. Chan, R.A. Huggins, Y. Cui, J. Phys. Chem. C 113 (2009) 11390-11398.
[124] K. Kang, H.-S. Lee, D.-W. Han, G.-S. Kim, D. Lee, G. Lee, Y.-M. Kang, M.-H. Jo, Appl. Phys. Lett. 96 (2010) 053110.
[125] P.R.N. Chan C K, O'Connell M J, Korgel B A, Cui Y. ACS Nano 2010, 4 (2010) 1443–1450.
[126] H. Kim, J. Cho, Nano Lett. 8 (2008) 3688-3691.
[127] K.M.G. Park M H, Joo J, Kim K, Kim J, Ahn S, Cui Y, Cho J. Nano Lett. 9 (2009) 3844-3847.
[128] T. Song, J. Xia, J.H. Lee, D.H. Lee, M.S. Kwon, J.M. Choi, J. Wu, S.K. Doo, H. Chang, W.I. Park, D.S. Zang, H. Kim, Y. Huang, K.C. Hwang, J.A. Rogers, U. Paik, Nano Lett. 10 (2010) 1710-1716.
[129] H. Kim, B. Han, J. Choo, J. Cho, Angew. Chem. 47 (2008) 10151-10154.
[130] R. Ma, Y. Liu, Y. Yang, M. Gao, H. Pan, Appl. Phys. Lett. 105 (2014) 213901.
[131] C. Xiao, N. Du, H. Zhang, D. Yang, J. Alloys Compd. 587 (2014) 807-811.
[132] Y. Chen, J.F. Qian, Y.L. Cao, H.X. Yang, X.P. Ai, ACS Appl. Mater. Interfaces 4 (2012) 3753-3758.
[133] K. Adpakpang, J.-e. Park, S.M. Oh, S.-J. Kim, S.-J. Hwang, Electrochim. Acta 136 (2014) 483-492.
[134] H. Jia, C. Stock, R. Kloepsch, X. He, J.P. Badillo, O. Fromm, B. Vortmann, M. Winter, T. Placke, ACS Appl. Mater. Interfaces 7 (2015) 1508-1515.
[135] X.L. Ji, L.F. Nazar, J. Mater. Chem. 20 (2010) 9821-9826.
[136] J.Q. Huang, X.F. Liu, Q. Zhang, C.M. Chen, M.Q. Zhao, S.M. Zhang, W.C. Zhu, W.Z. Qian, F. Wei, Nano Energy 2 (2013) 314-321.
[137] S. Iwamura, H. Nishihara, Y. Ono, H. Morito, H. Yamane, H. Nara, T. Osaka, T. Kyotani, Sci.Rep. 5 (2015) 8085.
[138] R. Hu, M. Zhu, H. Wang, J. Liu, O. Liuzhang, J. Zou, Acta Mater. 60 (2012) 4695-4703.
[139] H. Jung, Y.-U. Kim, M.-S. Sung, Y. Hwa, G. Jeong, G.-B. Kim, H.-J. Sohn, J. Mater. Chem. 21 (2011)

11213-11216.
[140] S.-B. Son, S.C. Kim, C.S. Kang, T.A. Yersak, Y.-C. Kim, C.-G. Lee, S.-H. Moon, J.S. Cho, J.-T. Moon, K.H. Oh, S.-H. Lee, Adv. Energy Mater. 2 (2012) 1226-1231.
[141] C. Loka, H. Yu, K.-S. Lee, J. Cho, J. Power Sources 244 (2013) 259-265.
[142] M.R. Jo, Y.U. Heo, Y.C. Lee, Y.M. Kang, Nanoscale 6 (2014) 1005-1010.
[143] G. Schmuelling, M. Winter, T. Placke, ACS Appl. Mater. Interfaces 7 (2015) 20124-20133.
[144] G. Zhao, Y. Meng, N. Zhang, K. Sun, Mater. Lett. 76 (2012) 55-58.
[145] P. Liu, J. Zheng, Y. Qiao, H. Li, J. Wang, M. Wu, J. Solid State Electrochem. 18 (2014) 1799-1806.
[146] K.-F. Chiu, S.-H. Su, H.-J. Leu, C.-Y. Wu, Surf. Coat.Technol. 267 (2015) 70-74.
[147] Y. He, X. Yu, Y. Wang, H. Li, X. Huang, Adv. Mater. 23 (2011) 4938-4941.
[148] K. Xu, Y. He, L. Ben, H. Li, X. Huang, J. Power Sources 281 (2015) 455-460.
[149] N. Paul, J. Brumbarov, A. Paul, Y. Chen, J.F. Moulin, P. Muller-Buschbaum, J. Kunze-Liebhauser, R. Gilles, J. Appl. Crystallogr. 48 (2015) 444-454.
[150] K.-S. Park, K.-M. Min, S.-D. Seo, G.-H. Lee, H.-W. Shim, D.-W. Kim, Mater. Res. Bull. 48 (2013) 1732-1736.
[151] J. Wu, X. Qin, H. Zhang, Y.-B. He, B. Li, L. Ke, W. Lv, H. Du, Q.-H. Yang, F. Kang, Carbon 84 (2015) 434-443.
[152] B. Li, F. Yao, J.J. Bae, J. Chang, M.R. Zamfir, L. Duc Toan, P. Duy Tho, H. Yue, Y.H. Lee, Sci. Rep. 5 (2015)7659.
[153] Z. Lu, J. Zhu, D. Sim, W. Zhou, W. Shi, H.H. Hng, Q. Yan, Chem. Mater. 23 (2011) 5293-5295.
[154] V.V. Kulish, O.I. Malyi, M.-F. Ng, P. Wu, Z. Chen, RSC Adv. 3 (2013) 4231-4236.
[155] O. Malyi, V.V. Kulish, T.L. Tan, S. Manzhos, Nano Energy 2 (2013) 1149-1157.
[156] X. Yu, F. Xue, H. Huang, C. Liu, J. Yu, Y. Sun, X. Dong, G. Cao, Y. Jung, Nanoscale 6 (2014) 6860-6865.
[157] W.-S. Kim, Y. Hwa, J.-H. Shin, M. Yang, H.-J. Sohn, S.-H. Hong, Nanoscale 6 (2014) 4297-4302.
[158] X.H. Wang, L.M. Sun, X.N. Hu, R.A. Susantyoko, Q. Zhang, J. Power Sources 280 (2015) 393-396.
[159] J. Ryu, D. Hong, S. Choi, S. Park, ACS Nano 10 (2016) 2843-2851.
[160] R. Zhang, Y. Du, D. Li, D. Shen, J. Yang, Z. Guo, H.K. Liu, A.A. Elzatahry, D. Zhao, Adv. Mater. 26 (2014) 6749-6755.
[161] Y. Xu, Y. Zhu, C. Wang, J. Mater. Chem. A 2 (2014) 9751-9757.
[162] L. Yue, W. Zhang, J. Yang, L. Zhang, Electrochim. Acta 125 (2014) 206-217.
[163] A. Magasinski, P. Dixon, B. Hertzberg, A. Kvit, J. Ayala, G. Yushin, Nat. Mater. 9 (2010) 353-358.
[164] Y. Hwa, W.-S. Kim, S.-H. Hong, H.-J. Sohn, Electrochim. Acta 71 (2012) 201-205.
[165] T.H. Hwang, Y.M. Lee, B.S. Kong, J.S. Seo, J.W. Choi, Nano Lett. 12 (2012) 802-807.
[166] N. Liu, H. Wu, M.T. McDowell, Y. Yao, C. Wang, Y. Cui, Nano Lett. 12 (2012) 3315-3321.
[167] X. Li, P. Meduri, X. Chen, W. Qi, M.H. Engelhard, W. Xu, F. Ding, J. Xiao, W. Wang, C. Wang, J. Mater. Chem. 22 (2012) 11014-11017.
[168] H. Tao, L.Z. Fan, W.L. Song, M. Wu, X. He, X. Qu, Nanoscale 6 (2014) 3138-3142.
[169] L.Y. Yang, H.Z. Li, J. Liu, Z.Q. Sun, S.S. Tang, M. Lei, Sci. Rep. 5 (2015)10908.
[170] N.T. Hieu, J. Suk, D.W. Kim, O.H. Chung, J.S. Park, Y. Kang, Synth. Met. 198 (2014) 36-40.
[171] Y. Li, G. Xu, L. Xue, S. Zhang, Y. Yao, Y. Lu, O. Toprakci, X. Zhang, J. Electrochem. Soc. 160 (2013) A528-A534.
[172] A. Gohier, B. Laik, K.H. Kim, J.L. Maurice, J.P. Pereira-Ramos, C.S. Cojocaru, P. Van Tran, Adv. Mater. 24 (2012) 2592-2597.

[173] R. Epur, M. Ramanathan, M.K. Datta, D.H. Hong, P.H. Jampani, B. Gattu, P.N. Kumta, Nanoscale 7 (2015) 3504-3510.
[174] Y. Chen, N. Du, H. Zhang, D. Yang, J. Alloys Compd. 622 (2015) 966-972.
[175] L.L. Zhong, J.C. Guo, L. Mangolini, J. Power Sources 273 (2015) 638-644.
[176] Z.-l. Wang, D. Xu, Y. Huang, Z. Wu, L.-m. Wang, X.-b. Zhang, Chem. Commun. 48 (2012) 976-978.
[177] Y. Du, G. Zhu, K. Wang, Y. Wang, C. Wang, Y. Xia, Electrochem. Commun. 36 (2013) 107-110.
[178] Y. Wen, Y. Zhu, A. Langrock, A. Manivannan, S.H. Ehrman, C. Wang, Small 9 (2013) 2810-2816.
[179] Minseong Ko, Sujong Chae, Sookyung Jeong, Pilgun Oh, J. Cho., ACS Nano 8 (2014) 591–8599.
[180] J. Ji, H. Ji, L.L. Zhang, X. Zhao, X. Bai, X. Fan, F. Zhang, R.S. Ruoff, Adv. Mater. 25 (2013) 4673-4677.
[181] M. Zhou, T. Cai, F. Pu, H. Chen, Z. Wang, H. Zhang, S. Guan, ACS Appl. Mater. Interfaces 5 (2013) 3449-3455.
[182] Z.F. Li, H. Zhang, Q. Liu, Y. Liu, L. Stanciu, J. Xie, ACS Appl. Mater. Interfaces 6 (2014) 5996-6002.
[183] X. Zhou, Y.X. Yin, A.M. Cao, L.J. Wan, Y.G. Guo, ACS Appl. Mater. Interfaces 4 (2012) 2824-2828.
[184] S. Murugesan, J.T. Harris, B.A. Korgel, K.J. Stevenson, Chem. Mater. 24 (2012) 1306-1315.
[185] S. Fang, L. Shen, G. Xu, P. Nie, J. Wang, H. Dou, X. Zhang, ACS Appl. Mater. Interfaces 6 (2014) 6497-6503.
[186] K.J.G. Jeong G, Park M S, Seo M, Hwang S M, Kim Y U, Kim Y J, Kim J H, Dou S X. Acs Nano 8 (2014) 2977-2985.
[187] A.R. Park, D.Y. Son, J.S. Kim, J.Y. Lee, N.G. Park, J. Park, J.K. Lee, P.J. Yoo, ACS Appl. Mater. Interfaces 7 (2015) 18483-18490.
[188] Y.Z. Han, P.F. Qi, X. Feng, S.W. Li, X.T. Fu, H.W. Li, Y.F. Chen, J.W. Zhou, X.G. Li, B. Wang, ACS Appl. Mater. Interfaces 7 (2015) 2178-2182.
[189] Y. Chen, S. Zeng, J.F. Qian, Y.D. Wang, Y.L. Cao, H.X. Yang, X.P. Ai, ACS Appl. Mater. Interfaces 6 (2014) 3508-3512.
[190] A.M. Chockla, K.C. Klavetter, C.B. Mullins, B.A. Korgel, Chem. Mater. 24 (2012) 3738-3745.
[191] Y. Xiao, D. Hao, H. Chen, Z. Gong, Y. Yang, ACS Appl. Mater. Interfaces 5 (2013) 1681-1687.
[192] E. Mullane, T. Kennedy, H. Geaney, C. Dickinson, K.M. Ryan, Chem. Mater. 25 (2013) 1816-1822.
[193] W. McSweeney, O. Lotty, J.D. Holmes, C. O'Dwyer, ECS Trans. 35 (2011) 25-34.
[194] M.Y. Ge, J.P. Rong, X. Fang, C.W. Zhou, Nano Lett. 12 (2012) 2318-2323.
[195] S. Jing, H. Jiang, Y. Hu, C. Li, Nanoscale 6 (2014) 14441-14445.
[196] A.M. Chockla, J.T. Harris, V.A. Akhavan, T.D. Bogart, V.C. Holmberg, C. Steinhagen, C.B. Mullins, K.J. Stevenson, B.A. Korgel, J. Am. Chem. Soc. 133 (2011) 20914-20921.
[197] A. Gohier, B. Laïk, J.-P. Pereira-Ramos, C.S. Cojocaru, P. Tran-Van, J. Power Sources 203 (2012) 135-139.
[198] T.D. Bogart, D. Oka, X.T. Lu, M. Gu, C.M. Wang, B.A. Korgel, Acs Nano 8 (2014) 915-922.
[199] Y. Yao, N. Liu, M.T. McDowell, M. Pasta, Y. Cui, Energy Environ. Sci. 5 (2012) 7927-7930.
[200] H. Chen, Y. Xiao, L. Wang, Y. Yang, J. Power Sources 196 (2011) 6657-6662.
[201] S.-H. Baek, J.-S. Park, Y.-M. Jeong, J.H. Kim, J. Alloys Compd. 660 (2016) 387-391.
[202] A. Kohandehghan, K. Cui, M. Kupsta, E. Memarzadeh, P. Kalisvaart, D. Mitlin, J. Mater. Chem. A 2 (2014) 11261-11279.
[203] A. Kohandehghan, P. Kalisvaart, M. Kupsta, B. Zahiri, B.S. Amirkhiz, Z.P. Li, E.L. Memarzadeh, L.A. Bendersky, D. Mitlin, J. Mater. Chem. A 1 (2013) 1600-1612.
[204] B. Wang, X. Li, X. Zhang, B. Luo, Y. Zhang, L. Zhi, Adv. Mater. 25 (2013) 3560-3565.

[205] K.W. Lim, J.I. Lee, J. Yang, Y.K. Kim, H.Y. Jeong, S. Park, H.S. Shin, ACS Appl. Mater. Interfaces 6 (2014) 6340-6345.
[206] Z. Lu, J. Zhu, D. Sim, W. Shi, Y.Y. Tay, J. Ma, H.H. Hng, Q. Yan, Electrochim. Acta 74 (2012) 176-181.
[207] Y. Zhu, W. Liu, X. Zhang, J. He, J. Chen, Y. Wang, T. Cao, Langmuir 29 (2013) 744-749.
[208] J.G. Ren, C. Wang, Q.H. Wu, X. Liu, Y. Yang, L. He, W. Zhang, Nanoscale 6 (2014) 3353-3360.
[209] Y. Yang, J.G. Ren, X. Wang, Y.S. Chui, Q.H. Wu, X.F. Chen, W.J. Zhang, Nanoscale 5 (2013) 8689-8694.
[210] J.K. Yoo, J. Kim, Y.S. Jung, K. Kang, Adv. Mater. 24 (2012) 5452-5456.
[211] Z. Wen, G. Lu, S. Mao, H. Kim, S. Cui, K. Yu, X. Huang, P.T. Hurley, O. Mao, J. Chen, Electrochem. Commun. 29 (2013) 67-70.
[212] A.T. Tesfaye, R. Gonzalez, J.L. Coffer, T. Djenizian, ACS Appl. Mater. Interfaces 7 (2015) 20495-20498.
[213] Z. Lu, T. Wong, T.-W. Ng, C. Wang, RSC Adv. 4 (2014) 2440-2446.
[214] B. Hertzberg, A. Alexeev, G. Yushin, J. Am. Chem. Soc. 132 (2010) 8548-8549.
[215] J. Liu, N. Li, M.D. Goodman, H.G. Zhang, E.S. Epstein, B. Huang, Z. Pan, J. Kim, J.H. Choi, X. Huang, J. Liu, K.J. Hsia, S.J. Dillon, P.V. Braun, ACS Nano 9 (2015) 1985-1994.
[216] L.M. Sun, X.H. Wang, R.A. Susantyoko, Q. Zhang, J. Mater. Chem. A 2 (2014) 15294-15297.
[217] H. Wu, G. Chan, J.W. Choi, I. Ryu, Y. Yao, M.T. McDowell, S.W. Lee, A. Jackson, Y. Yang, L. Hu, Y. Cui, Nat. Nanotechnol. 7 (2012) 310-315.
[218] M.R. Zamfir, H.T. Nguyen, E. Moyen, Y.H. Lee, D. Pribat, J. Mater. Chem. A 1 (2013) 9566-9586.
[219] J. Cho, J. Mater. Chem. 20 (2010) 4009-4014.
[220] Y. Liu, B. Chen, F. Cao, H.L.W. Chan, X. Zhao, J. Yuan, J. Mater. Chem. 21 (2011) 17083-17086.
[221] B.M. Bang, H. Kim, H.-K. Song, J. Cho, S. Park, Energy Environ.Sci. 4 (2011) 5013-5019.
[222] B.M. Bang, J.I. Lee, H. Kim, J. Cho, S. Park, Adv. Energy Mater. 2 (2012) 878-883.
[223] T. Wada, T. Ichitsubo, K. Yubuta, H. Segawa, H. Yoshida, H. Kato, Nano Lett. 14 (2014) 4505-4510.
[224] J. Zhu, C. Gladden, N. Liu, Y. Cui, X. Zhang, Phys. Chem. Chem. Phys. 15 (2013) 440-443.
[225] M.Y. Ge, J.P. Rong, X. Fang, A.Y. Zhang, Y.H. Lu, C.W. Zhou, Nano Res. 6 (2013) 174-181.
[226] M. Ge, Y. Lu, P. Ercius, J. Rong, X. Fang, M. Mecklenburg, C. Zhou, Nano Lett. 14 (2014) 261-268.
[227] Z. Jiang, C. Li, S. Hao, K. Zhu, P. Zhang, Electrochim. Acta 115 (2014) 393-398.
[228] C. Li, P. Zhang, Z. Jiang, Electrochim. Acta 161 (2015) 408-412.
[229] W. He, H. Tian, F. Xin, W. Han, J. Mater. Chem. A 3 (2015) 17956-17962.
[230] H. Tian, X. Tan, F. Xin, C. Wang, W. Han, Nano Energy 11 (2015) 490-499.
[231] J. Feng, Z. Zhang, L. Ci, W. Zhai, Q. Ai, S. Xiong, J. Power Sources 287 (2015) 177-183.
[232] X. Han, H. Chen, J. Liu, H. Liu, P. Wang, K. Huang, C. Li, S. Chen, Y. Yang, Electrochim. Acta 156 (2015) 11-19.
[233] Z. Bao, M.R. Weatherspoon, S. Shian, Y. Cai, P.D. Graham, S.M. Allan, G. Ahmad, M.B. Dickerson, B.C. Church, Z. Kang, H.W. Abernathy Iii, C.J. Summers, M. Liu, K.H. Sandhage, Nature 446 (2007) 172-175.
[234] N. Liu, K. Huo, M.T. McDowell, J. Zhao, Y. Cui, Sci. Rep. 3 (2013) 1919.
[235] H. Zhong, H. Zhan, Y.-H. Zhou, J. Power Sources 262 (2014) 10-14.
[236] W. Wang, Z. Favors, R. Ionescu, R. Ye, H.H. Bay, M. Ozkan, C.S. Ozkan, Sci. Rep. 5 (2015) 8717.
[237] Y.M. Kim, J. Ahn, S.-H. Yu, D.Y. Chung, K.J. Lee, J.-K. Lee, Y.-E. Sung, Electrochim. Acta 151 (2015) 256-262.
[238] Q. Li, L. Yin, X. Gao, RSC Adv. 5 (2015) 35598-35607.

[239] H.-C. Tao, L.-Z. Fan, X. Qu, Electrochim. Acta 71 (2012) 194-200.
[240] M.-S. Wang, L.-Z. Fan, M. Huang, J. Li, X. Qu, J. Power Sources 219 (2012) 29-35.
[241] Y. Zhao, X. Liu, H. Li, T. Zhai, H. Zhou, Chem. Commun. 48 (2012) 5079-5081.
[242] Y. Yao, M.T. McDowell, I. Ryu, H. Wu, N. Liu, L. Hu, W.D. Nix, Y. Cui, Nano Lett. 11 (2011) 2949-2954.
[243] D.Y. Chen, X. Mei, G. Ji, M. Lu, J. Xie, J. Lu, J.Y. Lee, Angew. Chem. 51 (2012) 2409-2413.
[244] F.H. Du, B. Li, W. Fu, Y.J. Xiong, K.X. Wang, J.S. Chen, Adv. Mater. 26 (2014) 6145-6150.
[245] X.K. Huang, J. Yang, S. Mao, J.B. Chang, P.B. Hallac, C.R. Fell, B. Metz, J.W. Jiang, P.T. Hurley, J.H. Chen, Adv. Mater. 26 (2014) 4326-4332.
[246] T. Morita, N. Takami, J. Electrochem. Soc. 153 (2006) A425-A430.
[247] C.-M. Park, W. Choi, Y. Hwa, J.-H. Kim, G. Jeong, H.-J. Sohn, J. Mater. Chem. 20 (2010) 4854-4860.
[248] J.I. Lee, K.T. Lee, J. Cho, J. Kim, N.S. Choi, S. Park, Angew. Chem. Int. Ed. 51 (2012) 2767-2771.
[249] J.I. Lee, N.S. Choi, S. Park, Energy Environ. Sci. 5 (2012) 7878-7882.
[250] J. Ryu, S. Choi, T. Bok, S. Park, Nanoscale 7 (2015) 6126-6135.
[251] J.-I. Lee, Y. Ko, M. Shin, H.-K. Song, N.-S. Choi, M.G. Kim, S. Park, Energy Environ. Sci. 8 (2015) 2075-2084.
[252] Z. Du, S.N. Ellis, R.A. Dunlap, M.N. Obrovac, J. Electrochem. Soc. 163 (2016) A13-A18.
[253] S. Chae, M. Ko, S. Park, N. Kim, J. Ma, J. Cho, Energy Environ. Sci. 9 (2016) 1251-1257.
[254] Y.H. Huang, Q. Bao, J.G. Duh, C.T. Chang, J. Mater. Chem. A 4 (2016) 9986-9997.
[255] A.G. Kannan, S.H. Kim, H.S. Yang, D.W. Kim, RSC Adv. 6 (2016) 25159-25166.
[256] X. Ding, X. Liu, Y. Huang, X. Zhang, Q. Zhao, X. Xiang, G. Li, P. He, Z. Wen, J. Li, Y. Huang, Nano Energy 27 (2016) 647-657.
[257] D.A. Agyeman, K. Song, G.-H. Lee, M. Park, Y.-M. Kang, Adv. Energy Mater. 6 (2016) 1600904.
[258] Y. Ma, R. Younesi, R. Pan, C. Liu, J. Zhu, B. Wei, K. Edström, Adv. Funct. Mater. 26 (2016) 6797-6806.
[259] Y. Li, K. Yan, H.-W. Lee, Z. Lu, N. Liu, Y. Cui, Nature Energy 1 (2016) 15029.
[260] M. Ko, S. Chae, J. Ma, N. Kim, H.-W. Lee, Y. Cui, J. Cho, Nature Energy 1 (2016) 16113.
[261] L. Zhang, R. Rajagopalan, H. Guo, X. Hu, S. Dou, H. Liu, Adv. Funct. Mater. 26 (2016) 440-446.
[262] M.N. Obrovac, V.L. Chevrier, Chem. Rev. 114 (2014) 11444-11502.
[263] M.F.L. De Volder, S.H. Tawfick, R.H. Baughman, A.J. Hart, Science 339 (2013) 535-539.
[264] Q. Xu, J.-Y. Li, J.-K. Sun, Y.-X. Yin, L.-J. Wan, Y.-G. Guo, Adv. Energy Mater. (2016) 1601481.
[265] A. Casimir, H. Zhang, O. Ogoke, J.C. Amine, J. Lu, G. Wu, Nano Energy 27 (2016) 359-376.
[266] NEXEON. http://www.nexeon.co.uk/technology-2/ (accessed 06.11.2016) .
[267] 3M. http://www.3m.com/3M/en_US/energy-storage-us#lithium (accessed 06.11.2016) .
[268] Amprius. http://www.amprius.com/news/news_amprius_20160523.htm (accessed 06.11.2016) .
[269] XGS. http://xgsciences.com/blog/2013/04/12/new-battery-anode/ (accessed 06.11.2016) .
[270] Hitachi.http://www.companyowl.com/i/n/new-hitachi-maxell-liion-battery-increases-battery-power-60-taking-extra-space/201397 (accessed 06.11.2016) .
[271] BTR. http://www.btrchina.com/product/index123.html (accessed 06.11.2016) .

Table of Content

The research on the Si-based lithium-ion battery anode has been systematically reviewed in a chronicle perspective from early 1990s to 2016, where the evolution trends of the structure feature and modification strategy of Si have been elaborated.

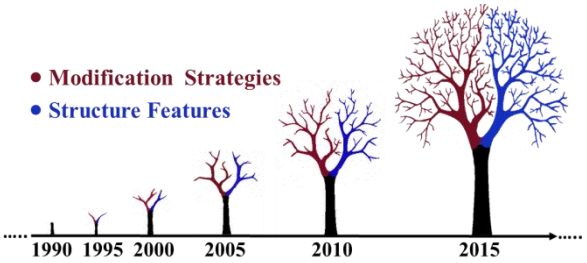

Author Portrait and Bio-sketch

Xiuxia Zuo:

Xiuxia Zuo is now a Ph.D. student at the Ningbo Institute of Materials Technology and Engineering (NIMTE), Chinese Academy of Sciences. She completed her undergraduate studies at the North University of China (2004), followed by a master degree in materials from Beijing Institute of Technology in 2007. After master studies, she has worked as a research assistant at the Ningbo Institute of Materials Technology & Engineering (NIMTE), CAS. Her research focuses on nanohybrid materials for lithium ion battery.

Prof. Dr. Jin Zhu:

Prof. Dr. Jin Zhu is a full professor and head of the Institute of Materials Technology in Ningbo Institute of Materials Technology and Engineering, Chinese Academy of Sciences (NIMTE). Dr. Zhu got his Ph.D. at Marquette University and did postdoctoral study at Cornell University in the United States. Prior to returning China in 2009, Dr. Zhu had worked at several US companies. His current research interests are on bio-based polymers, flame retardant materials and functional nanocomposites. He has published over 100 research papers and more than 50 granted patents. Dr. Zhu is a specialist of China “National Thousand Talent Program”.

Prof. Dr. Peter Müller-Buschbaum:

Peter Müller-Buschbaum is professor at Technische Universität München, heading the chair of Functional Materials since 2006. He is heading the keylab 'TUM.solar' on solar energy conversion and storage and the 'Network for Renewable Energies' (NRG) of the 'Munich School of Engineering' (MSE). He is the German representative at the 'European Polymer Federation' (EPF) for polymer physics. He is elected chairman of the 'Hamburg User Committee' (HUC) at the synchrotron radiation laboratory DESY, member of the 'European Synchrotron User Organization' (EUSO) and associate editor of "ACS Applied Materials & Interfaces". His research focuses on polymer nanohybrids with advanced scattering experiments.

Prof. Dr. Ya-Jun Cheng:

Dr. Ya-Jun Cheng is an associate professor at the Ningbo Institute of Materials Technology & Engineering (NIMTE, CAS). Since 2015 he has been working in the group of Prof. Dr. Peter G Bruce as a Marie Sklodowska-Curie Fellow. He received the BS degree from Peking University, China, followed by the master from the University of Siegen, Germany, and the Ph. D. studies at the Max-Planck Institute for Polymer Research in Mainz, Germany. He worked in the National Institute of Standards and Technology, USA before he joined the NIMTE, CAS. His research focuses on the synthesis and applications of polymer/inorganic nanohybrids.